Published for the International Glaciological Society

Assessing Future Ice Shelf Collapse Vulnerability in the ISMIP6 Ensemble

Journal:	*Journal of Glaciology*
Manuscript ID	Draft
Manuscript Type:	Article
Date Submitted by the Author:	n/a
Complete List of Authors:	Reynolds, Benjamin; University at Buffalo, Department of Earth Sciences Crooks Nowicki, Sophie; University at Buffalo, Department of Earth Sciences; University at Buffalo, RENEW Institute
Keywords:	Ice shelves, Crevasses, Melt - surface, Ice-shelf break-up, Ice-sheet modelling
Abstract:	Understanding the possibility of future ice shelf collapses similar to the Larsen B is critical for improving sea-level-rise projections due to the restraint on upstream flow that ice shelves provide. Prior research has provided a criterion for assessing the vulnerability of ice shelf to hydrofracture. We apply these calculations to the model ensemble results from the Ice Sheet Modeling Intercomparison Project for CMIP6 (ISMIP6). With these ensemble results, we evaluate the predicted shelf vulnerability through time with forcings from several climate scenarios, climate models, basal melt parametrizations, and a range of fracture toughness values. Additionally, for the ISMIP6 experiments that included a collapse forcing (based on surface melt availability alone), we evaluate whether the ice subjected to the collapse forcing was vulnerable. We find that shelf vulnerability generally decreases through 2100 as ice thickness decreases, indicating a potential negative feedback. Differences in initial vulnerability between models as well as sensitivity to fracture toughness, however, tend to outweigh the change from stress evolution. For the shelves where collapse was imposed in the corresponding ISMIP6

Author contacts: Benjamin Reynolds (br77@buffalo.edu), Sophie Nowicki (sophien@buffalo.edu)

	experiment (Larsen C, George VI, Wilkins), between 20% and 70% of collapsed shelf area was vulnerable depending on fracture toughness.

Journal of Glaciology, Vol. 00, No. 000, 0000

Assessing Future Ice Shelf Collapse Vulnerability in the ISMIP6 Ensemble

Benjamin REYNOLDS,[1] Sophie NOWICKI,[1,2]

[1]*Department of Earth Sciences, University at Buffalo, Buffalo, NY, USA*

[2]*RENEW Institute, University at Buffalo, Buffalo, NY, USA*

Correspondence: Benjamin Reynolds <br77@buffalo.edu>

ABSTRACT. Understanding the possibility of future ice shelf collapses similar to the Larsen B is critical for improving sea-level-rise projections due to the restraint on upstream flow that ice shelves provide. Prior research has provided a criterion for assessing the vulnerability of ice shelf to hydrofracture. We apply these calculations to the model ensemble results from the Ice Sheet Modeling Intercomparison Project for CMIP6 (ISMIP6). With these ensemble results, we evaluate the predicted shelf vulnerability through time with forcings from several climate scenarios, climate models, basal melt parametrizations, and a range of fracture toughness values. Additionally, for the ISMIP6 experiments that included a collapse forcing (based on surface melt availability alone), we evaluate whether the ice subjected to the collapse forcing was vulnerable. We find that shelf vulnerability generally decreases through 2100 as ice thickness decreases, indicating a potential negative feedback. Differences in initial vulnerability between models as well as sensitivity to fracture toughness, however, tend to outweigh the change from stress evolution. For the shelves where collapse was imposed in the corresponding ISMIP6 experiment (Larsen C, George VI, Wilkins), between 20% and 70% of collapsed shelf area was vulnerable depending on fracture toughness.

INTRODUCTION

While the loss of ice shelves does not directly contribute to sea-level rise, ice shelves hold back upstream ice via buttressing (Fürst and others, 2016; Sun and others, 2020). Major speedups of upstream ice following the 2002 collapse of the Larsen B were observed (Rignot and others, 2004; Rott and others, 2011), increasing the sea-level contribution from upstream glaciers. Surface meltwater pond formation prior to multiple Antarctic Peninsula shelf collapses led to the proposal of hydrofracture as the collapse mechanism (Scambos and others, 2000). Hydrofracture occurs when surface meltwater enters pre-existing crevasses and propagates them through the shelf (van der Veen, 1998; Scambos and others, 2000). This theory has led to research in understanding the past and future of surface melt, the extent of surface crevassing, and the mechanism by which sudden collapse propagates when surface melt and crevasses coincide. These lines of work will hopefully converge to create process models that allow for the accurate implementation of ice shelf collapse in ice sheet models.

Scambos and others (2000) noted the high number of melt days prior to collapse events at the Prince Gustav, Larsen inlet, Larsen A, Larsen B, and Wilkins ice shelves. Subsequent work by Trusel and others (2015) assessed the meltwater production at the Larsen A and B during their collapse periods and projected meltwater production into the future as a function of climate scenario to show the impact of emissions on future collapse extent. Whether meltwater production alone is the best predictor of supraglacial lake formation has been questioned on the basis of firn's ability to store water in pore space. Other proposed methods for predicting the start of pond formation include using firn air content depletion via firn models (Munneke and others, 2014) or using the ratio of melt over accumulation as an indicator for firn depletion (Pfeffer and others, 1991; Donat-Magnin and others, 2021). The timing of future pond formation as a function climate scenario using these criteria has also been evaluated (e.g. Veldhuijsen and others, 2024; Donat-Magnin and others, 2021; van Wessem and others, 2023). Work on remote sensing measurements of pond volume (e.g. Trusel and others, 2013; Moussavi and others, 2020) has begun to allow more direct testing of these criteria for predicting pond initiation and volume (e.g. van Wessem and others, 2023).

At the same time, methods of predicting the extent of crevassing and whether crevasses would be susceptible to hydrofracture have been in development. Scambos and others (2000) assessed the "critical depth" that pre-existing crevasses must be such that hyrdrofracture occurs given assumptions about fracture toughness, water levels in crevasses, and firn density. The application of linear elastic fracture mechanics (LEFM) to crevasse depths (e.g. van der Veen, 1998; Jiménez and Duddu, 2018) allows for the prediction of where crevasses should exist based on stress and density profiles. Lai and others (2020) derived an LEFM-based dimensionless stress threshold that simplified the delineation of regions that should and should not have surface crevassing. They validated this threshold by identifying crevasses with machine learning and showing that the vast majority of identified crevasses exist where the threshold predicts existence of stable crevasses. Finally, they overlapped their mapping of where crevassing is predicted with the mapping of where ice shelves provide buttressing from Fürst and others (2016) to reach the conclusion that approximately 60% of Antarctic ice shelf area is both vulnerable to hydrofracture (given melt) and important to upstream ice velocity.

With the developing ability to predict where crevasses and surface ponds will overlap from the above lines of work, the last step is to model the actual collapse mechanism whereby hydrofracture of individual crevasses leads to the rapid and large scale break-up of a significant fraction of an ice shelf. Scambos and others (2009) presented two-dimensional flowline modeling results showing how the flexural response from a calving event can cause additional calving with sufficient meltwater. Banwell and others (2013) proposed a process and analytical model whereby the flexural response from lake formation and then drainage causes additional crevassing and drainages from surrounding lakes yielding a chain reaction. This proposed chain reaction leaves a pattern of intersecting crevasses that can explain rapid collapse. This mechanism has been further assessed by models of viscoelastic shelf flexure during lake formation and draining (MacAyeal and others, 2015) and by a cellular automata model of the interaction between melt pond hydrofracture events (Robel and Banwell, 2019). While these and other efforts will hopefully provide a more mechanistic method of implementing ice shelf collapse in ice sheet models, there is presently a gap between these methods and simple implementations used so far. In the most recent ice sheet model ensemble, the Ice Sheet Model Intercomparison Project for CMIP6 (ISMIP6) (Nowicki and others, 2016), ice shelf collapse was parametrized based on surface melt alone (Nowicki and others, 2020). An intermediate step might be to apply the crevasse existence criterion of Lai and others (2020) and prescribe collapse of regions where crevasses overlap with surface ponds based on criterion from melt production, firn air content depletion, or melt over accumulation.

We seek to better understand how crevasse-based ice shelf vulnerability may evolve into the future by applying this criterion from Lai and others (2020) to results from ISMIP6. This work furthers understanding of future ice shelf vulnerability in general but also provides a preview of what may be expected if this criterion is applied in future ice sheet modeling efforts. In ISMIP6, ice sheet modelers ran a set of common experiments defined by input climate scenarios, climate models, and process parametrizations. Through this, ISMIP6 provides projections of the Greenland and Antarctic contributions to sea-level rise that include both climate-forcing and ice-sheet-modeling driven uncertainty (Goelzer and others, 2020; Seroussi and others, 2020; Payne and others, 2021). By further postprocessing the ISMIP6 Antarctica results, we can make projections of ice-shelf-vulnerability evolution considering these same unknowns. In our reanalysis, we also consider the impacts of fracture toughness on both the initial and evolved ice-shelf vulnerabilities.

As noted, the parametrization of ice shelf collapse implemented in some ISMIP6 experiments was based only on surface melt (Nowicki and others, 2020), so we can assess how the collapse forcing might have changed with the stress preconditioning criterion from Lai and others (2020). These experiments also allow for study of how partial ice shelf collapse can affect ice shelf vulnerability of the remaining shelf fraction to assess the importance of using an evolving parametrization.

METHODS

Surface Stress Calculation

While each ice sheet model in the ISMIP6 ensemble will have directly calculated deviatoric stresses, these are not provided in the standard, gridded output that modelers reported. Because of this, we use the velocity output that all models reported on the ISMIP6 standard, eight-kilometer grid to compute deviatoric stress at the surface. The gradient of the velocity fields (calculated with central differences) gives strain rates, and we calculate the deviatoric stress tensor following Cuffey and Patterson (2010). For models that output evolving surface temperatures, we calculated the surface stress accordingly. For models that do not report an evolving temperature, we assume the temperature of Comiso (2000), which was used as a boundary condition for the thermal solver of at least two of the models (Seroussi and others, 2020). Table 1 shows which models' results were analyzed with reported versus assumed surface temperatures. The assumption of rheology (Cuffey and Patterson, 2010) and (in some cases) surface temperature may result in a mismatch between a model's stress and the recalculated stress. Nonetheless, the direction and approximate magnitude of change in stress through time will still be captured.

Shelf Vulnerability Calculation

Lai and others (2020) derived equations for dimensionless resistive stress and a critical value of this dimensionless resistive stress that causes crevassing regardless of initial flaw size. They argue that this is a criterion for shelf vulnerability to hydrofracture when surface meltwater is present, as it guarantees

Table 1. ISMIP6 models' temperature and velocity outputs used for reanalysis.

Model name	Temperature	Velocity
AWI_PISM1	reported	surface
DOE_MALI	reported	surface
ILTS_PIK_SICOPOLIS1	reported	surface
IMAU_IMAUICE1	Comiso	mean
IMAU_IMAUICE2	Comiso	mean
JPL1_ISSM	Comiso	mean
LSCE_GRISLI2	reported	surface
NCAR_CISM	reported	surface
UCIJPL_ISSM	Comiso*	mean
ULB_fETISh_16km	reported	surface
ULB_fETISh_32km	reported	surface
UTAS_ElmerIce	Comiso*	surface
VUB_AISMPALEO	reported	surface

*Confirmed to match surface temperature used as thermal model boundary condition in appendix of Seroussi and others (2020).

the presence of crevasses to be hydrofractured. Their dimensionless resistive stress, $\tilde{R}_{xx}$, is

$$\tilde{R}_{xx} = \frac{R_{xx}}{\rho_i g H} \tag{1}$$

where R_{xx} is resistive stress, ρ_i is ice density, g is gravitational acceleration, and H is ice thickness. The dimensionless resistive stress threshold, $\tilde{R}^*_{xx}$ is

$$\tilde{R}^*_{xx} = \left(\frac{3\sqrt{6}}{2\pi} \frac{f^{1/2}}{F^{3/2}} \tilde{K}_{IC} \right)^{2/3} \tag{2}$$

where $\tilde{K}_{IC}$ is dimensionless fracture toughness and F and f are linear elastic fracture mechanics (LEFM) functions that can be approximated for shallow crevasses as $F \approx 1.122$ and $f \approx 1.068$. Lai and others (2020) provide the generalized equations that apply when crevasses are a significant fraction of ice thickness. Dimensionless fracture toughness is given by

$$\tilde{K}_{IC} = \frac{K_{IC}}{\rho_i g H^{3/2}} \tag{3}$$

where K_{IC} is fracture toughness. Fracture toughness is the one free parameter in these equations and is the property of ice that describes its resistance to crevasse formation. van der Veen (1998) specified the plausible range of fracture toughness as 100 to 400 $KPa\ m^{1/2}$ based on lab tests of real glacial and synthetic ice by Fischer and others (1995) and Rist and others (1996). We use 200 $KPa\ m^{1/2}$ for all analyses except when specifically studying sensitivity to fracture toughness. See the Fracture Toughness Sensitivity section below for a brief review of experimental fracture toughness results.

Mirroring Lai and others (2020), we neglect the effect of firn on both the density and rheology of the ice shelf surfaces. We also do not consider the change of ice temperature with depth or seasonal change in surface temperature. The one difference between the calculations we use and those of Lai and others (2020) is in the calculation of the resistive stress from the deviatoric stresses. We calculate the resistive stress, R_{xx} as

$$R_{xx} = 2\tau_1 + \tau_2 \tag{4}$$

where τ_1 and τ_2 are the maximum and minimum principal deviatoric stress from the surface (planar) deviatoric stress tensor. These deviatoric stresses are calculated with effective strain rate, $\dot{\epsilon}_{eff}$, that recognizes mass continuity ($\dot{\epsilon}_{zz} = -\dot{\epsilon}_{xx} - \dot{\epsilon}_{yy}$) but neglects vertical shear strain rates ($\dot{\epsilon}_{xz} = \dot{\epsilon}_{yz} = 0$) such that

$$\dot{\epsilon}_{eff} = \sqrt{\frac{1}{2}\left(\dot{\epsilon}_{xx}^2 + \dot{\epsilon}_{yy}^2 + \dot{\epsilon}_{zz}^2\right) + \dot{\epsilon}_{xy}^2}. \tag{5}$$

Lai and others (2020) applied the one-dimensional version of Glen's flow law in either the maximum principal stress direction or the flow direction:

$$R_{xx} = 2B\dot{\epsilon}_1^{1/3} \tag{6}$$

$$R_{xx} = 2B\dot{\epsilon}_{flow\,dir.}^{1/3} \tag{7}$$

where B is ice rigidity, $\dot{\epsilon}_1$ is the maximimum principal strain rate, and $\dot{\epsilon}_{flow\,dir.}$ is the strain rate in the flow direction. Our use of the maximum principal stress direction will tend to increase shelf vulnerability as sometimes the flow direction and maximum principal stress directions are misaligned. Our inclusion of the minimum principal stress term and effective strain rate calculation reduces the vulnerability in shear zones, as the pure shear strain rate state has a minimum principal deviatoric stress that is equal in magnitude but opposite in sign to the maximum principal deviatoric stress ($\dot{\tau}_2 = -\dot{\tau}_1$).

Shelf Vulnerability Sensitivity Analyses

We first analyze the shelf-vulnerability-evolution impact of climate scenario with two representative concentration pathways (RCPs), climate models with three atmosphere-ocean global circulation models (AOGCMs), and basal melt parametrization with four sensitivity tunings. We also analyze the sensitivity of initial and evolving vulnerability to ice's fracture toughness. In these analyses, we show the mean and standard deviation across models of the percentage of the ice shelf that is vulnerable. These metrics are calculated for 2014 (the end of model initialization), 2050, 2075, and 2100. The total ice shelf areas can increase through grounding line retreat or decrease through calving (for models that included a calving law). To avoid this artificially changing the vulnerable fraction, the fractions are calculated against the initial shelf areas. Some models that include calving have major reductions in shelf area such that a very high or low vulnerable fraction could be reported from a shelf remnant. To avoid this possible source of error, vulnerable fractions are only included in the average if the shelf area remains above 80% of its initial value.

The ISMIP6 experiments included a standard basal melt parametrization but also allowed models to use a custom parametrization. To include as many models as possible in our comparisons, we group the experiments that are identical except for the use of the standard versus open basal melt parametrizations. In cases where a model participated in both melt experiments, we take the submission to the experiment with the standard basal melt parametrization. For example, exp01 and exp05 were both forced by the NorESM1-M climate model under the RCP8.5 scenario with exp01 using the open melt parametrization and exp05 using the standard parametrization. In this case, all exp05 submissions are included along with exp01 submissions only from models that did not submit to exp05. Table 2 shows the experiment groupings used in all comparisons.

Climate Scenario Sensitivity

The ISMIP6 Antarctica experiments include projections under the RCP2.6 and RCP8.5 scenarios driven by the NorESM1-M climate model. This was the only climate model with both RCP8.5 and RCP2.6 in the Tier 1 ISMIP6 experiments, which have the most participating models (Seroussi and others, 2020). We select the corresponding experiments (exp05/exp01 and exp07/exp03) to study the sensitivity of ice shelf vulnerability evolution to climate scenario with one climate model.

Table 2. ISMIP6 Experiments and associated parameters used in all comparison analyses for studying the sensitivity of ice shelf vulnerability to RCP, AOGCM, basal melt parametrization, and fracture toughness. Entries in bold indicate the forcing or parameter that varies between the ensemble results groups.

Analysis	Experiment	AOGCM	Scenario	Ocean Forcing	Ocean Sensitivity	Fracture Toughness
RCP	exp05/exp01	NorESM1-M	**RCP8.5**	Standard/Open	Medium	200 $KPa\ m^{1/2}$
	exp07/exp03	NorESM1-M	**RCP2.6**	Standard/Open	Medium	200 $KPa\ m^{1/2}$
AOGCM	exp05/exp01	**NorESM1-M**	RCP8.5	Standard/Open	Medium	200 $KPa\ m^{1/2}$
	exp06/exp02	**MIROC-ESM-CHEM**	RCP8.5	Standard/Open	Medium	200 $KPa\ m^{1/2}$
	exp08/exp04	**CCSM4**	RCP8.5	Standard/Open	Medium	200 $KPa\ m^{1/2}$
Basal	exp10	NorESM1-M	RCP8.5	Standard	**Low**	200 $KPa\ m^{1/2}$
Melt	exp05	NorESM1-M	RCP8.5	Standard	**Medium**	200 $KPa\ m^{1/2}$
	exp09	NorESM1-M	RCP8.5	Standard	**High**	200 $KPa\ m^{1/2}$
	exp13	NorESM1-M	RCP8.5	Standard	**PIGL**	200 $KPa\ m^{1/2}$
Fracture	exp05/exp01	NorESM1-M	RCP8.5	Standard	Medium	**100 KPa $\mathbf{m^{1/2}}$**
Toughness	exp05/exp01	NorESM1-M	RCP8.5	Standard	Medium	**200 KPa $\mathbf{m^{1/2}}$**
	exp05/exp01	NorESM1-M	RCP8.5	Standard	Medium	**300 KPa $\mathbf{m^{1/2}}$**
	exp05/exp01	NorESM1-M	RCP8.5	Standard	Medium	**400 KPa $\mathbf{m^{1/2}}$**

Climate Model Sensitivity

The tier 1 ISMIP6 experiments included forcings from three AOGCMs. Climate models that perform well against reanalysis of the Antarctic climate while also sampling lower and higher warming were selected by the ISMIP6 team (Barthel and others, 2020). Although the Tier 2 experiments included forcings from three additional climate models, using them would reduce the number of ice sheet models in our analysis from 16 to 10. For this reason, we compare the ice sheet vulnerability through time under forcings from the three climate models included in the Tier 1 experiments: NorESM1-M, MIROC-ESM-CHEM, and CCSM4 (exp05/exp01, exp06/exp02, exp08/exp04). The climate scenario used in these experiments is RCP8.5.

Basal Melt Parametrization Sensitivity

The ISMIP6 protocol provides four basal melt parametrizations for Antarctic ice shelves. The development of these parametrizations is specified in Jourdain and others (2020). The low, medium, and high basal melt parametrizations correspond to the 5th, 50th, and 95th percentile tuning paramaters from all Antarctic ice shelves. The Pine Island Glacier (PIGL) melt parametrization is a tuning that reproduces the high basal melt rates near the grounding line of Pine Island Glacier under the premise that the high sensitivity observed at Pine Island could be indicative of future response to ocean warming. We will asses the evolution of shelf vulnerability with each of these basal melt paremetrizations (exp10, exp05, exp09, and exp13).

Thickness Change Correlation

That stress increases linearly with ice thickness in laterally confined or unconfined ice shelves has been derived and used to infer ice rheology in numerous studies (e.g. Thomas, 1973; Millstein and others, 2022). For example, when longitudinal spreading dominates, the longitudinal deviatoric stress (τ_{xx}) is

$$\tau_{xx} = \frac{1}{4}\rho_i g(1 - \rho_i/\rho_{sw})H \tag{8}$$

where ρ_{sw} is the density of seawater (Millstein and others, 2022). With the assumption of purely longitudinal extension, lateral deviatoric stress, τ_{yy} is negligible making the resistive stress:

$$R_{xx} = 2\tau_{xx}. \tag{9}$$

From this relationship, we may expect that as increased basal melt causes shelf thinning, stress and thus shelf vulnerable area will decrease across some shelf regions. To better understand how much of shelf vulnerability change can be explained by thickness decrease, we will plot the correlation of average resistive stress change, average critical dimensionless restive stress exceedance change, and shelf vulnerable fraction change against average shelf thickness change. The change in average resistive stress is calculated as

$$\Delta\overline{R_{xx}} = avg\left(R_{xx,f} - R_{xx,o}\right) \tag{10}$$

where $R_{xx,f}$ is the final per-grid-point resistive stress and $R_{xx,o}$ is the initial per-grid-point resistive stress. The average change in dimensionless resistive stress threshold exceedance is calculated as

$$\Delta\overline{(\tilde{R}_{xx} - \tilde{R}^*_{xx})} = \tag{11}$$

$$avg\left(\left(\tilde{R}_{xx,f} - \tilde{R}^*_{xx,f}\right) - \left(\tilde{R}_{xx,o} - \tilde{R}^*_{xx,o}\right)\right) \tag{12}$$

where $\tilde{R}_{xx,f}$ and $\tilde{R}_{xx,o}$ are the final and initial dimensionless resistive stresses and $\tilde{R}^*_{xx,f}$ and $\tilde{R}^*_{xx,o}$ are the final and intial dimensionless resistive stress thresholds for crevasse formation. Recall that the dimensionless resistive stress is a function of the stress and thickness (Equation (1)) and that the critical dimensionless resistive stress is a function of thickness and fracture toughness but not stress (Equation (2)). Change in shelf vulnerable area fraction is calculated as

$$\Delta Vuln\ Fraction = \frac{A_{vulnerable,f} - A_{vulnerable,o}}{A_{total,o}} \tag{13}$$

where $A_{vulnerable,f}$ is the final area shelf area, $A_{total,o}$ is the initial total shelf area, and $A_{vulnerable,o}$ is the initial vulnerable shelf area. As before, any shelf that drops below 80% of its initial area will be excluded from these analyses to avoid artificial results from shelf remnants. The correlation of these changes in shelf stress and vulnerability against thickness change will be shown for every model and experiment combination that makes up the sensitivity analyses to climate scenario, climate model, and basal melt parametrization (Table 2).

When analyzing the correlation with thickness change of resistive stress and of dimensionless resitive stress threshold exceedance, we can plot a theoretical prediction starting from an averaged initial thickness. For a given shelf, we take the spatially-averaged initial thicknesses from all ice sheet models and average those to get this starting thickness. Predicted change in resistive stress is calculated with change from this initial thickness using Equations (8, 9). Predicted change in exceedance of the dimensionless resistive stress threshold can then be calculated with Equations (1-3) taking the predicted resistive stress change and fracture toughness used in the ice sheet model reanalyses as input.

Finally, it is important to distinguish between thickness change being used here and in the ISMIP6 results papers. To calculate sea-level rise that excludes model drift that is deemed artificial, change in thickness reported in Seroussi and others (2020) is the thickness change in the experiment run minus the thickness change in a control run that had a constant forcing. Here, we simply use the thickness change in the experiment, as that thickness change corresponds to stress balance equations in the ice sheet model.

Fracture Toughness Sensitivity

van der Veen (1998) reviewed fracture toughness tests of real glacial samples as well as synthetic ice by Fischer and others (1995) and Rist and others (1996) and recommended a range of 100 to 400 $KPa\ m^{1/2}$. The high end value is anchored by exactly one result from the glacial samples of Rist and others (1996), whose other glacial ice results (excluding firn) fall between 140 and 260 $KPa\ m^{1/2}$. Their synthetic ice tests fell between 100 and 300 $KPa\ m^{1/2}$ with more scatter for larger grain sizes. The synthetic ice tests of Fischer and others (1995) gave fracture toughness values between 100 and 210 $KPa\ m^{1/2}$ with an average of 146 $KPa\ m^{1/2}$. More tests on synthetic ice by Litwin and others (2012) yielded results between 100 and

200 $KPa\ m^{1/2}$ with some lower values as melting temperature is approached. This result was consistent with other synthetic ice studies they reviewed. We will assess the importance of further constraining this parameter by analyzing shelf vulnerability with fracture toughness values of 100, 200, 300, and 400 $KPa\ m^{1/2}$. This is performed on the projections from exp05 and exp01 (standard and open basal melt parametrization for RCP8.5 forced by NorESM1-M) as all models participated in at least one of these two experiments. For all other analyses in this paper, we use 200 $KPa\ m^{1/2}$, which falls near the average of the glacial ice tests by Rist and others (1996). Given these samples came from boreholes into the Ronne ice shelf, we deem it appropriate to assign them extra weight.

Evaluation of Ice Vulnerability under the ISMIP6 Shelf Collapse Forcing

ISMIP6 included two experiments with an ice shelf collapse forcing (exp11 and exp12). The only difference between these experiments is that exp11 used open basal melt parametrizations while exp12 employed the standard medium parametrization. All models that participated in exp11 also participated in exp12; we only analyze the exp12 submissions. The collapse forcing was applied in all participating models based on the atmospheric forcing alone and did not consider stress-based ice shelf vulnerability.

Under the exp11 and exp12 forcing, the Larsen C, George VI, Wilkins, and Abbot ice shelves are predicted to see complete collapse by 2100. The Larsen C sees collapse near its ice forcing by 2025 and collapse of the remaining shelf between 2055 and 2065. The George VI sequence is similar with an early collapse of the Northern end and a 2055 to 2065 collapse of the rest. Most of the Wilkins shelf is predicted to collapse near the start of the experiment. The Abbot is predicted to see most of its collapse between 2075 and 2085 (Fig. 1).

We assess where the forced collapse was applied to vulnerable and non-vulnerable ice based on the crevasse-presence criterion from Lai and others (2020). In our postprocessing, we vary whether or not shelf vulnerability is evolved as well as the value of fracture toughness. These analyses help assess the importance of these factors in future paremetrizations of shelf collapse based on both melt and stress. We perform four versions of this analysis:

1. EVO100: Evolving vulnerability with fracture toughness of 100 $KPa\ m^{1/2}$
2. NON-EVO100: Non-evolving vulnerability with fracture toughness of 100 $KPa\ m^{1/2}$
3. EVO400: Evolving vulnerability with fracture toughness of 400 $KPa\ m^{1/2}$

4. NON-EVO400: Non-evolving vulnerability with fracture toughness of 400 $KPa\ m^{1/2}$

Collapse sequences with buttressing number

We will show several examples of collapse sequences as implemented in individual ice sheet models to understand how shelf collapse may or may not cause upstream shelf vulnerability. We will show both how shelf vulnerability and normal buttressing number change through time. Normal buttressing number calculations for ice shelves come from Fürst and others (2016). In Fürst and others (2016), normal buttressing number, K_n, is calculated as

$$K_n = 1 - \frac{\mathbf{n} \cdot \mathbf{R}\mathbf{n}}{N_0} \tag{14}$$

where $\mathbf{n}$ is a horizontal direction, $\mathbf{R}$ is the depth-averaged resistive stress tensor, and N_0 is the resistive stress stress that would exist if there were an ice cliff rather than continued shelf extent. This value is given by

$$N_0 = \frac{1}{2}\rho_i \left(1 - \frac{\rho_i}{\rho_{sw}}\right) gH. \tag{15}$$

Ideally, the stress used in our analysis would be the depth-averaged resistive stress as above. This calculation, however, would require the depth-averaged ice rigidity (or flow factor) or vertical temperature profiles to recalculate it. The ISMIP6 model outputs include only the surface and base temperatures. While we could attempt to estimate depth-averaged rigidity by assuming a temperature profile with these end points, we instead take the surface stress to avoid adding another variable. This unavoidable simplification means we cannot quantitatively link the buttressing factor of removed ice to upstream change in vulnerability. Despite this limitation, sequential plots of buttressing number as calculated with surface stress still aid in qualitative understanding of when shelf collapse may effect more vulnerability. Fürst and others (2016) considered both the maximum principal stress direction and flow direction for $\mathbf{n}$ and recommended the maximum principal stress direction. We follow this recommendation.

Shelf Selection

The ISMIP6 models have considerable differences in shelf extent that arise from their varying spinup methods (Seroussi and others, 2020). For smaller ice shelves, these differences are more pronounced and may override comparison of ice shelf vulnerability based on differences in stress evolution. For this reason, we use large shelves in our analyses. For sensitivity analyses (RCP, AOGCM, Basal Melt, Fracture Toughness), we consider the Ross, Filchner-Ronne, Amery, and Larsen C shelves. The ISMIP6 shelf collapse forcing

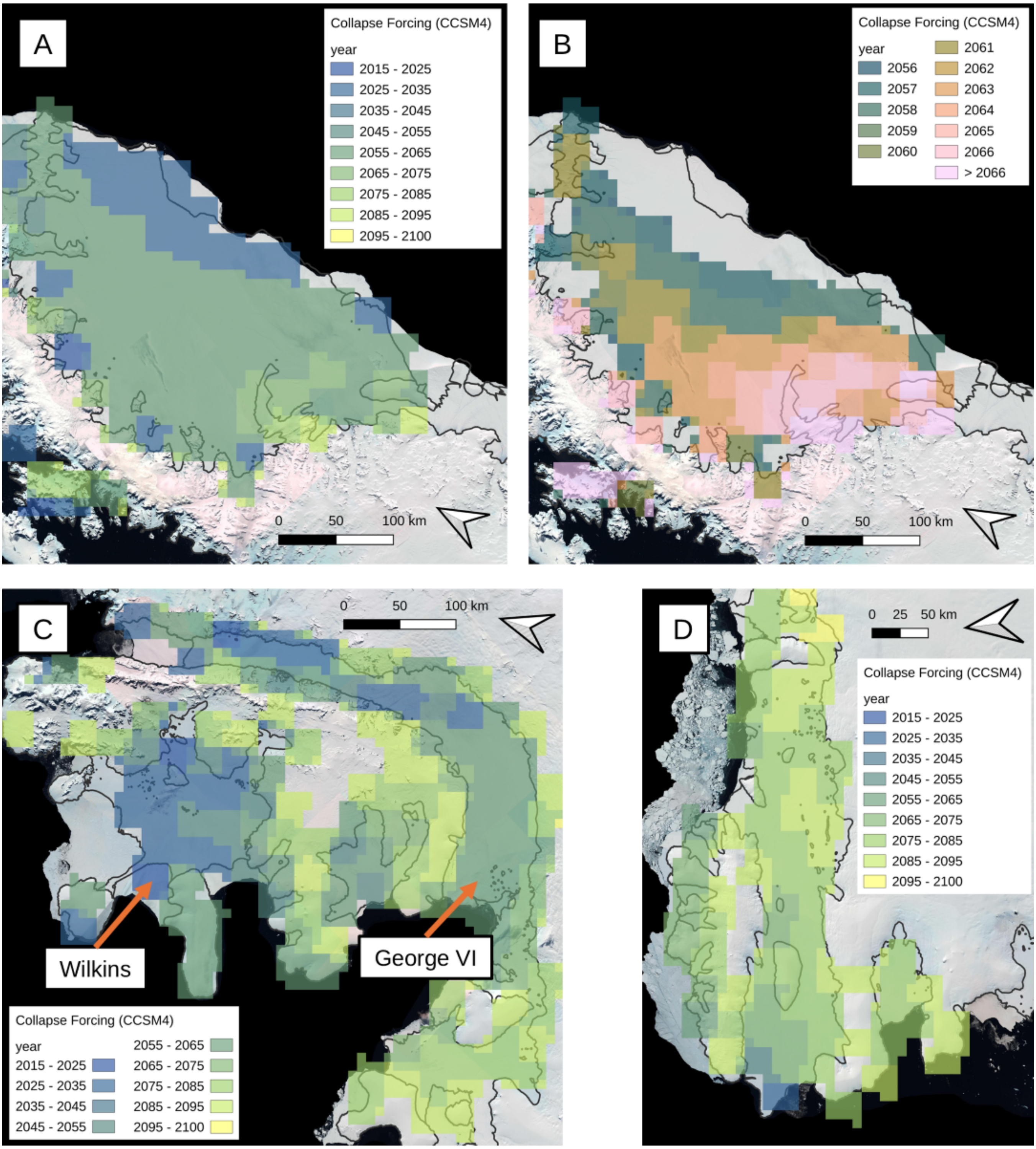

Fig. 1. ISMIP6 exp11 and exp12 collapse forcing dates for (A) the Larsen C between 2015 and 2100, (B) the Larsen C from 2056 to 2066, (C) the Wilkins and George VI shelves from 2015 to 2100, and (D) Abbot from 2015 to 2100. A, C, and D use 10-year intervals while B shows the per-year collapse forcing. The collapse forcing is plotted on the Landsat Image Mosaic of Antarctica (courtesy of the U.S. Geological Survey) and MEaSUREs grounding line and ice-sheet extent boundaries (Mouginot and others, 2017) included in the Quantarctica mapping environment (Matsuoka and others, 2021).

primarily impacted the Larsen C, George VI, Wilkins, and Abbott ice shelves. The Wilkins domains across models vary too significantly for comparison, so we analyze the other three shelves in evaluating the ice vulnerability under the ISMIP6 collapse mask.

RESULTS

Climate Scenario Sensitivity

Figure 2 shows the average vulnerable fraction of the Ross, Filchner-Ronne, Larsen C, and Amery ice shelves in 2014, 2050, 2075, and 2100 under RCP8.5 and RCP2.6 driven by the NorESM1-M climate model. The bars are the average fraction of total shelf area that is vulnerable from all the participating models and the error bars show the standard deviation of vulnerable fraction across the models. For each of these shelves, there is minimal change in vulnerable area through the end of the century under the RCP2.6 scenario. Under the RCP8.5 scenario, the Filchner-Ronne still has minimal change. The three other shelves, however, all see some reduction in vulnerable fraction by the end of the century. It is important to reiterate that this is with one climate model only.

The spatial pattern of model agreement on shelf vulnerability for the Ross shelf in 2014 and 2100 under RCP2.6 and RCP8.5 is shown in Figure 3. Color represents fraction of ice-sheet models that agree a given pixel is vulnerable. In the initial state as well as in 2100 under RCP2.6, nearly all models agree that the much of the ice front is vulnerable to hydrofracture. Under RCP8.5, however, three models see this region become non-vulnerable between 2075 and 2100. Many models have high vulnerability at the grounding line but lower vulnerability immediately downstream. This can be seen in Figure 3, but is partially hidden by the fact that the grounding line location varies per ice sheet model. Reviewing individual ice sheet model results, however, confirms this pattern. Individual results for each model can be found in a repository linked in the Data section. The majority of models become non-vulnerable near the grounding line by 2100 under RCP8.5 but not under RCP2.6. The horizontal lines come from a regridding artifact present for one of the model's postprocessed data.

Climate Model Sensitivity

Figure 4 shows the evolution in averaged shelf vulnerable fraction through time under RCP8.5 with three AOGCMs: NorESM1-M, MIROC-ESM-CHEM, and CCSM4. The Ross and Amery shelves see decreasing vulnerable fractions through 2100 with all AOGCMs. The Filchner-Ronne has a small but steady decrease in vulnerability under the CCSM4 forcing and negligible change under the NorESM1-M and MIROC-

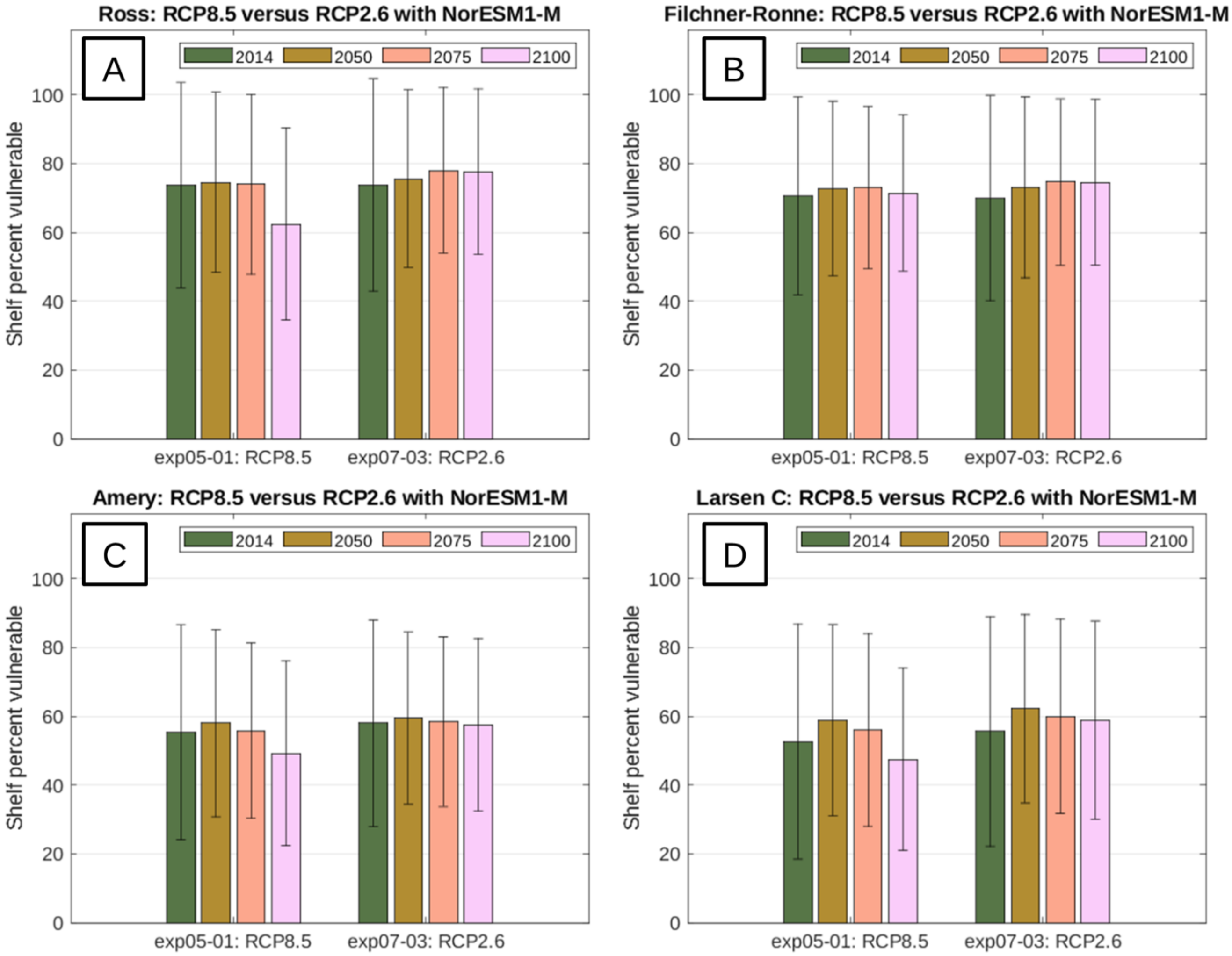

Fig. 2. Average shelf vulnerability fraction across ice sheet models in 2014, 2050, 2075, and 2100 for the (A) Ross, (B) Filchner-Ronne, (C) Larsen C, and (D) Amery shelves under RCP8.5 and RCP2.6. Reanalysis is of exp05 and exp01 for RCP8.5 and exp07 and exp03 for RCP2.6. All these experiments are forced by NorESM1-M. Exp05 and Exp07 use the standard basal melt parametrization while exp01 and exp03 use open basal melt parametrizations. The fracture toughness used in post processing was 200 $KPa\ m^{1/2}$. Error bars show +/- one standard deviation.

ESM-CHEM forcings. The Larsen C sees similar decreases in vulnerability under the forcings from the NorESM1-M and CCSM4 climate models but negligible change in vulnerability under the forcing from MIROC-ESM-CHEM.

Basal Melt Parametrization Sensitivity

ISMIP6 experiments included basal melt parametrizations tuned to the 5th, 50th, and 95th percentiles from shelves across Antarctica (low, medium, and high) as well as tuned to reproduced the high sensitivity to ocean warming observed at Pine Island (PIGL). Figure 5 shows the evolution in averaged shelf vulnerable

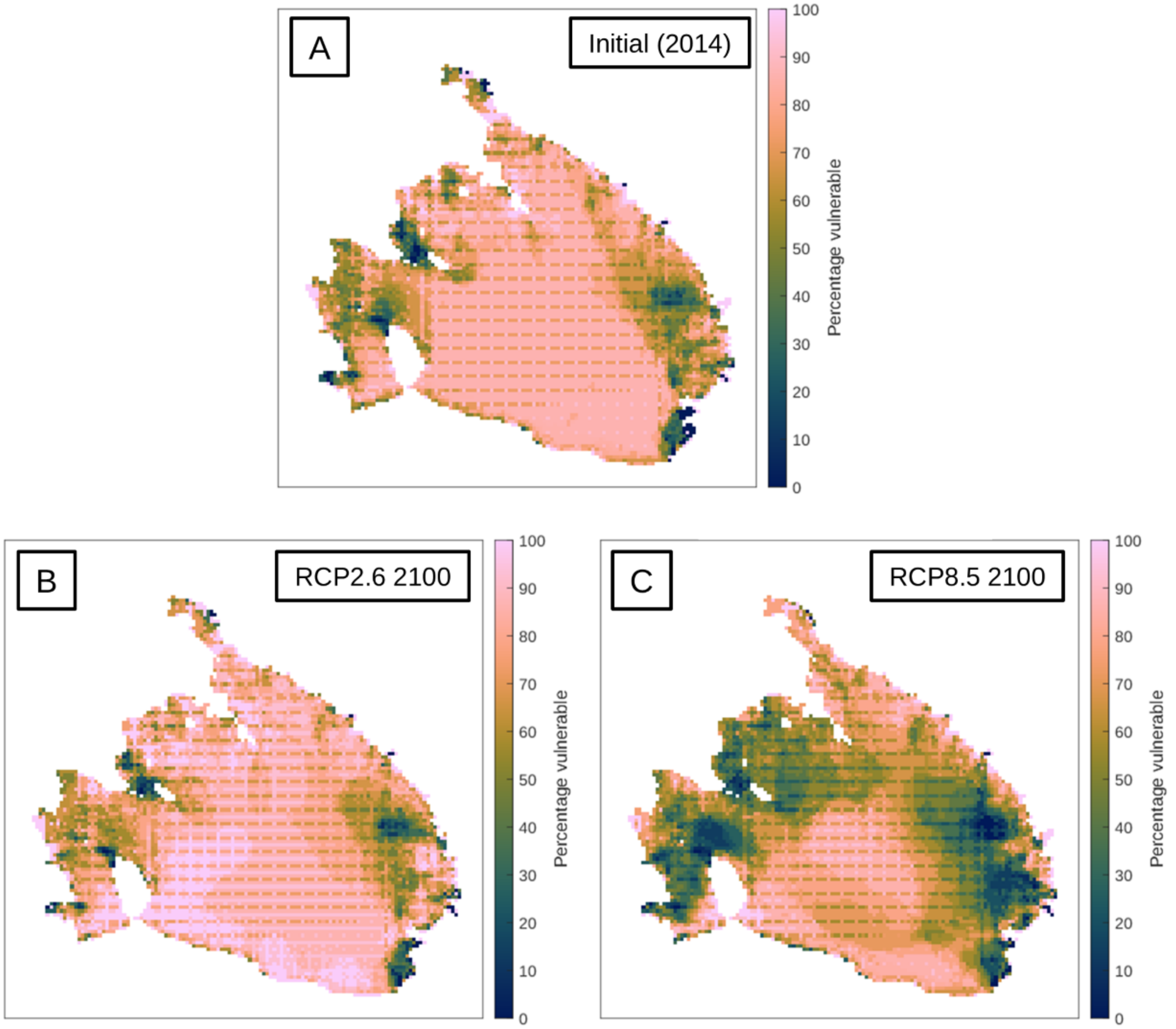

Fig. 3. Percentage of models that predict vulnerability for each grid point (A) after initialization in 2014, (B) in 2100 under RCP2.6 (exp07 and exp03), and (C) in 2100 under RCP8.5 (exp05 and exp01) using the NorESM1-M climate model.

fraction through time with these four basal melt parametrizations. For all shelves, an increase in basal melt rate corresponds to a faster decrease in shelf vulnerability. Under the low, medium, and high basal melt parametrizations, there is little change in vulnerability through 2075. For the Ross and Amery shelves, the PIGL melt parametrization causes the decrease in vulnerability to start by 2050. For the Filchner-Ronne, there is little decrease in shelf vulnerability for all parametrizations except the PIGL tuning. For the Larsen C, the PIGL tuning mainly adds to the decrease in vulnerability at the end of the century but has little effect through 2075. In general, there is little sensitivity to the change in basal melt rate caused by the low,

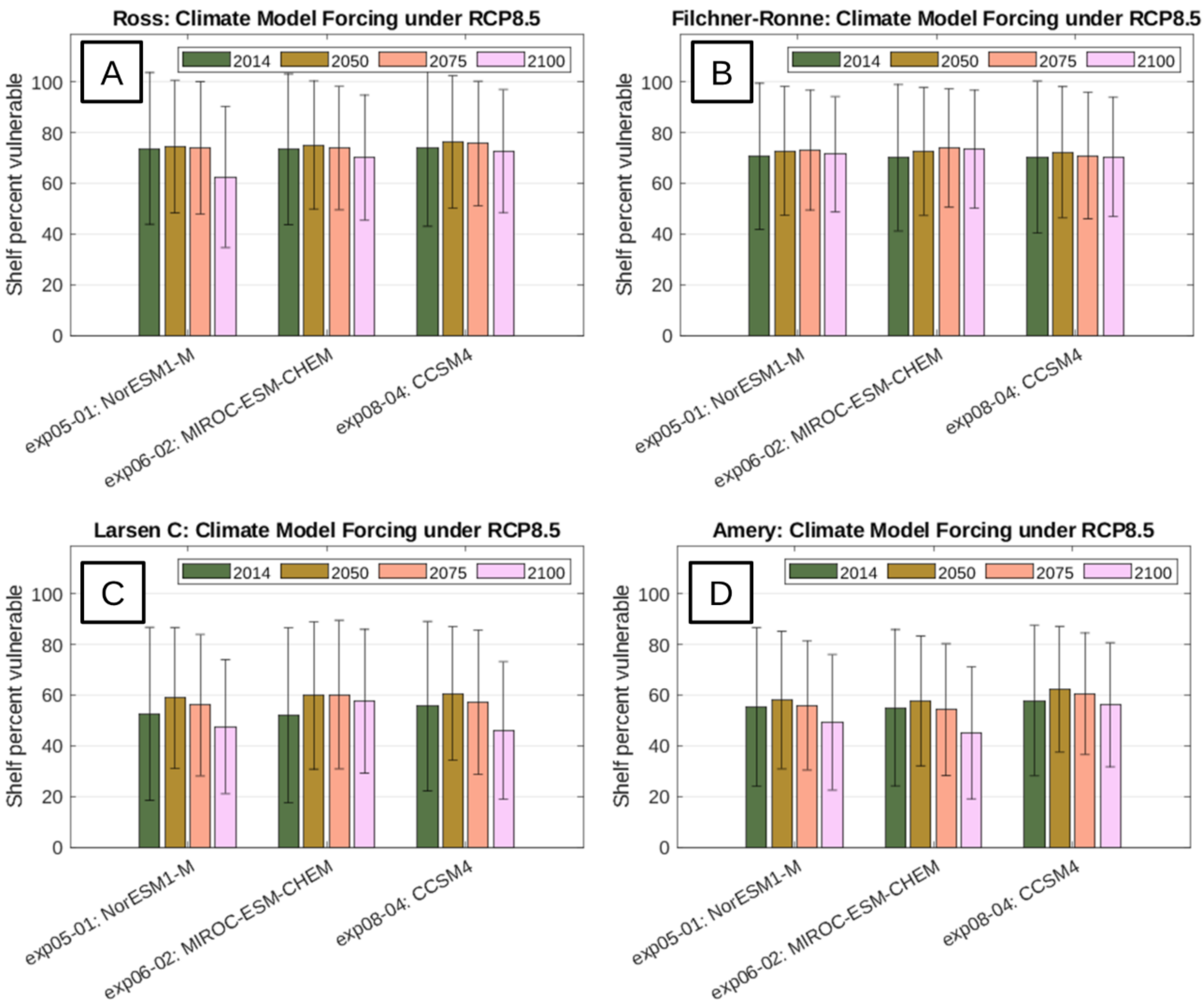

Fig. 4. Average shelf vulnerability fraction across ice sheet models in 2014, 2050, 2075, and 2100 for the (A) Ross, (B) Filchner-Ronne, (C) Larsen C, and (D) Amery shelves with three AOGCM forcings under RCP8.5. The fracture toughness used in post processing was 200 $KPa\ m^{1/2}$. Error bars show +/- one standard deviation.

medium, and high tunings while the PIGL tuning is enough to cause changes earlier in the century and to significantly reduce the vulnerability at the end of the century.

As with comparing climate scenarios, the change in predicted shelf vulnerability through time as a function of basal melt parametrization can also be seen from sequences of single-year plots of per-pixel ice-sheet model agreement of vulnerability. Figure 6 shows this result for the initial state (2014) as well as in 2100 with the standard medium and PIGL basal melt parametrizations for the Ross and Filchner-Ronne. Before considering change we note that the Filchner-Ronne, like the Ross, is predicted to be vulnerable in the center of flow near the front by most models and near the inlet glaciers by fewer models. At the Filchner-

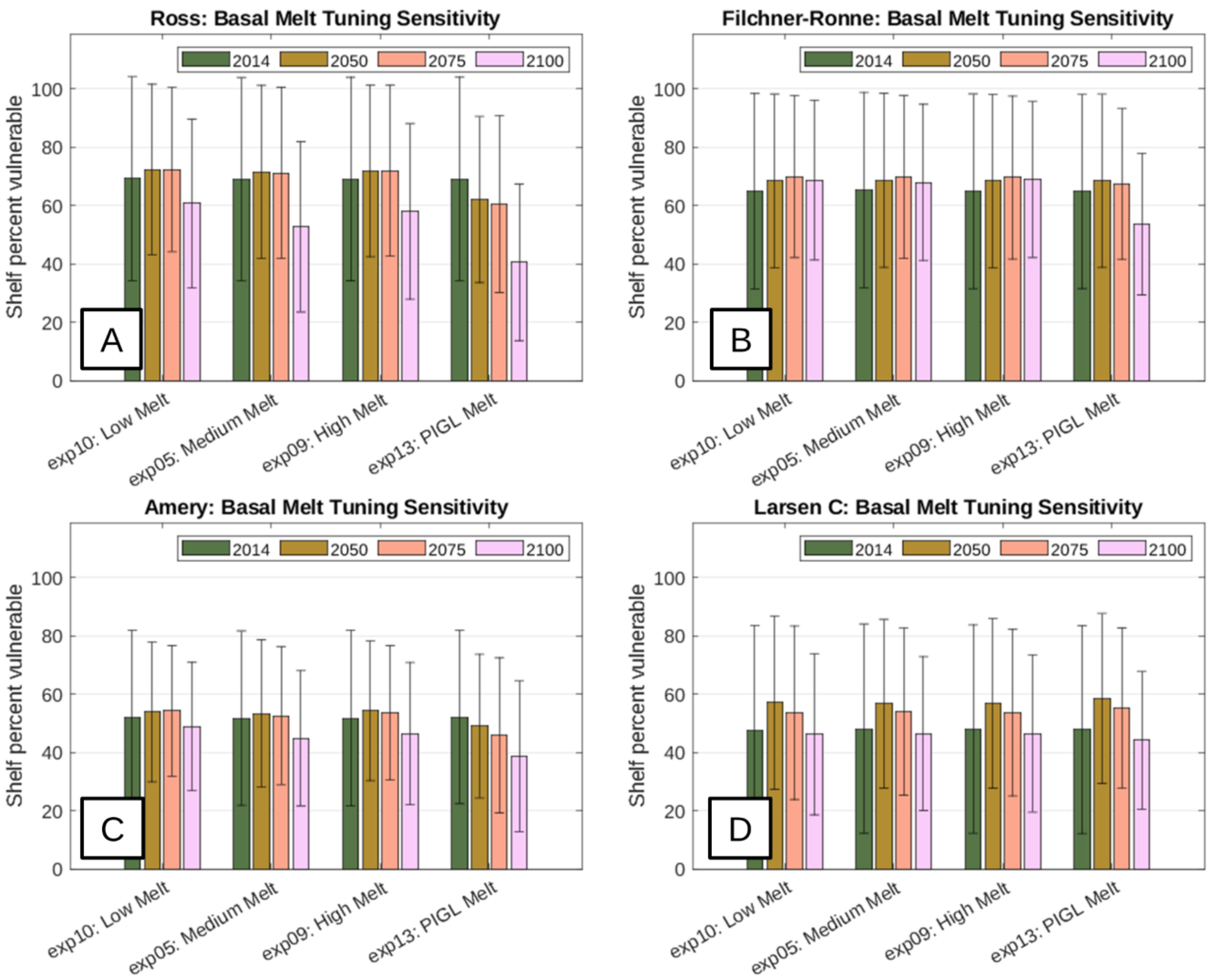

Fig. 5. Average shelf vulnerability fraction across ice sheet models in 2014, 2050, 2075, and 2100 for the (A) Ross, (B) Filchner-Ronne, (C) Larsen C, and (D) Amery shelves with four basal melt tunings. All experiments shown used NorESM1-M under the RCP8.5 scenario. The fracture toughness used in post processing was 200 $KPa\ m^{1/2}$. Error bars show +/- one standard deviation.

Ronne, it is also again the case that individual models report higher vulnerability near the grounding line than immediately downstream, but that this pattern is partially hidden by differences in grounding line positions between models. At the Ross under the PIGL melt parametrization, most models predict non-vulnerability in 2100 except for small regions at the front (Fig. 6e). While the Filchner-Ronne maintains more vulnerability under PIGL melt, this vulnerability is concentrated locally near the front with most models agreeing on non-vulnerability elsewhere (Fig. 6f).

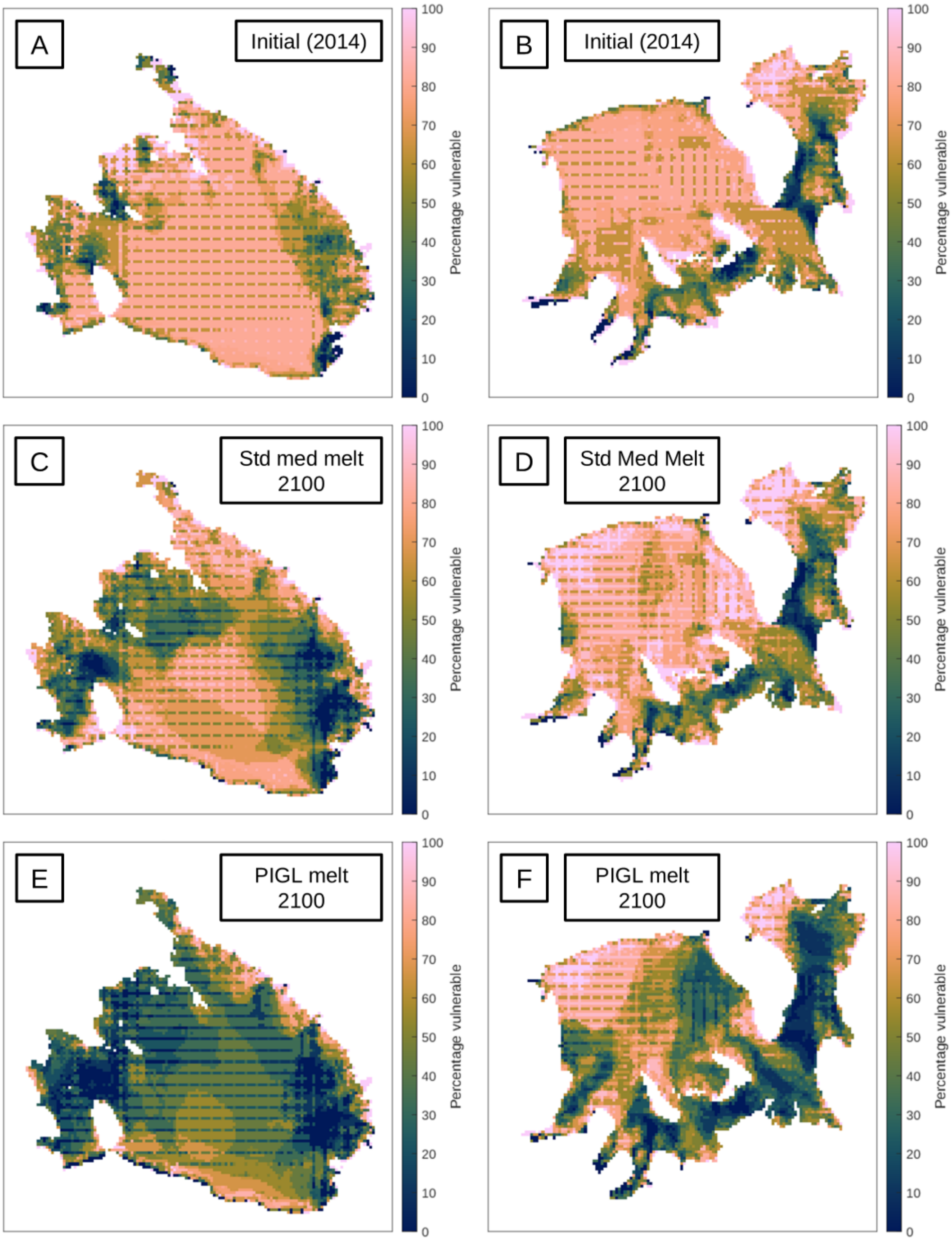

Fig. 6. Percentage of models predicting vulnerability for each grid point for the Ross in (A) the initial state, (C) 2100 with the standard basal melt parametrization, and (E) 2100 with the PIGL basal melt parametrization and the same for the Filchner-Ronne (B, D, and F).

Correlation with Thickness Change

As noted in the methods section, shelf thickness reduction would be expected to drive a decrease in stress and a corresponding reduction in shelf vulnerable area. Figure 7 shows the change in average resistive stress (across the shelf), average exceedance of the dimensionless resistive stress threshold, and shelf vulnerable fraction plotted against thickness change for each ice sheet model. Results come from all experiments used to study climate scenario, climate model, and basal melt parametrization sensitivity at the Ross and Larsen C ice shelves in 2100. Apart from two instances of the same ice sheet model that show an offset, a linear relationship between change in average thickness and in average resistive stress is apparent at the Ross (Fig. 7a). The same is true at the Larsen C (Fig. 7b), but with more noise relative to the change magnitude. The Ross sees higher thickness change predicted. At the Ross, going from resistive stress change to dimensionless resistive stress threshold exceedance change recasts the linear relationship into a curve. For the Larsen C, this change is obfuscated by the higher noise. Finally, change in shelf vulnerable area with average thickness change becomes much more scattered with small changes in thickness sometimes corresponding with large changes in shelf vulnerability for both ice shelves.

Fracture Toughness Sensitivity

By selecting one experiment and changing the value of ice's fracture toughness during post processing, we can assess the sensitivity of initial and evolving shelf vulnerability to fracture toughness. We selected exp05 and exp01 (NorESM1-M, RCP8.5) for their high participation and then varied fracture toughness between 100 and 400 $KPa\ m^{1/2}$ in increments of 100 $KPa\ m^{1/2}$. Figure 8 shows the average vulnerable area fraction from all ice sheet models through time with these fracture toughness values. At the Ross, Filchner-Ronne, and Amery shelves, the difference in initial vulnerability with the low and high end fracture toughnesses is 20% of the shelf area or less. The Larsen C is more sensitive to fracture toughness with a change in initial vulnerable fraction of roughly 40% of the shelf area. The ice-sheet-model-averaged vulnerable area itself is approximately halved in size. For all shelves, a fracture toughness of 100 $KPa\ m^{1/2}$ yields an increase in vulnerable fraction to 2050 and a 2100 vulnerable fraction that is identical or slightly higher than the 2014 value. This is reversed with a fracture toughness of 400 $KPa\ m^{1/2}$. At all shelves, the average vulnerable fraction decreases to 2050 and is lower in 2100 than in 2014. With 100 $KPa\ m^{1/2}$, there is also less variability between models in vulnerable shelf fraction. This is due to the saturation of vulnerable fraction to nearly 100%. Each of the higher fracture toughness values shifts the vulnerable fractions off of 100% but by varying amounts causing the higher variability.

To better understand the trends observed in the averaged plots, we next show the vulnerable and non-vulnerable (safe) areas for each model for the Ross and Larsen C shelves with fracture toughness values of 100 $KPa\ m^{1/2}$ and 400 $KPa\ m^{1/2}$. Figure 9 shows the shelf area that is vulnerable (lower bar) and not

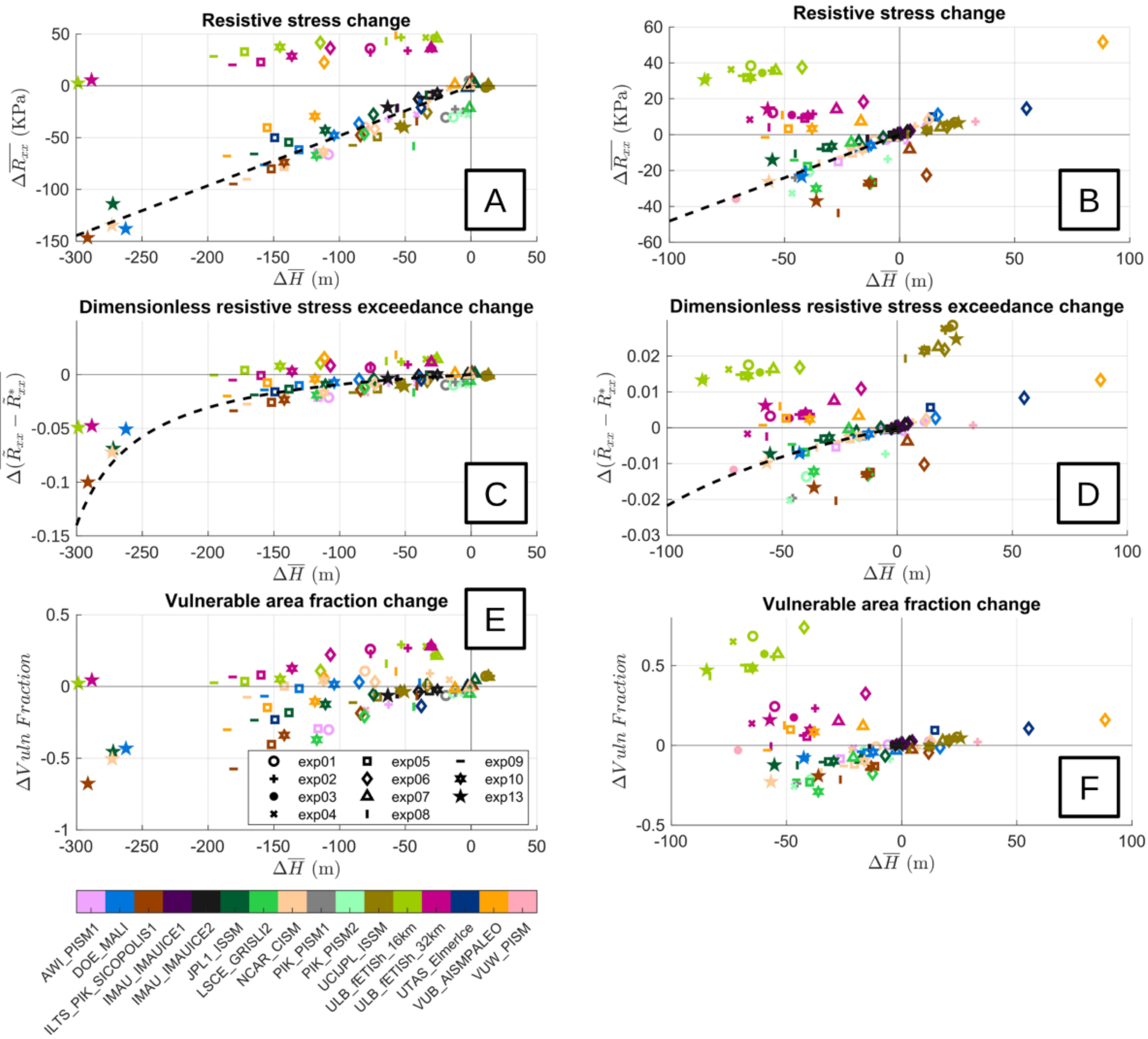

Fig. 7. Change in (A) resistive stress, (C) dimensionless resistive stress exceedance, and (E) shelf vulnerable fraction with thickness change for the Ross shelf and the same (B, D, F) for the Larsen C shelf. Marker shapes indicate experiments and marker colors indicate models. Dashed black lines indicate the theoretical predictions whose calculations are discussed in the Thickness Change Correlation part of the Methods section. The fracture toughness used in post processing was 200 $KPa\ m^{1/2}$.

vulnerable (upper bar) for each year and for each model for the Ross ice shelf analyzed with a fracture toughness of 100 $KPa\ m^{1/2}$. The combined bar height is the total shelf area. The observed bar on the right shows the result when the calculations are applied to the 2014-2017 MEaSUREs velocity product (Rignot and others, 2022) with surface temperature from Comiso (2000). The observed behavior that lower fracture toughness causes less change in vulnerable area through time can be seen for several models

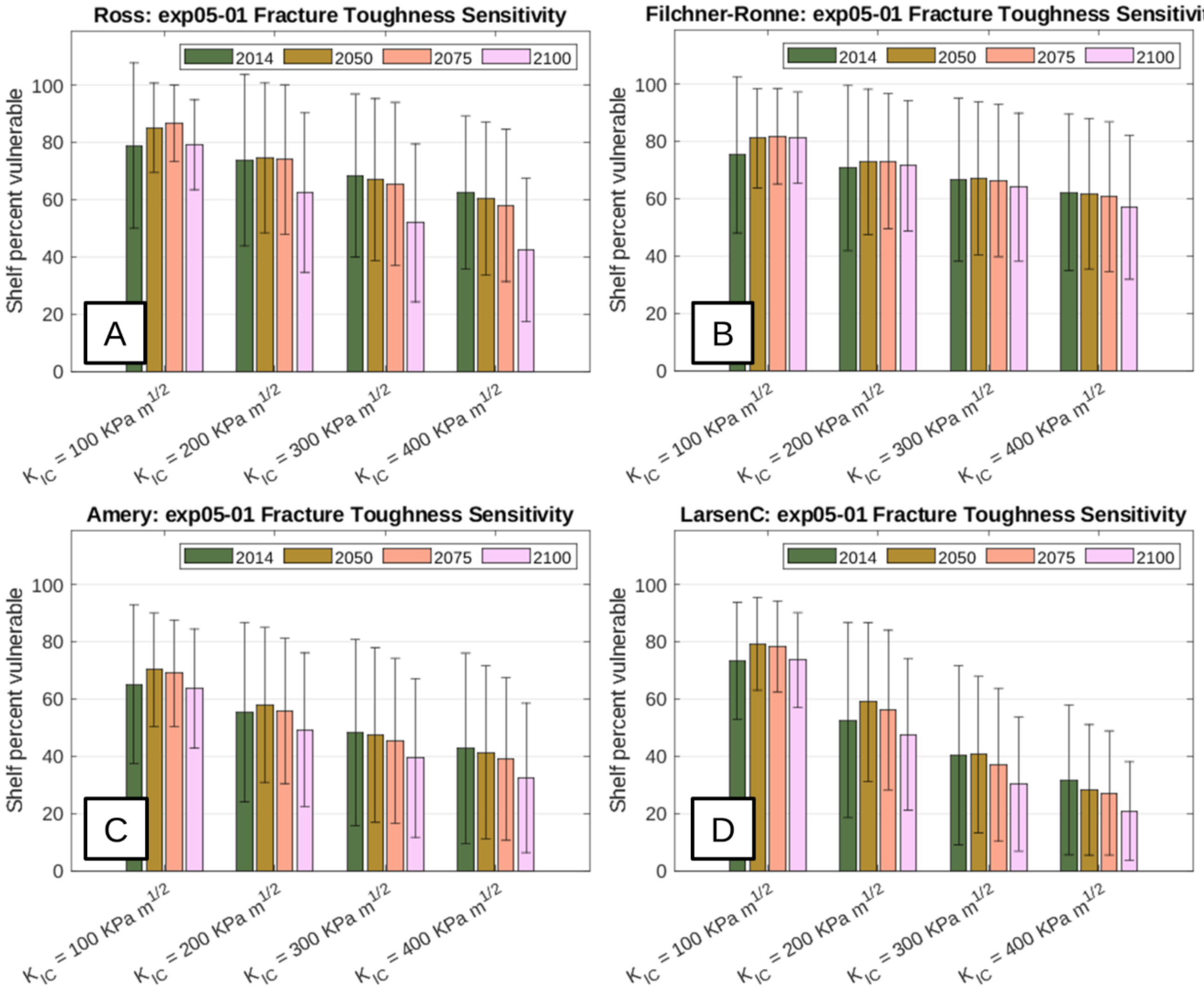

Fig. 8. Average shelf vulnerability fraction across ice sheet models in 2014, 2050, 2075, and 2100 for the (A) Ross, (B) Filchner-Ronne, (C) Larsen C, and (D) Amery shelves with fracture toughness values of 100, 200, 300, and 400 $KPa\, m^{1/2}$. Exp05 and exp01 results were analyzed, which are driven by a NorESM1-M RCP8.5 forcing with standard medium (exp05) or open (exp01) melt parametrizations. Error bars show +/- one standard deviation.

(AWI_PISM1, ILTS_PIK_SICOPOLIS, JPL1_ISSM, LSCE_GRISLI2, NCAR_CISM). Figure 10 shows the vulnerable and non-vulnerable shelf areas for the Larsen C. While two models (ULB fETISH 16km and 32km) have complete losses of vulnerable area with the higher fracture toughness, all models have major decreases contributing to the high sensitivity observed for the Larsen C. The same behavior of higher fracture toughness causing a larger change through time in individual models can be observed. For both shelves, the low change in vulnerability through time with low values of fracture toughness is caused at least in part by saturation: the stress threshold is exceeded by a large margin across most of the shelf so a decrease in stress will not cause much ice to move across the threshold.

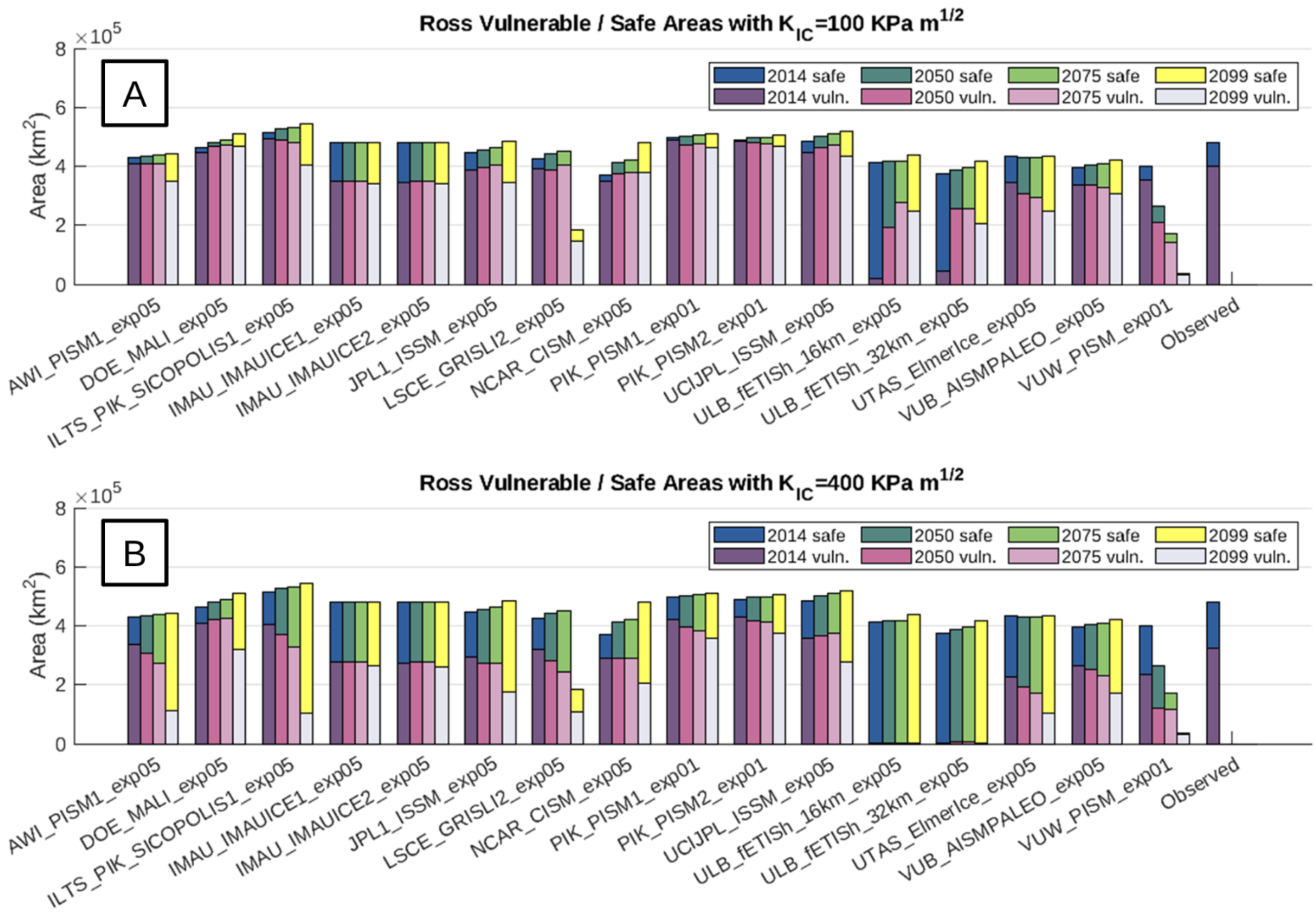

Fig. 9. Per model vulnerable and safe shelf area evolution through time for the Ross ice shelf with fracture toughness values of (A) 100 $KPa\, m^{1/2}$ and (B) 400 $KPa\, m^{1/2}$. Reanalysis is of exp05 and exp01 which are forced by NorESM1-M under an RCP8.5 scenario with standard medium and open basal melt parametrizations respectively. The "observed" bar on the right side comes from applying the same vulnerability calculations directly to the MEaSUREs 2014-2017 velocity mosaic (Rignot and others, 2022) with surface temperature from Comiso (2000).

Evaluation of Ice Vulnerability under the ISMIP6 Shelf Collapse Forcing

ISMIP6 included a collapse forcing based on meltwater availability in exp11 and exp12. Both experiments used the CCSM4 climate model under the RCP8.5 scenario but with open basal melt parametrizations in exp11 and the standard medium parametrization in exp12. For the Larsen C, George VI, and Abbot ice shelves, we analyzed the fraction of collapsed area that was predicted to be vulnerable in exp12. Figure 1 showed the collapse forcing years for these shelves. The average percentage of the collapsed shelf area that was predicted to be vulnerable at the time of collapse with and without evolving vulnerability and with fracture toughness values of 100 $KPa\, m^{1/2}$ and 400 $KPa\, m^{1/2}$ is given as Figure 11. For the Larsen C, The use of evolving vulnerability appears to have little effect with both ensembles using 100 $KPa\, m^{1/2}$ having

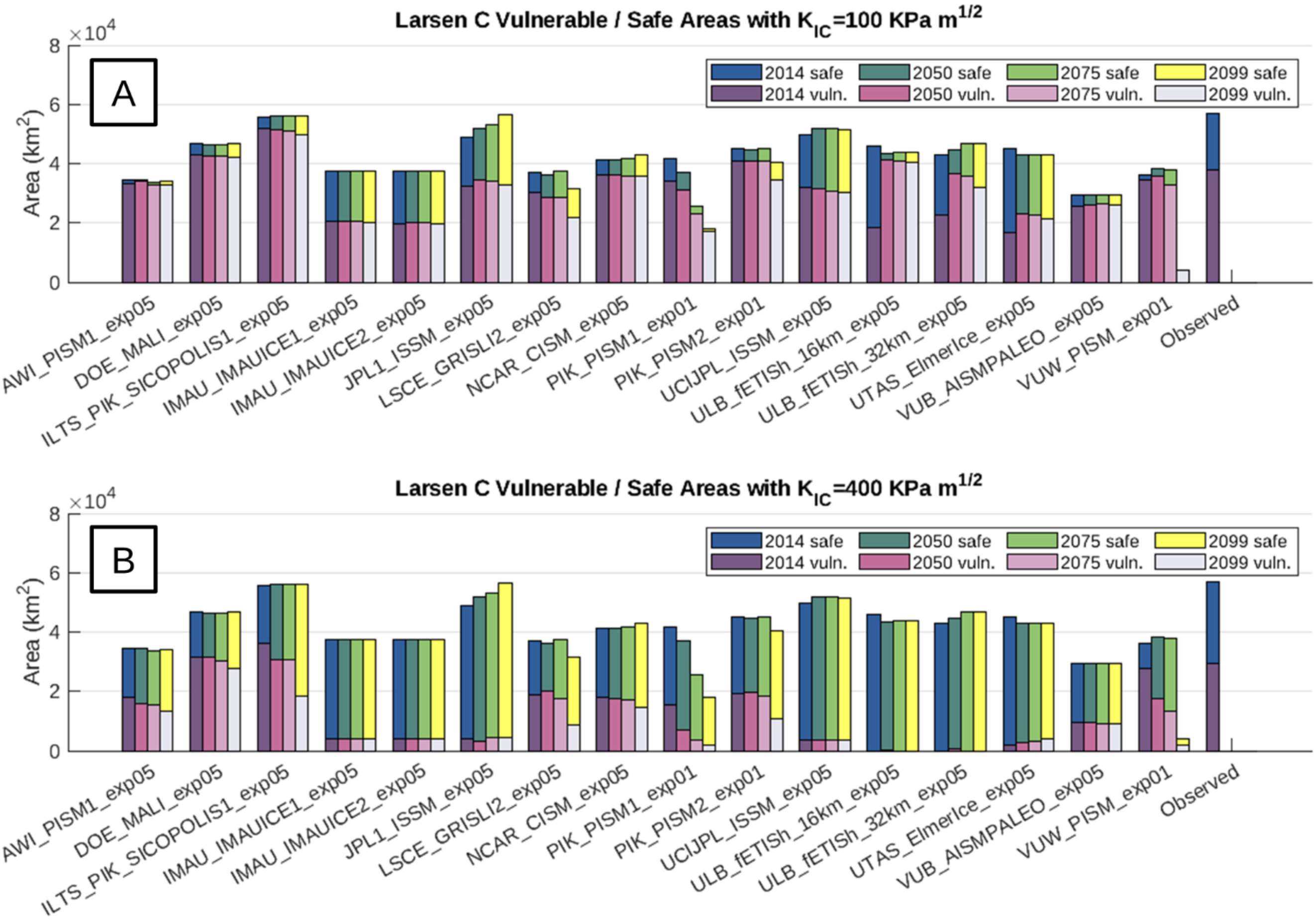

Fig. 10. Per model vulnerable and safe shelf area evolution through time for the Larsen C ice shelf with fracture toughness values of (A) 100 $KPa\ m^{1/2}$ and (B) 400 $KPa\ m^{1/2}$. Reanalysis is of exp05 and exp01 which are forced by NorESM1-M under an RCP8.5 scenario with standard medium and open basal melt parametrizations respectively. The "observed" bar on the right side comes from applying the same vulnerability calculations directly to the MEaSUREs 2014-2017 velocity mosaic (Rignot and others, 2022) with surface temperature from Comiso (2000).

around 65% vulnerability and both ensembles using 400 $KPa\ m^{1/2}$ averaging around 28% vulnerability. The George VI and Abbot shelves, however, are more affected by evolving vulnerability with increases in vulnerable fraction corresponding to the use of evolving shelf vulnerability. Whether the majority of collapse was vulnerable at the Larsen C varies with fracture toughness. At the George VI and Abbot however, no more than 40% of collapsed area was vulnerable for any of the analyses. While evolving vulnerability does not appear to make a major difference to the Larsen C results, looking at individual ice sheet model results shows that there is an impact that happens to cancel out on average.

Figure 12 panels A and B show the areas of collapse that were forced and vulnerable, forced and not vulnerable, and not forced for each model with and without evolving vulnerability and a fracture toughness

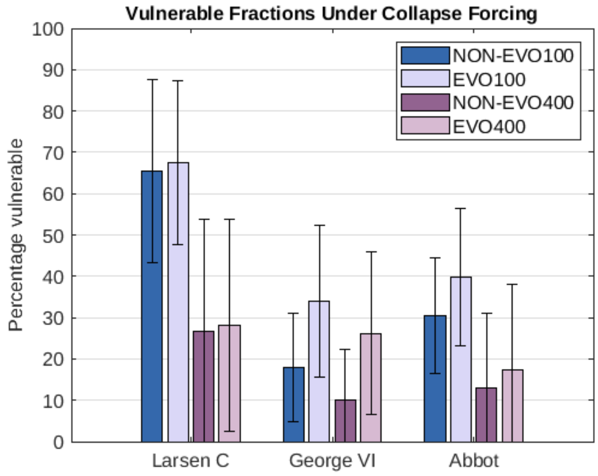

Fig. 11. Mean fraction of shelf collapse in 2100 (exp12) that was vulnerable for the NON-EVO100 (fracture toughness of 100 $KPa\ m^{1/2}$ without evolving vulnerability), EVO100 (fracture toughness of 100 $KPa\ m^{1/2}$ with evolving vulnerability), NON-EVO400 (fracture toughness of 400 $KPa\ m^{1/2}$ without evolving vulnerability), and EVO400 (fracture toughness of 400 $KPa\ m^{1/2}$ with evolving vulnerability) analyses for the Larsen C, George VI, and Abbot ice shelves. Error bars show +/- one standard deviation of the ice sheet-model-ensemble.

of 100 $KPa\ m^{1/2}$ for the Larsen C. The unforced collapse may be because of a shelf extent beyond the modern day extent for the which the forcing was applied. Five models saw an increase in collapse of non-vulnerable shelf area; two models had increased collapse areas predicted to be vulnerable, and two models had little change. Even for the models with little change, the spatial patterns of vulnerable and non-vulnerable collapsed area were significantly different but balanced each other out. This can be seen for the JPL1_ISSM model in Figure 12 panels C and D. Evolving vulnerability caused a reduction in vulnerable area at the front but an increase upstream where collapse of buttressing ice add stress.

Note that, for models that included calving, shelf retreat due to calving may be misclassified as being due to the collapse forcing. Of the models that participated in exp12, this includes AWI_PISM, ILTS_PIK_SICOPOLIS, and LSCE_GRISLI2. Systematically identifying calving retreat versus collapse forcing retreat was difficult as the timing of collapse forcing retreat varies across models. Manual review of retreat shows shows that ILTS_PIK_SICOPOLIS is minimally affected while AWI_PISM and LSCE_GRISLI2 have calving retreat that is mostly categorized as vulnerable collapsed area. The calving retreat generally only slightly outruns the collapse forcing, because the collapse forcing is applied in short, rapid bursts.

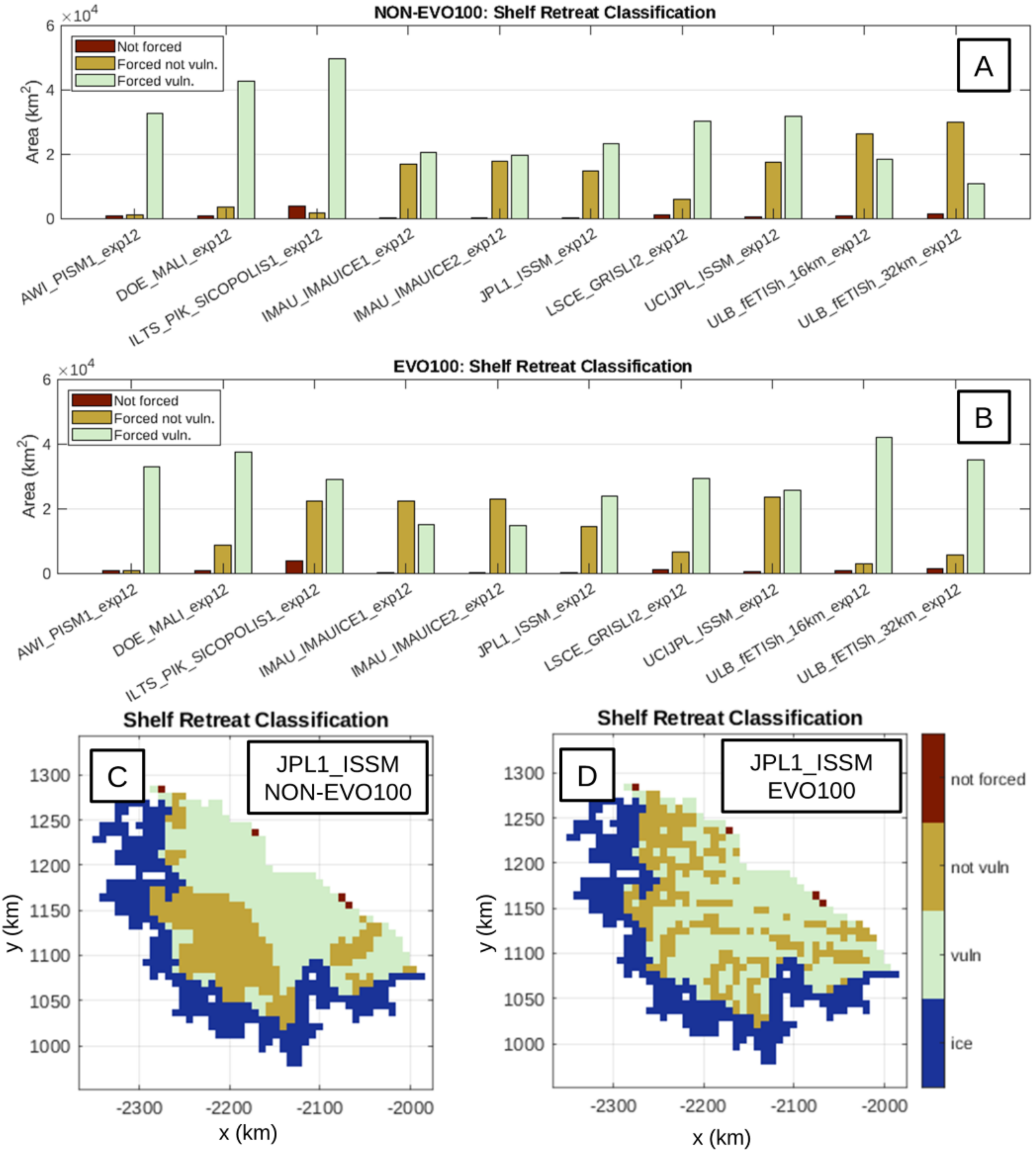

Fig. 12. Forced collapse area that was vulnerable, forced collapse area that was not vulnerable, and non-forced collapse area for the Larsen C ice shelf (A) without evolving vulnerability and (B) with evolving vulnerability and classification in 2100 for the JPL1_ISSM ice sheet model with the (C) NON-EVO100 and (D) EVO100 analyses.

Evaluation of Collapse-Shelf-Vulnerability Feedback

To better understand how collapse forcing can influence upstream vulnerability, we next consider several examples of individual models responding to multi-year collapse sequences. We plot the shelf vulnerability alongside the buttressing number to show how the safety band idea of Fürst and others (2016) applies to vulnerability feedback. Figure 13 shows this for the DOE MALI submission in 2025 to 2027 from the EVO400 analysis. A major portion (roughly 10,000 km^2 or 15% of the shelf) of the front of the Larsen C shelf is removed under the collapse forcing. This collapsed region, however, has a buttressing number under approximately 0.2 and there is little upstream change in shelf vulnerability accordingly. Later in 2059 through 2061 (Fig. 14), a corner of the shelf is removed by the forcing that has higher buttressing (around 0.6 and up) is collapsed. This causes the adjacent region of the shelf to go from non vulnerable to vulnerable in 2060 such that collapse forcing in 2061 now affects vulnerable ice.

A more pronounced example of the importance of evolving shelf vulnerability is shown in Figure 15 for the UCIJPL_ISSM submission in the EVO100 analysis. Shelf area removed by the collapse forcing in 2055 to 2057 causes a major region (roughly 3000 km^2) to become vulnerable. That region subsequently collapses between 2060 and 2064. Therefore, if an evolving stress-based criterion were included for collapse determination, this region would collapse despite not being initially vulnerable.

DISCUSSION

A Negative Basal Melt Feedback?

At first glance, the process of increasing basal melt causing thinning which reduces stress and thus shelf vulnerability to hydrofracture would constitute a negative feedback. Correlation plots of stress change versus thickness change of the Ross showed that large thickness decrease overwhelms other factors and drives stress decrease (Fig. 7) . While buttressing reduces with thinning, the risk of a complete loss of buttressing through shelf collapse goes down. At least three neglected factors complicate determining whether this negative feedback really is present. First, local regions of elevated basal melt (particularly basal channels in shear margins) could counter this stress reduction. Basal melt channels with increased melt rate may preferentially develop in shear margins due to several proposed causes (Alley and others, 2019). In shear margins, stress is not driven by the thickness of the ice itself, but by the speed difference between merging bodies of ice. Because of this, as shear margin thickness goes down, shear margin stress may increase as there is less thickness to carry an externally driven load. This can lead to mechanical damage in shear margins further weakening them (e.g. Lhermitte and others, 2020). Additionally, thinning shear margins may then provide less resistance to the ice in the center of flow increasing stress there as well. The calving retreat of Pine Island has been attributed to this by some studies (Alley and others, 2019;

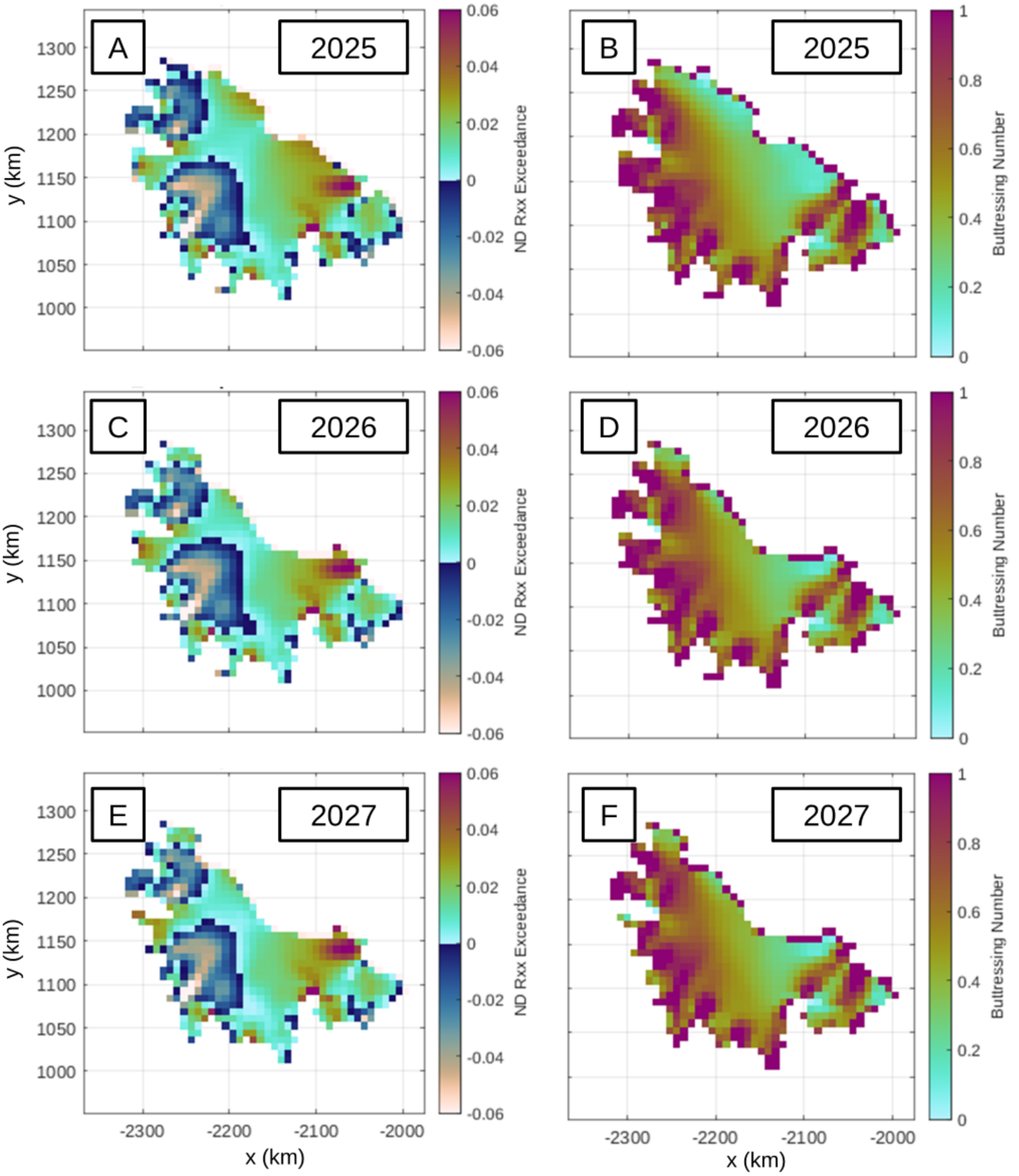

Fig. 13. Exceedance of dimensionless resistive stress threshold (A, C, E) and buttressing number (B, D, F) in 2025 to 2027 for the Larsen C shelf with the DOE_MALI ISMIP6 submission in the EVO100 analysis.

Lhermitte and others, 2020), but upstream surface crevassing has also been observed to have increased (Surawy-Stepney and others, 2023) potentially indicating hydrofracture vulnerability increase. It is worth

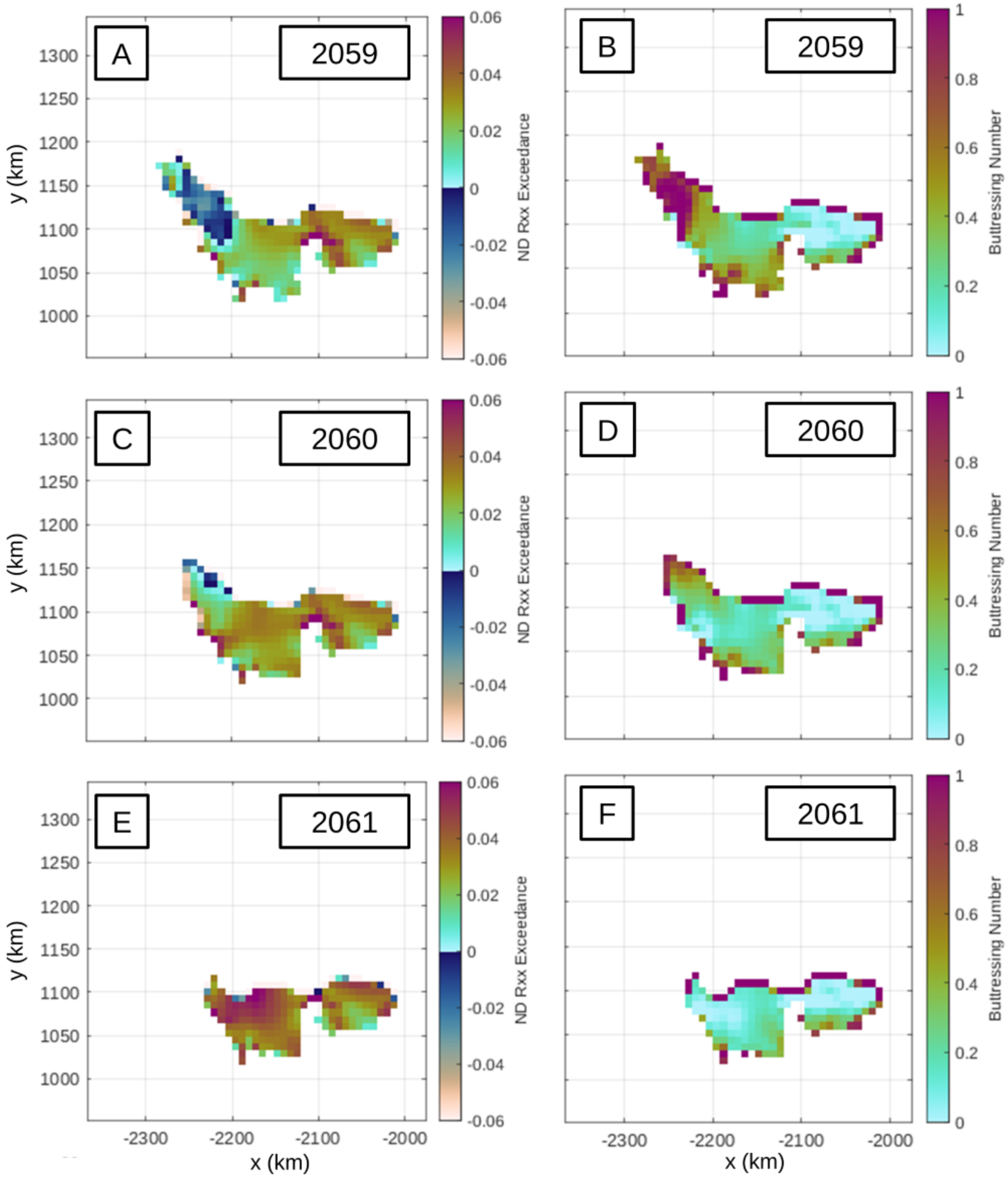

Fig. 14. Exceedance of dimensionless resistive stress threshold (A, C, E) and buttressing number (B, D, F) in 2059 to 2061 for the Larsen C shelf with the DOE_MALI ISMIP6 submission in the EVO100 analysis.

455 noting that this will be more complex at larger shelves with less developed shear zones than those of the
456 Pine Island Glacier shelf.

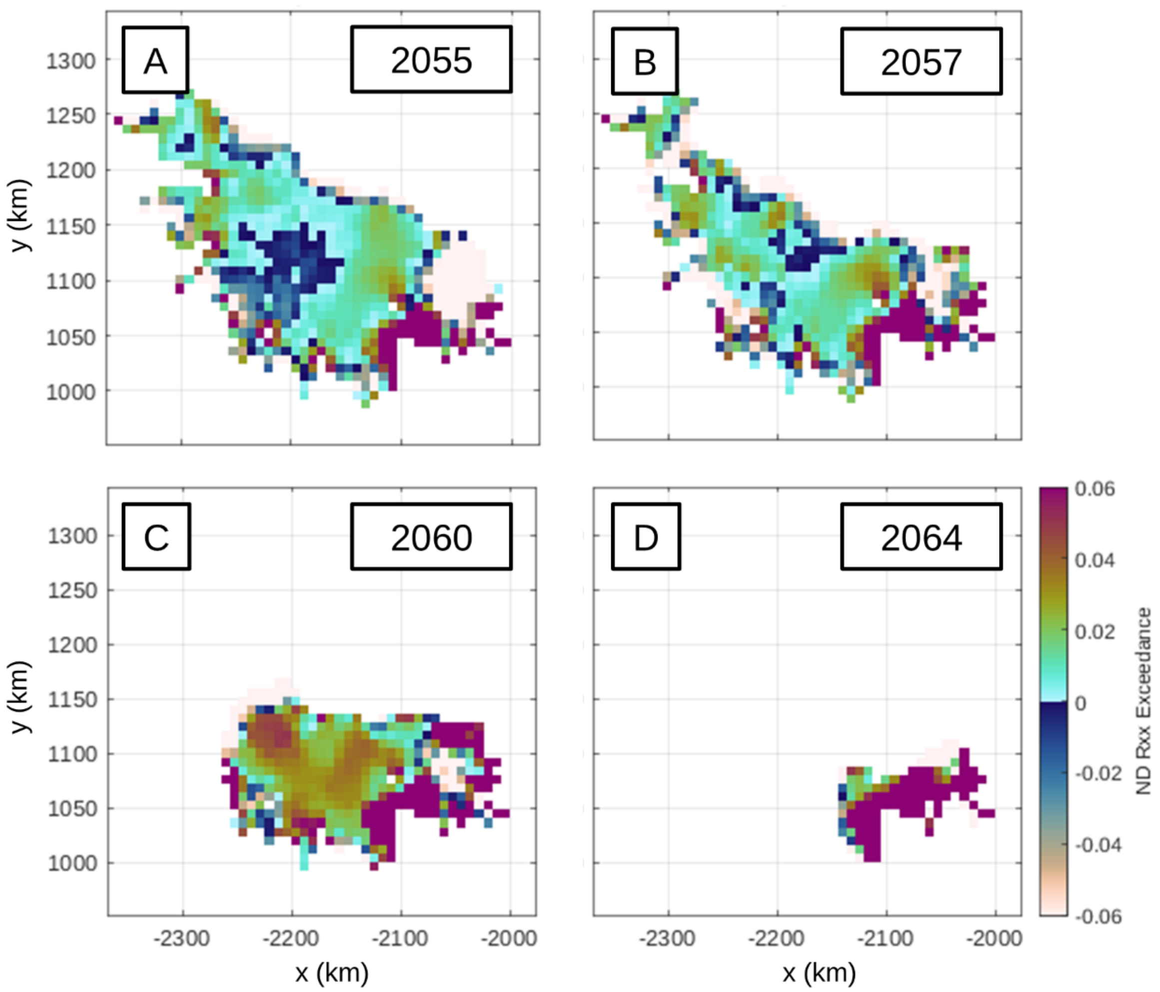

Fig. 15. Exceedance of dimensionless resistive stress threshold in (A) 2055, (B) 2057, (C) 2060, and (D) 2064 for the Larsen C shelf with the UCIJPL_ISSM ISMIP6 submission in the EVO100 analysis.

The second potential factor that could void this negative feedback is the presence of relict crevasses. When the stress drops beneath the threshold, any previously created crevasses remain and, when a crevasse is already present, less stress is needed to prevent closure because of the crevasse's stress intensity factor effects. Therefore, analysis of crevasse removal via ablation and healing is necessary to assess whether the stress reduction shown yields a significant reduction in crevassed area. The third potential factor is increasing stress from short-term environmental drivers like ocean swells. As thickness decreases, swells cause higher stress countering some the stress reduction from gravity-driven flow as discussed in Bassis and others (2024). Finally, the buttressing provided by a shelf goes down with thickness as well. So, whether the amount of thickness decrease that reduces vulnerability to where collapse does not occur is enough thinning that the shelf is largely passive is also an open question.

Shelf Vulnerability Sensitivities

Except where calving changes ice shelf flow patterns, evolution in shelf vulnerability mostly equates to evolution in shelf thickness (Fig. 7). Accordingly, basal melt parametrization is the strongest control of future shelf vulnerability. This comes with the caveat that, in the ISMIP6 protocol, experiments changing basal melt parametrizations were applied with the RCP8.5 climate scenario and, for the Ross, the climate model used projected the most local ocean warming of the three considered (Fig. 4). Lower amounts of ocean warming under more mild climate scenarios or more favorable climate models could prevent basal melt parametrization from being a major driver of shelf vulnerability decrease. In general, the differences between models' initial vulnerability is larger than the evolution in vulnerability that occurs except when the high ends of climate forcing, climate model, and basal melt parametrization stack. For some shelves (the Larsen C and the Amery), the same is true of fracture toughness in the range of 100 to 400 $KPa\ m^{1/2}$ while other shelves are less sensitive to fracture toughness (the Ross and Filchner-Ronne). This suggests that improving model initialization to better match modern stress states and further constraining ice shelf fracture toughness are the highest return efforts for improving predictions of ice shelf vulnerability. This is particularly true if the PIGL melt parametrization, which did cause significant change in vulnerability for some shelves, is confirmed to be overly sensitive for the future melt response of other ice shelves.

ISMIP6 Shelf Collapse Forcing

Under the ISMIP6 collapse forcing, even with the low-end fracture toughness of 100 $KPa\ m^{1/2}$, five of 11 ice sheet models had collapse forcing applications where more than one third of the collapsed area was not vulnerable (Fig. 12). Given the other shelves have fairly similar predicted vulnerable area fractions (all are within 60% to 80% for 100 $KPa\ m^{1/2}$, Fig. 8), this finding would likely apply if the large shelves see significant surface melt after 2100. And if fracture toughness is higher, this becomes even more prevalent. This suggests that the inclusion of a stress criterion will prevent collapse of some shelves in some models with a strong fracture-toughness influence. The importance of shelf collapse to sea-level rise as demonstrated by ABUMIP (Sun and others, 2020) and by comparisons in ISMIP6 2300 (Seroussi and others, 2024) of Antarctic contribution with and without collapse makes refining collapse parametrization and fracture toughness estimates critical. That the parametrization presented in Lai and others (2020) with a range of realistic fracture toughness values can create such a range of vulnerability ice-sheet models indicates that sensitivity to parametrization updates will be major.

Collapse-Shelf-Vulnerability Feedback

At the Larsen C, the lack of major change in the mean or standard deviation of the fraction of forced collapse that was vulnerable when evolving vulnerability is used was unexpected. This finding was ultimately explained through the changes across ice sheet models, and even changes within an individual ice sheet model, balancing out. The evolution of ice shelf vulnerability is always significant in arranging which regions are vulnerable, but with wide-ranging bulk effects. The averaged vulnerable fractions of collapsed ice at the George VI and Abbot ice shelves were strongly dependant on whether evolving stress was considered.

The first takeaway, then, is simply that it is important to include shelf vulnerability evolution in future parametrizations of shelf collapse. An important consideration will be the minimum collapse area of overlapping shelf vulnerability and surface melt. When evolving vulnerability is used, the vulnerability is patchy for many models. This means that there would be individual or small groups of grids or elements upstream that could be collapsed which would like cause downstream ice to become vulnerable. But if larger overlap areas are required, collapse vulnerability feedback may be prevented. Collapse process models are needed to understand if there is an area requirement of overlapping melt availability and surface crevasses. If collapse is allowed to be per grid point or element, model resolution may artificially control the outcome.

CONCLUSION

We applied the ice shelf vulnerability criterion from Lai et al. (2020) to the results of the ISMIP6 ice sheet model ensemble. We found that ice shelf vulnerability decreases mostly correlated with ice shelf thinning. This suggests a negative feedback where ocean warming improves shelf stability, but the impact of relict crevasses, stress effects of more regional melting, and stress from short-term environmental sources need further study. Except for cases where sensitive melt parametrizations (PIGL) complement high-emissions climate scenarios (RCP8.5), shelf vulnerability evolution is a smaller factor than initial differences between ice sheet models and the effects of fracture toughness uncertainty in determining end-of century shelf vulnerability.

Because the ISMIP6 shelf collapse forcing was based on surface melt alone, the inclusion of the stress criterion was certain to find that collapse was overprescribed. For the George VI and Abbot shelves, the average vulnerable fraction of collapsed ice was no more than 40% with any selection of vulnerability evolution and fracture toughness. At the Larsen C, vulnerable fraction ranged from approximately 65% to 40% depending primarily on fracture toughness. With low-end fracture toughness (100 $KPa\ m^{1/2}$), three of 10 models had vulnerability predicted for one half or less of collapsed ice at the Larsen C. With high-end fracture toughness (400 $KPa\ m^{1/2}$), seven of 10 models had less than one half vulnerability. So the timing and extent of collapse, per this parametrization of collapse vulnerability, is likely to have been later and less than was applied in the ISMIP6 collapse experiment for many models. Evolving stress state changed the vulnerable and non-vulnerable regions impacted by the collapse forcing but not in a consistent manner. Major feedbacks of collapse causing increased upstream vulnerability were observed. This result highlights the importance of understanding whether collapse requires a certain area threshold of overlapping vulnerability and melt, as collapse of small regions can cause more vulnerability allowing for subsequent collapse.

In order to understand whether Antarctica's largest shelves may collapse, which would unleash higher long-term sea-level rise (Sun and others, 2020), we must analyze a longer time period. Future work will assess shelf vulnerability evolution in the extended, 2300 ISMIP6 ensemble (Seroussi and others, 2024) with the same analyses. In the 2300 simulations with some climate forcings, melt is predicted on the major shelves (Ross and Filchner-Ronne) and a collapse forcing was applied. The major amount of ice being held back by these shelves means whether they ultimately collapse will have major implications for the trajectory of Antarctic sea-level rise contribution in multi-century timescales.

ACKNOWLEDGMENTS

First, this research was dependent on the availability of the ISMIP6 ensemble results. Accordingly, we thank the Climate and Cryosphere (CliC) effort, which provided support for ISMIP6 through sponsoring of workshops, hosting the ISMIP6 website and wiki, and promoted ISMIP6. We acknowledge the World Climate Research Programme, which, through its Working Group on Coupled Modelling, coordinated and promoted CMIP5 and CMIP6. We thank the climate modeling groups for producing and making available their model output, the Earth System Grid Federation (ESGF) for archiving the CMIP data and providing access, the University at Buffalo for ISMIP6 data distribution and upload, and the multiple funding agencies who support CMIP5 and CMIP6 and ESGF. We thank the ISMIP6 steering committee, the ISMIP6 model selection group and ISMIP6 dataset preparation group for their continuous engagement in defining ISMIP6. Additionally, we thank the Ghub project (Sperhac and others, 2021), which now hosts the archived ISMIP6 wiki, as well the Center for Computational Research (CCR) at the University at Buffalo, which provided the computing resources used for this work. We also appreciate useful conversations with current and former members of the ISMIP7 shelf collapse focus group including Luke Trusel, Jeremy Bassis, Hélène Seroussi, Maya Fields, and Sanne Veldhuijsen. The scientific color maps come from Crameri and others (2020).

SUPPLEMENTARY MATERIAL

The supplementary material includes the complete set of summarized result plots (vulnerable fractions, spatial agreement of vulnerability, and per-model vulnerable and non-vulnerable shelf area) organized by ice shelf. [PDF included in submission.]

DATA

For the analyses studying sensitivity to RCP, AOGCM, basal melt parametrization, and fracture toughness, the resistive stress, resistive stress misfit relative to MEaSUREs, thickness, and dimensionless resistive stress exceedance plots for all individual ice sheet models are available here: https://zenodo.org/records/14681268 (Reynolds and Nowicki, 2025). Access to ISMIP6 model outputs is available through Ghub here: https://theghub.org/resources?id=4748.

REFERENCES

Alley KE, Scambos TA, Alley RB and Holschuh N (2019) Troughs developed in ice-stream shear margins precondition ice shelves for ocean-driven breakup. *SCIENCE ADVANCES*, **5**(10), ISSN 2375-2548 (doi: 10.1126/sciadv.aax2215)

Banwell AF, MacAyeal DR and Sergienko OV (2013) Breakup of the Larsen B Ice Shelf triggered by chain reaction drainage of supraglacial lakes. *Geophysical Research Letters*, **40**(22), 5872–5876, ISSN 1944-8007 (doi: 10.1002/2013GL057694), _eprint: https://onlinelibrary.wiley.com/doi/pdf/10.1002/2013GL057694

Barthel A, Agosta C, Little CM, Hattermann T, Jourdain NC, Goelzer H, Nowicki S, Seroussi H, Straneo F and Bracegirdle TJ (2020) CMIP5 model selection for ISMIP6 ice sheet model forcing: Greenland and Antarctica. *The Cryosphere*, **14**(3), 855–879, ISSN 1994-0424 (doi: 10.5194/tc-14-855-2020), publisher: Copernicus Publications

Bassis JN, Crawford A, Kachuck SB, Benn DI, Walker C, Millstein J, Duddu R, Åström J, Fricker H and Luckman A (2024) Stability of Ice Shelves and Ice Cliffs in a Changing Climate. *Annual Review of Earth and Planetary Sciences*, **52**(1), annurev–earth–040522–122817, ISSN 0084-6597, 1545-4495 (doi: 10.1146/annurev-earth-040522-122817)

Comiso JC (2000) Variability and Trends in Antarctic Surface Temperatures from In Situ and Satellite Infrared Measurements. *Journal of Climate*, **13**(10), 1674–1696, ISSN 0894-8755, 1520-0442 (doi: 10.1175/1520-0442(2000)013¡1674:VATIAS¿2.0.CO;2), publisher: American Meteorological Society Section: Journal of Climate

Crameri F, Shephard GE and Heron PJ (2020) The misuse of colour in science communication. *Nature Communications*, **11**(1), 5444, ISSN 2041-1723 (doi: 10.1038/s41467-020-19160-7), publisher: Nature Publishing Group

Cuffey KM and Patterson W (2010) *The Physics of Glaciers*. Elsevier, Burlington, MA, 4 edition

Donat-Magnin M, Jourdain NC, Kittel C, Agosta C, Amory C, Gallée H, Krinner G and Chekki M (2021) Future surface mass balance and surface melt in the Amundsen sector of the West Antarctic Ice Sheet. *The Cryosphere*, **15**(2), 571–593, ISSN 1994-0416 (doi: 10.5194/tc-15-571-2021), publisher: Copernicus GmbH

Fischer MP, Alley RB and Engelder T (1995) Fracture toughness of ice and firn determined from the modified ring test. *Journal of Glaciology*, **41**(138), 383–394, ISSN 0022-1430, 1727-5652 (doi: 10.3189/S0022143000016257)

Fürst JJ, Durand G, Gillet-Chaulet F, Tavard L, Rankl M, Braun M and Gagliardini O (2016) The safety band of Antarctic ice shelves. *Nature Climate Change*, **6**(5), 479–482, ISSN 1758-6798 (doi: 10.1038/nclimate2912), publisher: Nature Publishing Group

Goelzer H, Nowicki S, Payne A, Larour E, Seroussi H, Lipscomb WH, Gregory J, Abe-Ouchi A, Shepherd A, Simon E, Agosta C, Alexander P, Aschwanden A, Barthel A, Calov R, Chambers C, Choi Y, Cuzzone J, Dumas C, Edwards T, Felikson D, Fettweis X, Golledge NR, Greve R, Humbert A, Huybrechts P, Le clec'h S, Lee V, Leguy G, Little C, Lowry DP, Morlighem M, Nias I, Quiquet A, Rückamp M, Schlegel NJ, Slater DA, Smith RS, Straneo F, Tarasov L, van de Wal R and van den Broeke M (2020) The future sea-level contribution of the Greenland ice sheet: a multi-model ensemble study of ISMIP6. *The Cryosphere*, **14**(9), 3071–3096, ISSN 1994-0424 (doi: 10.5194/tc-14-3071-2020), publisher: Copernicus Publications

Jiménez S and Duddu R (2018) On the evaluation of the stress intensity factor in calving models using linear elastic fracture mechanics. *Journal of Glaciology*, **64**(247), 759–770, ISSN 0022-1430, 1727-5652 (doi: 10.1017/jog.2018.64)

Jourdain NC, Asay-Davis X, Hattermann T, Straneo F, Seroussi H, Little CM and Nowicki S (2020) A protocol for calculating basal melt rates in the ISMIP6 Antarctic ice sheet projections. *The Cryosphere*, **14**(9), 3111–3134, ISSN 1994-0424 (doi: 10.5194/tc-14-3111-2020), publisher: Copernicus Publications

Lai CY, Kingslake J, Wearing MG, Chen PHC, Gentine P, Li H, Spergel JJ and van Wessem JM (2020) Vulnerability of Antarctica's ice shelves to meltwater-driven fracture. *NATURE*, **584**(7822), 574–+, ISSN 0028-0836, 1476-4687 (doi: 10.1038/s41586-020-2627-8), num Pages: 19 Place: Berlin Publisher: Nature Research Web of Science ID: WOS:000563223200017

Lhermitte S, Sun S, Shuman C, Wouters B, Pattyn F, Wuite J, Berthier E and Nagler T (2020) Damage accelerates ice shelf instability and mass loss in Amundsen Sea Embayment. *PROCEEDINGS OF THE NATIONAL ACADEMY OF SCIENCES OF THE UNITED STATES OF AMERICA*, **117**(40), 24735–24741, ISSN 0027-8424 (doi: 10.1073/pnas.1912890117), num Pages: 7 Place: Washington Publisher: Natl Acad Sciences Web of Science ID: WOS:000579059100025

Litwin KL, Zygielbaum BR, Polito PJ, Sklar LS and Collins GC (2012) Influence of temperature, composition, and grain size on the tensile failure of water ice: Implications for erosion on Titan. *Journal of Geophysical Research: Planets*, **117**(E8), ISSN 2156-2202 (doi: 10.1029/2012JE004101), _eprint: https://onlinelibrary.wiley.com/doi/pdf/10.1029/2012JE004101

MacAyeal DR, Sergienko OV and Banwell AF (2015) A model of viscoelastic ice-shelf flexure. *Journal of Glaciology*, **61**(228), 635–645, ISSN 0022-1430, 1727-5652 (doi: 10.3189/2015JoG14J169)

Matsuoka K, Skoglund A, Roth G, de Pomereu J, Griffiths H, Headland R, Herried B, Katsumata K, Le Brocq A, Licht K, Morgan F, Neff PD, Ritz C, Scheinert M, Tamura T, Van de Putte A, van den Broeke M, von Deschwanden A, Deschamps-Berger C, Van Liefferinge B, Tronstad S and Melvær Y (2021) Quantarctica, an integrated mapping environment for Antarctica, the Southern Ocean, and sub-Antarctic islands. *Environmental Modelling & Software*, **140**, 105015, ISSN 1364-8152 (doi: 10.1016/j.envsoft.2021.105015)

Millstein JD, Minchew BM and Pegler SS (2022) Ice viscosity is more sensitive to stress than commonly assumed. *Communications Earth & Environment*, **3**(1), 1–7, ISSN 2662-4435 (doi: 10.1038/s43247-022-00385-x), number: 1 Publisher: Nature Publishing Group

Mouginot J, Scheuchl B and Rignot E (2017) Antarctic Boundaries for IPY 2007-2009 from Satellite Radar, Version 2 (doi: https://doi.org/10.5067/AXE4121732AD)

Moussavi M, Pope A, Halberstadt ARW, Trusel LD, Cioffi L and Abdalati W (2020) Antarctic Supraglacial Lake Detection Using Landsat 8 and Sentinel-2 Imagery: Towards Continental Generation of Lake Volumes. *Remote Sensing*, **12**(1), 134, ISSN 2072-4292 (doi: 10.3390/rs12010134), number: 1 Publisher: Multidisciplinary Digital Publishing Institute

Munneke PK, Ligtenberg SRM, Broeke MRVD and Vaughan DG (2014) Firn air depletion as a precursor of Antarctic ice-shelf collapse. *Journal of Glaciology*, **60**(220), 205–214, ISSN 0022-1430, 1727-5652 (doi: 10.3189/2014JoG13J183)

Nowicki S, Goelzer H, Seroussi H, Payne AJ, Lipscomb WH, Abe-Ouchi A, Agosta C, Alexander P, Asay-Davis XS, Barthel A, Bracegirdle TJ, Cullather R, Felikson D, Fettweis X, Gregory JM, Hattermann T, Jourdain NC, Kuipers Munneke P, Larour E, Little CM, Morlighem M, Nias I, Shepherd A, Simon E, Slater D, Smith RS, Straneo F, Trusel LD, van den Broeke MR and van de Wal R (2020) Experimental protocol for sea level projections from ISMIP6 stand-alone ice sheet models. *The Cryosphere*, **14**(7), 2331–2368, ISSN 1994-0424 (doi: 10.5194/tc-14-2331-2020), publisher: Copernicus Publications

Nowicki SMJ, Payne A, Larour E, Seroussi H, Goelzer H, Lipscomb W, Gregory J, Abe-Ouchi A and Shepherd A (2016) Ice Sheet Model Intercomparison Project (ISMIP6) contribution to CMIP6. *Geoscientific Model Development*, **9**(12), 4521–4545, ISSN 1991-959X (doi: 10.5194/gmd-9-4521-2016), publisher: Copernicus GmbH

Payne AJ, Nowicki S, Abe-Ouchi A, Agosta C, Alexander P, Albrecht T, Asay-Davis X, Aschwanden A, Barthel A, Bracegirdle TJ, Calov R, Chambers C, Choi Y, Cullather R, Cuzzone J, Dumas C, Edwards TL, Felikson D, Fettweis X, Galton-Fenzi BK, Goelzer H, Gladstone R, Golledge NR, Gregory JM, Greve R, Hattermann T, Hoffman MJ, Humbert A, Huybrechts P, Jourdain NC, Kleiner T, Munneke PK, Larour E, Le clec'h S, Lee V, Leguy G, Lipscomb WH, Little CM, Lowry DP, Morlighem M, Nias I, Pattyn F, Pelle T, Price SF, Quiquet A, Reese R, Rückamp M, Schlegel NJ, Seroussi H, Shepherd A, Simon E, Slater D, Smith RS, Straneo F, Sun S, Tarasov L, Trusel LD, Van Breedam J, van de Wal R, van den Broeke M, Winkelmann R, Zhao C, Zhang T and Zwinger T (2021) Future Sea Level Change Under Coupled Model Intercomparison Project Phase 5 and Phase 6 Scenarios From the Greenland and Antarctic Ice Sheets. *Geophysical Research Letters*, **48**(16), e2020GL091741, ISSN 1944-8007 (doi: 10.1029/2020GL091741), _eprint: https://onlinelibrary.wiley.com/doi/pdf/10.1029/2020GL091741

Pfeffer WT, Meier MF and Illangasekare TH (1991) Retention of Greenland runoff by refreezing; implications for projected future sea level change. *Journal of Geophysical Research*, **96**(C12), 22117–22124, ISSN 0148-0227 (doi: 10.1029/91JC02502), place: Washington, DC Publisher: American Geophysical Union

Reynolds B and Nowicki S (2025) Postprocessed Plots for "Ice-Shelf-Vulnerability- Parametrization Reanalysis of ISMIP6 Simulations Predicts Reduced Vulnerability with Shelf Thinning, Shows Importance of Improving Fracture Toughness Estimates and Model Initialization." (doi: 10.5281/zenodo.14681268)

Rignot E, Casassa G, Gogineni P, Krabill W, Rivera A and Thomas R (2004) Accelerated ice discharge from the Antarctic Peninsula following the collapse of Larsen B ice shelf. *Geophysical Research Letters*, **31**(18), ISSN 1944-8007 (doi: 10.1029/2004GL020697), _eprint: https://onlinelibrary.wiley.com/doi/pdf/10.1029/2004GL020697

Rignot E, Scheuchkl B, Mouginot J and Jeong S (2022) MEaSUREs Multi-year Reference Velocity Maps of the Antarctic Ice Sheet, Version 1 (doi: 10.5067/FB851ZIZYX5O)

Rist MA, Sammonds PR, Murrell SaF, Meredith PG, Oerter H and Doake CSM (1996) Experimental fracture and mechanical properties of Antarctic ice: preliminary results. *Annals of Glaciology*, **23**, 284–292, ISSN 0260-3055, 1727-5644 (doi: 10.3189/S0260305500013550)

Robel AA and Banwell AF (2019) A Speed Limit on Ice Shelf Collapse Through Hydrofracture. *GEOPHYSICAL RESEARCH LETTERS*, **46**(21), 12092–12100, ISSN 0094-8276, 1944-8007 (doi: 10.1029/2019GL084397), num Pages: 9 Place: Washington Publisher: Amer Geophysical Union Web of Science ID: WOS:000494348900001

Rott H, Müller F, Nagler T and Floricioiu D (2011) The imbalance of glaciers after disintegration of Larsen-B ice shelf, Antarctic Peninsula. *The Cryosphere*, **5**(1), 125–134, ISSN 1994-0416 (doi: 10.5194/tc-5-125-2011), publisher: Copernicus GmbH

Scambos T, Fricker HA, Liu CC, Bohlander J, Fastook J, Sargent A, Massom R and Wu AM (2009) Ice shelf disintegration by plate bending and hydro-fracture: Satellite observations and model results of the

2008 Wilkins ice shelf break-ups. *Earth and Planetary Science Letters*, **280**(1), 51–60, ISSN 0012-821X (doi: 10.1016/j.epsl.2008.12.027)

Scambos TA, Hulbe C, Fahnestock M and Bohlander J (2000) The link between climate warming and break-up of ice shelves in the Antarctic Peninsula. *Journal of Glaciology*, **46**(154), 516–530, ISSN 0022-1430, 1727-5652 (doi: 10.3189/172756500781833043)

Seroussi H, Nowicki S, Payne AJ, Goelzer H, Lipscomb WH, Abe-Ouchi A, Agosta C, Albrecht T, Asay-Davis X, Barthel A, Calov R, Cullather R, Dumas C, Galton-Fenzi BK, Gladstone R, Golledge NR, Gregory JM, Greve R, Hattermann T, Hoffman MJ, Humbert A, Huybrechts P, Jourdain NC, Kleiner T, Larour E, Leguy GR, Lowry DP, Little CM, Morlighem M, Pattyn F, Pelle T, Price SF, Quiquet A, Reese R, Schlegel NJ, Shepherd A, Simon E, Smith RS, Straneo F, Sun S, Trusel LD, Van Breedam J, van de Wal RSW, Winkelmann R, Zhao C, Zhang T and Zwinger T (2020) ISMIP6 Antarctica: a multi-model ensemble of the Antarctic ice sheet evolution over the 21st century. *The Cryosphere*, **14**(9), 3033–3070, ISSN 1994-0424 (doi: 10.5194/tc-14-3033-2020), publisher: Copernicus Publications

Seroussi H, Pelle T, Lipscomb WH, Abe-Ouchi A, Albrecht T, Alvarez-Solas J, Asay-Davis X, Barre JB, Berends CJ, Bernales J, Blasco J, Caillet J, Chandler DM, Coulon V, Cullather R, Dumas C, Galton-Fenzi BK, Garbe J, Gillet-Chaulet F, Gladstone R, Goelzer H, Golledge N, Greve R, Gudmundsson GH, Han HK, Hillebrand TR, Hoffman MJ, Huybrechts P, Jourdain NC, Klose AK, Langebroek PM, Leguy GR, Lowry DP, Mathiot P, Montoya M, Morlighem M, Nowicki S, Pattyn F, Payne AJ, Quiquet A, Reese R, Robinson A, Saraste L, Simon EG, Sun S, Twarog JP, Trusel LD, Urruty B, Van Breedam J, van de Wal RSW, Wang Y, Zhao C and Zwinger T (2024) Evolution of the Antarctic Ice Sheet Over the Next Three Centuries From an ISMIP6 Model Ensemble. *EARTHS FUTURE*, **12**(9), e2024EF004561, ISSN 2328-4277 (doi: 10.1029/2024EF004561), num Pages: 44 Place: Washington Publisher: Amer Geophysical Union Web of Science ID: WOS:001304094900001

Sperhac JM, Poinar K, Jones-Ivey R, Briner J, Csatho B, Nowicki S, Simon E, Larour E, Quinn J and Patra A (2021) GHub: Building a glaciology gateway to unify a community. *Concurrency and Computation: Practice and Experience*, **33**(19), e6130, ISSN 1532-0634 (doi: 10.1002/cpe.6130), _eprint: https://onlinelibrary.wiley.com/doi/pdf/10.1002/cpe.6130

Sun S, Pattyn F, Simon EG, Albrecht T, Cornford S, Calov R, Dumas C, Gillet-Chaulet F, Goelzer H, Golledge NR, Greve R, Hoffman MJ, Humbert A, Kazmierczak E, Kleiner T, Leguy GR, Lipscomb WH, Martin D, Morlighem M, Nowicki S, Pollard D, Price S, Quiquet A, Seroussi H, Schlemm T, Sutter J, Wal RSWvd, Winkelmann R and Zhang T (2020) Antarctic ice sheet response to sudden and sustained ice-shelf collapse (ABUMIP). *Journal of Glaciology*, **66**(260), 891–904, ISSN 0022-1430, 1727-5652 (doi: 10.1017/jog.2020.67)

Surawy-Stepney T, Hogg AE, Cornford SL and Hogg DC (2023) Mapping Antarctic crevasses and their evolution with deep learning applied to satellite radar imagery. *The Cryosphere*, **17**(10), 4421–4445, ISSN 1994-0416 (doi: 10.5194/tc-17-4421-2023), publisher: Copernicus GmbH

Thomas RH (1973) The Creep of Ice Shelves: Interpretation of Observed Behaviour. *Journal of Glaciology*, **12**(64), 55–70, ISSN 0022-1430, 1727-5652 (doi: 10.3189/S002214300002270X)

Trusel LD, Frey KE, Das SB, Munneke PK and van den Broeke MR (2013) Satellite-based estimates of Antarctic surface meltwater fluxes. *Geophysical Research Letters*, **40**(23), 6148–6153, ISSN 1944-8007 (doi: 10.1002/2013GL058138), _eprint: https://onlinelibrary.wiley.com/doi/pdf/10.1002/2013GL058138

Trusel LD, Frey KE, Das SB, Karnauskas KB, Kuipers Munneke P, van Meijgaard E and van den Broeke MR (2015) Divergent trajectories of Antarctic surface melt under two twenty-first-century climate scenarios. *Nature Geoscience*, **8**(12), 927–932, ISSN 1752-0908 (doi: 10.1038/ngeo2563), number: 12 Publisher: Nature Publishing Group

van der Veen CJ (1998) Fracture mechanics approach to penetration of surface crevasses on glaciers. *Cold Regions Science and Technology*, **27**(1), 31–47, ISSN 0165-232X (doi: 10.1016/S0165-232X(97)00022-0)

van Wessem JM, van den Broeke MR, Wouters B and Lhermitte S (2023) Variable temperature thresholds of melt pond formation on Antarctic ice shelves. *Nature Climate Change*, **13**(2), 161–166, ISSN 1758-6798 (doi: 10.1038/s41558-022-01577-1), publisher: Nature Publishing Group

Veldhuijsen SBM, van de Berg WJ, Kuipers Munneke P and van den Broeke MR (2024) Firn air content changes on Antarctic ice shelves under three future warming scenarios. *The Cryosphere*, **18**(4), 1983–1999, ISSN 1994-0416 (doi: 10.5194/tc-18-1983-2024), publisher: Copernicus GmbH

Supplement to: Assessing Future Ice Shelf Collapse Vulnerability in the ISMIP6 Ensemble

Benjamin Reynolds, Sophie Nowicki

April 2025

S1 Additional Thickness Correlation Figure for Amery and Filchner-Ronne

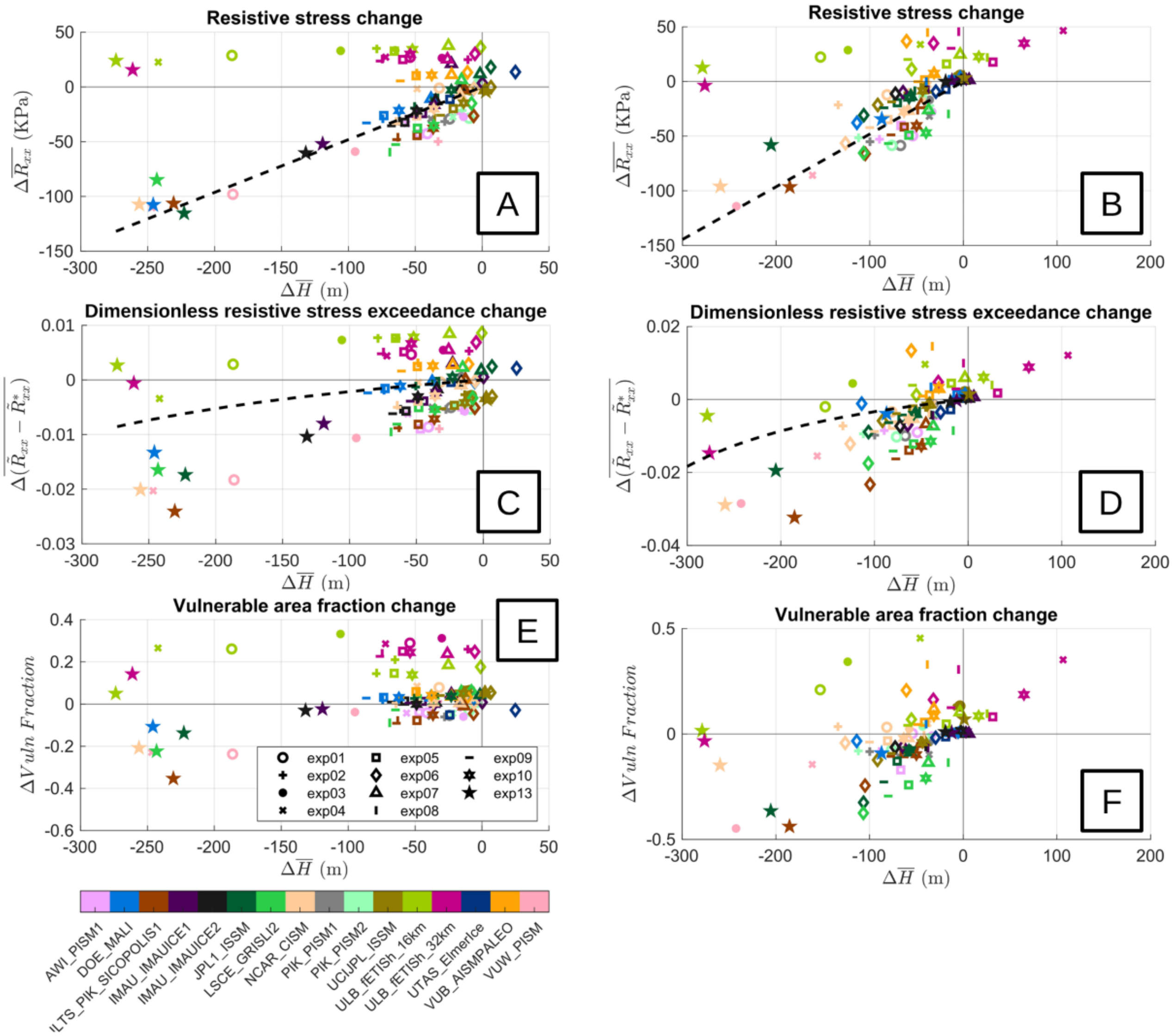

Figure S1: Change in (A) resistive stress, (C) dimensionless resistive stress exceedance, and (E) shelf vulnerable fraction with thickness change for the Filchner-Ronne and the same (B,D,F) for the Amery shelf. Marker shapes indicate experiments and marker colors indicate models. Dashed black lines indicate the theoretical predictions whose calculations are discussed in the Thickness Change Correlation part of the Methods section. The fracture toughness used in post processing was 200 $KPa\ m^{1/2}$.

S2 Comprehensive Figures Per-Shelf for Sensitivity Analyses

S2.1 Ross

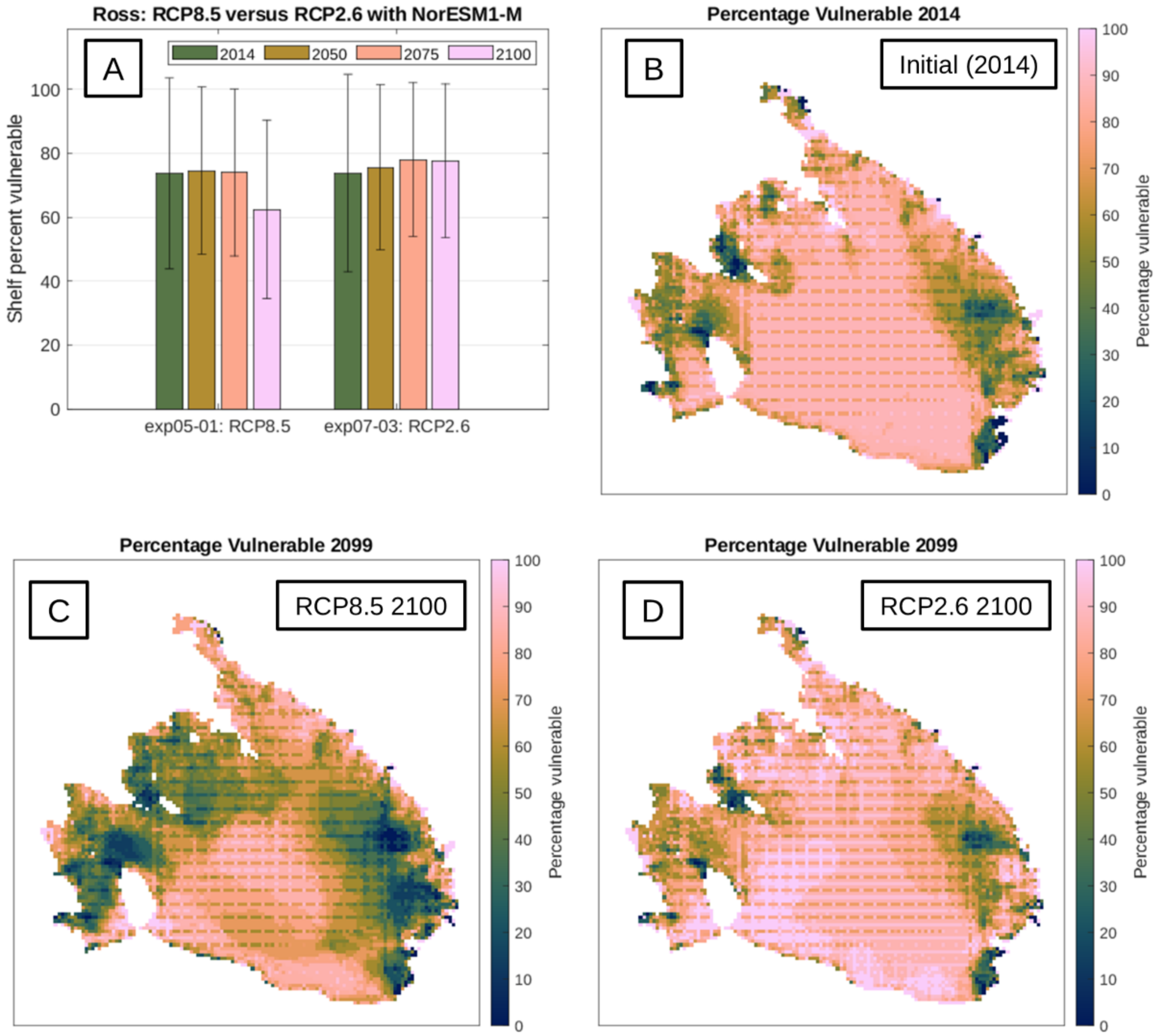

Figure S2: (A) Average shelf vulnerability fraction across ice sheet models in 2014, 2050, 2075, and 2100 under RCP8.5 and RCP2.6; (B) initial per-pixel vulnerability agreement across models; (C) 2100 vulnerability agreement under RCP8.5; and (D) 2100 vulnerability agreement under RCP2.6 driven by the NorESM1-M climate model for the Ross.

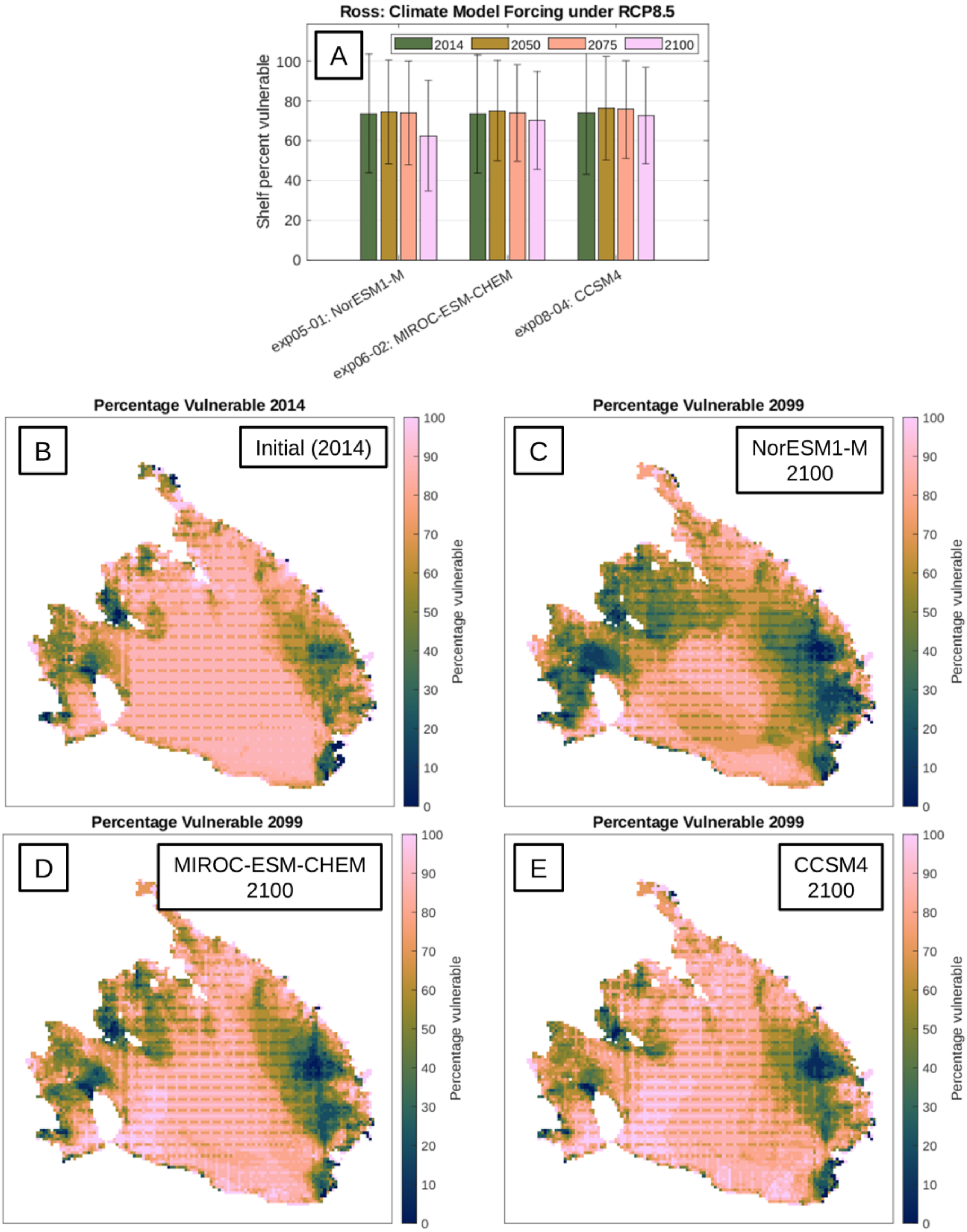

Figure S3: (A) Average shelf vulnerability fraction across ice sheet models in 2014, 2050, 2075, and 2100 using RCP8.5 with three climate models; (B) initial per-pixel vulnerability agreement across models; (C) 2100 vulnerability agreement driven by NorESM1-M; (D) 2100 vulnerability agreement driven by MIROC-ESM-CHEM; and (E) 2100 vulnerability agreement driven by CCSM4 for the Ross.

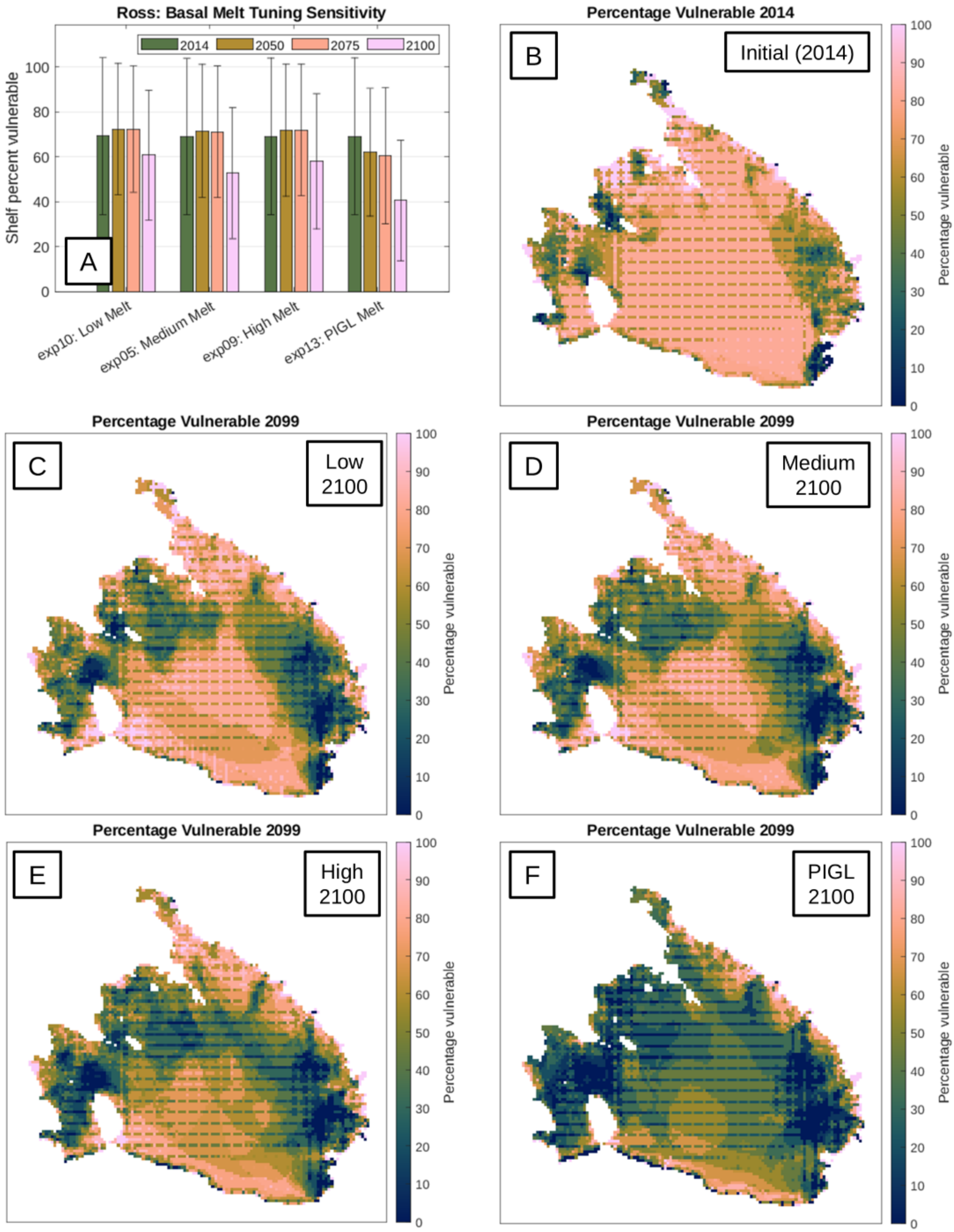

Figure S4: (A) Average shelf vulnerability fraction across ice sheet models in 2014, 2050, 2075, and 2100 using RCP8.5 with for basal melt parametrization tunings; (B) initial per-pixel vulnerability agreement across models; and 2100 vulnerability agreement with the (C) Low, (D) Medium, (E) High, and (F) PIGL basal melt parametrization tunings for the Ross.

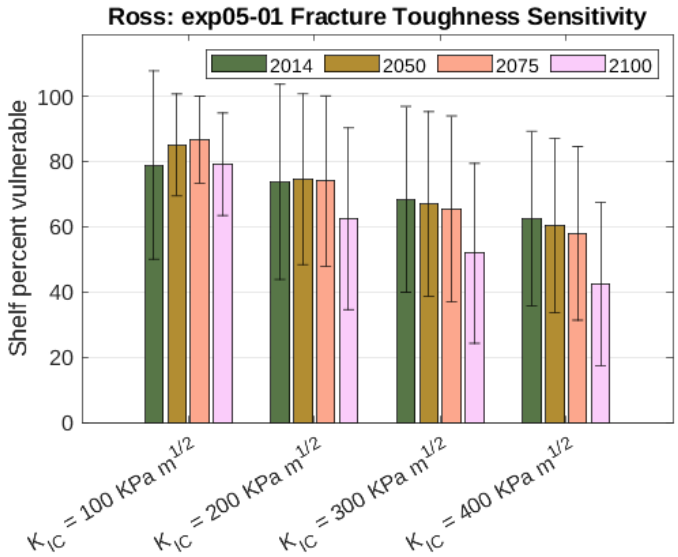

Figure S5: Average shelf vulnerability fraction across ice sheet models in 2014, 2050, 2075, and 2100 with fracture toughness values of 100, 200, 300, and 400 $KPa\ m^{1/2}$ under the RCP8.5 forcing with the NorESM1-M climate model for the Ross shelf.

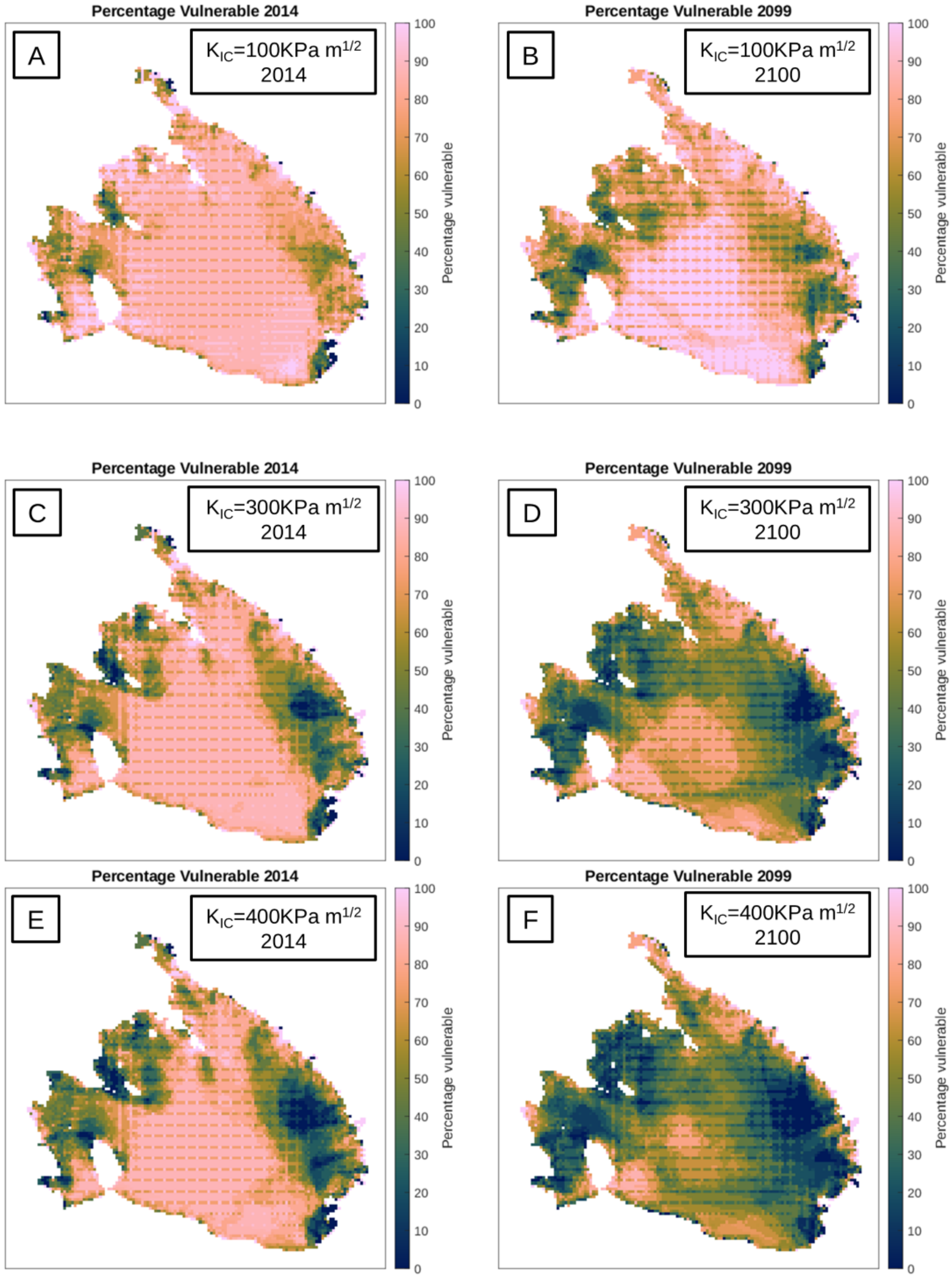

Figure S6: Initial and 2100 per-pixel vulnerability agreement across ice sheet models under RCP8.5 with NorESM1-M postprocessed with fracture toughness values of (A,B) 100, (C,D) 300, and (E,F) 400 $KPa\ m^{1/2}$ for the Ross. The equivalent plots with 200 $KPa\ m^{1/2}$ can be found as panels B and C of Fig. S3.

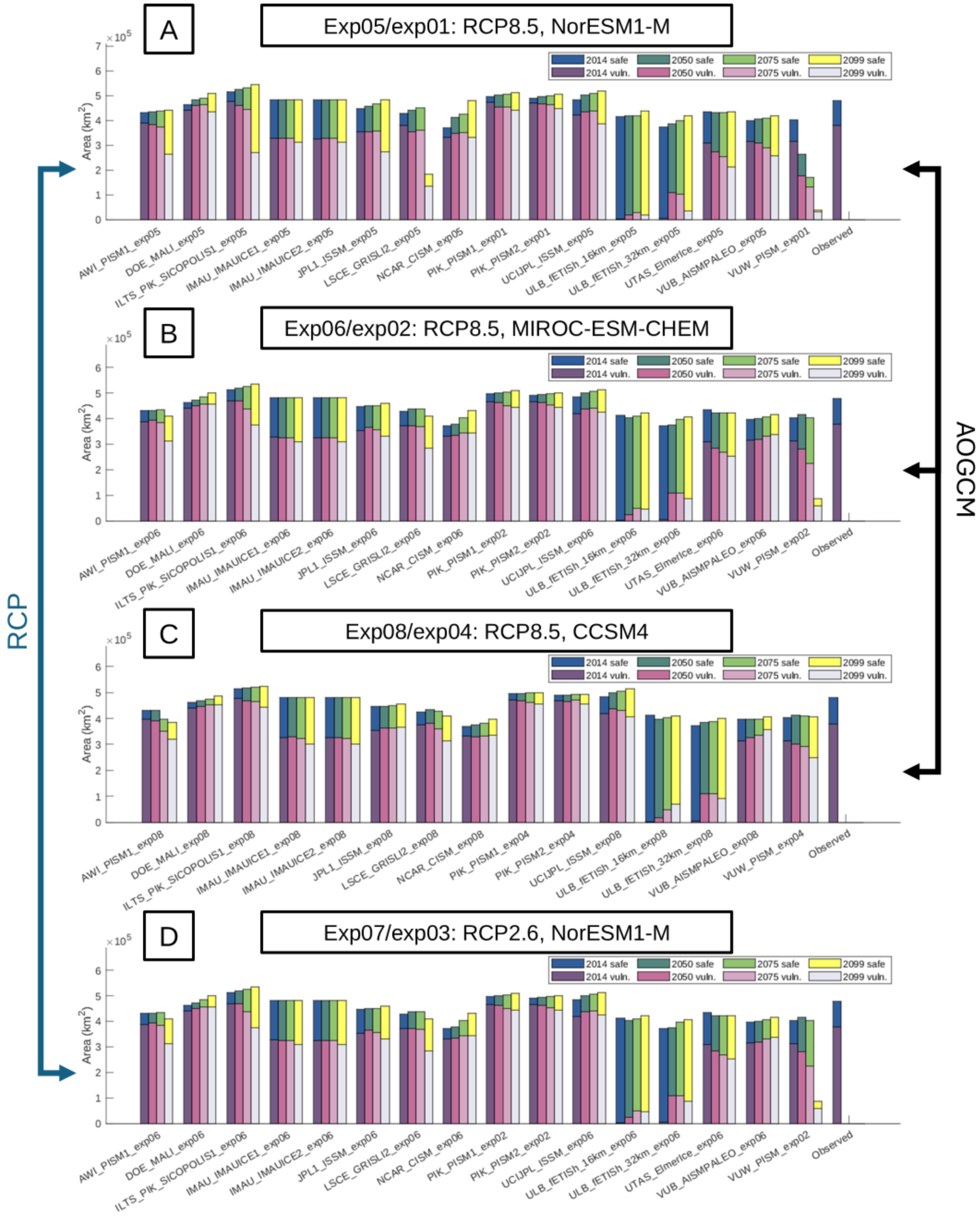

Figure S7: Vulnerable and safe ice shelf areas in each ice sheet model in 2014, 2050, 2075, and 2100 driven by (A) NorESM1-M with RCP8.5, (B) MIROC-ESM-CHEM with RCP8.5, (C) CCSM4 with RCP8.5, and (D) NorESM1-M with RCP2.6 for the Ross. Arrows indicate the analyses providing averages for the climate scenario (RCP) and climate model (AOGCM) analyses. The fracture toughness used is 200 $KPa\ m^{1/2}$.

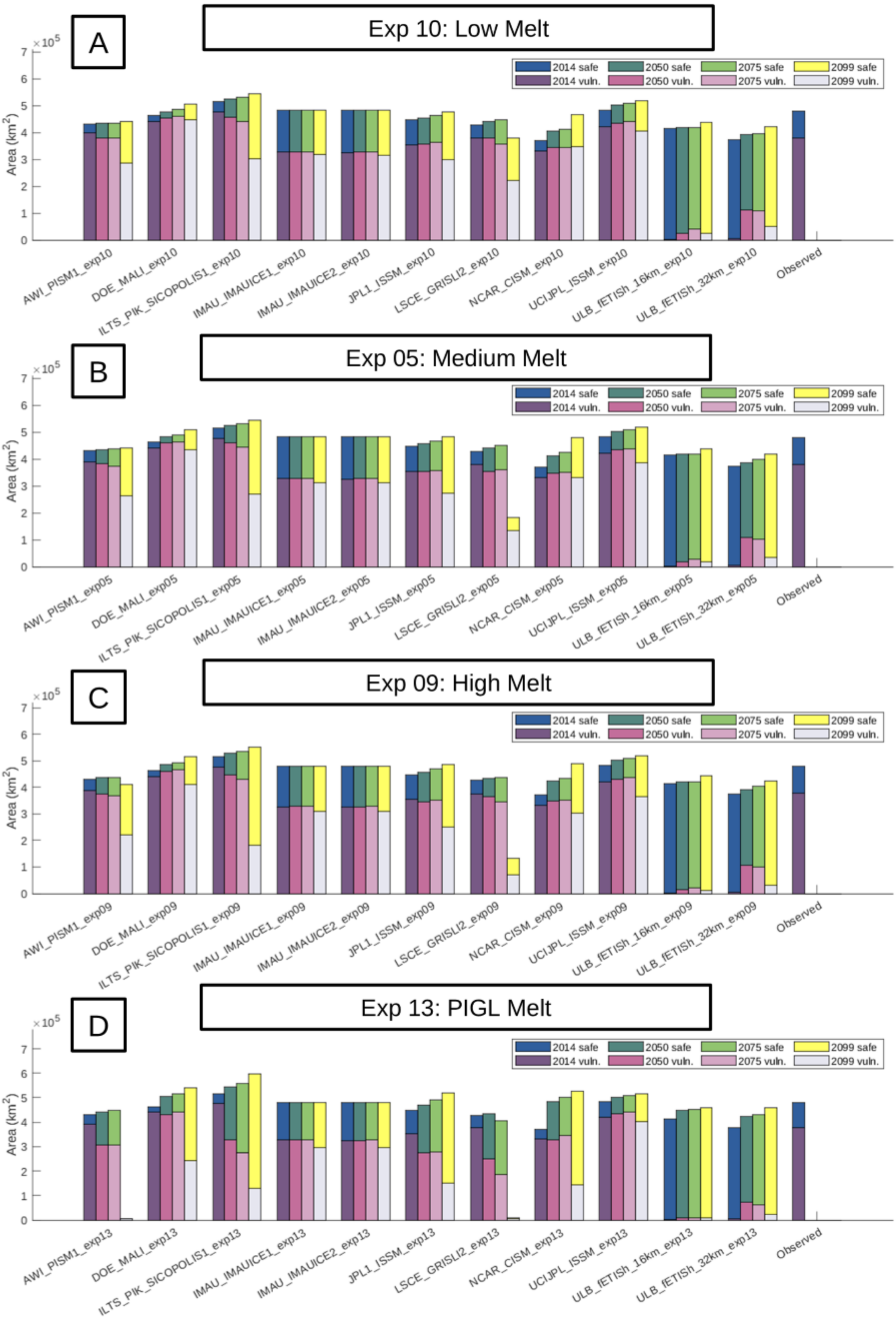

Figure S8: Vulnerable and safe ice shelf areas in each ice sheet model in 2014, 2050, 2075, and 2100 driven by the (A) low, (B) medium, (C) high, and (D) PIGL basal melt parametrizations for the Ross. The ice sheet models for all these experiments were driven by NorESM1-M under RCP8.5 and the fracture toughness used was $KPa\ m^{1/2}$.

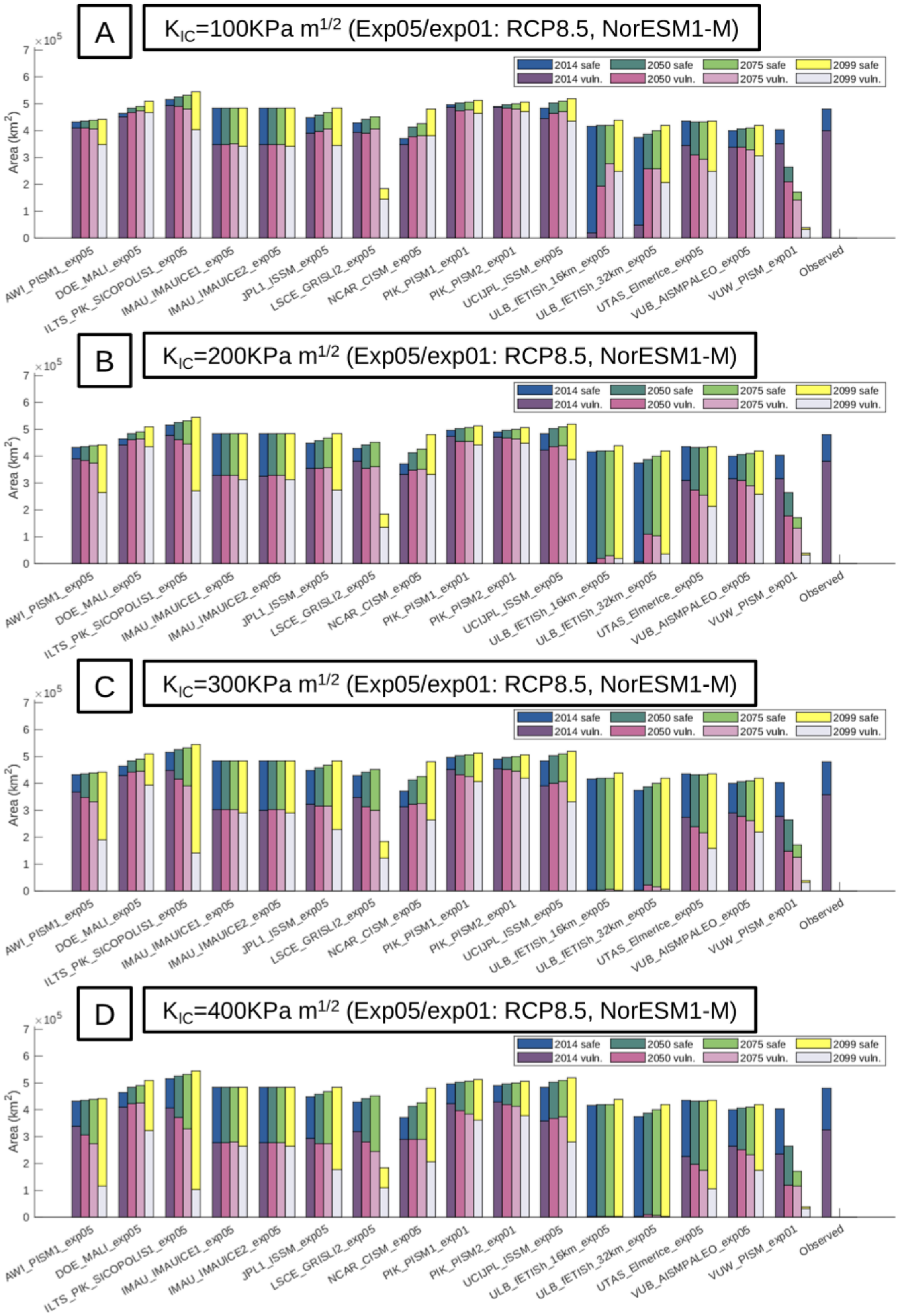

Figure S9: Vulnerable and safe ice shelf areas in each ice sheet model in 2014, 2050, 2075, and 2100 driven by NorESM1-M under RCP8.5 (exp05 and exp01) postprocessed with fracture toughenss values of (A) 100, (B) 200, (C) 300, and (D) 400 $KPa\ m^{1/2}$.

S2.2 Filchner-Ronne

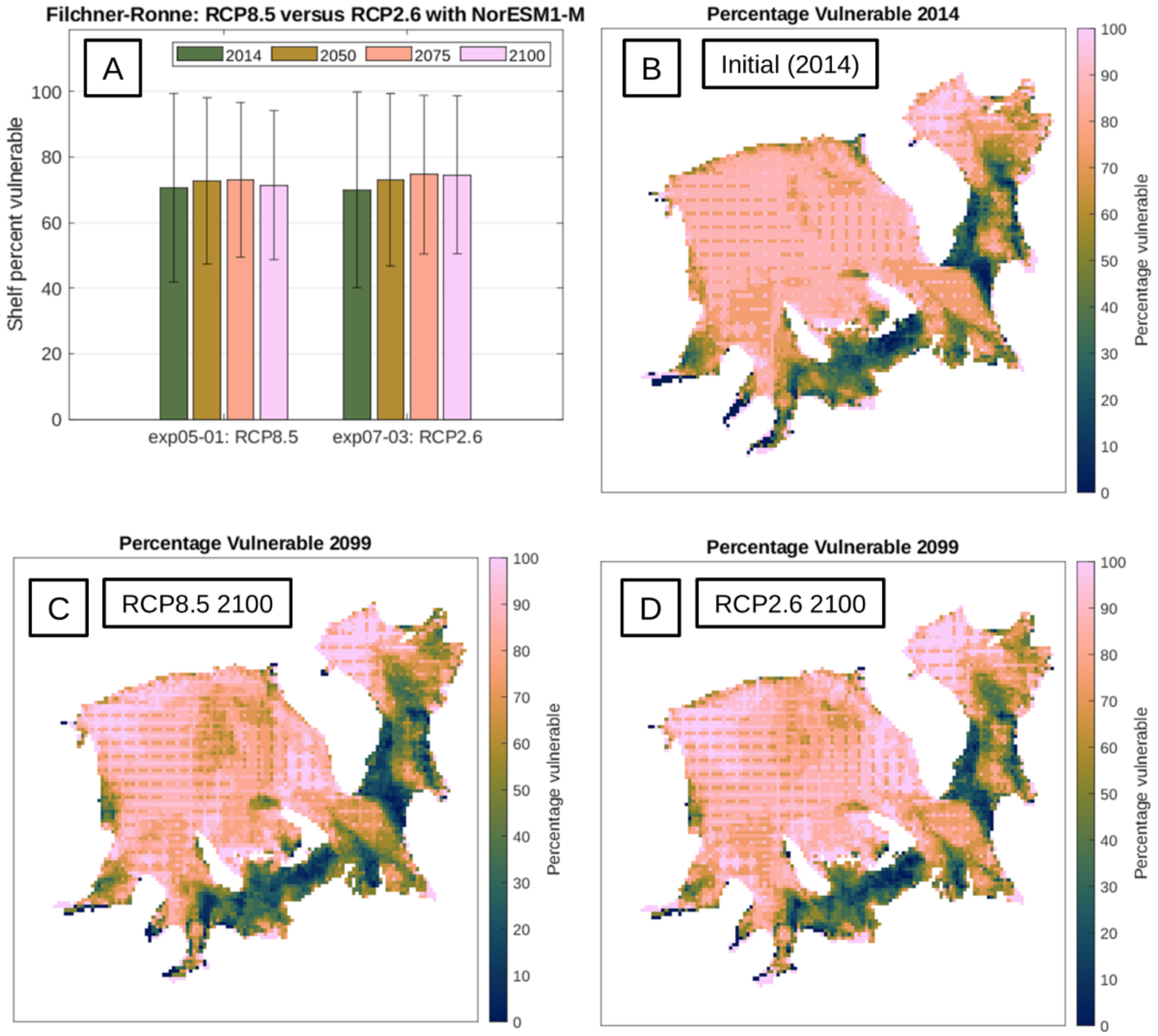

Figure S10: (A) Average shelf vulnerability fraction across ice sheet models in 2014, 2050, 2075, and 2100 under RCP8.5 and RCP2.6; (B) initial per-pixel vulnerability agreement across models; (C) 2100 vulnerability agreement under RCP8.5; and (D) 2100 vulnerability agreement under RCP2.6 driven by the NorESM1-M climate model for the Filchner-Ronne.

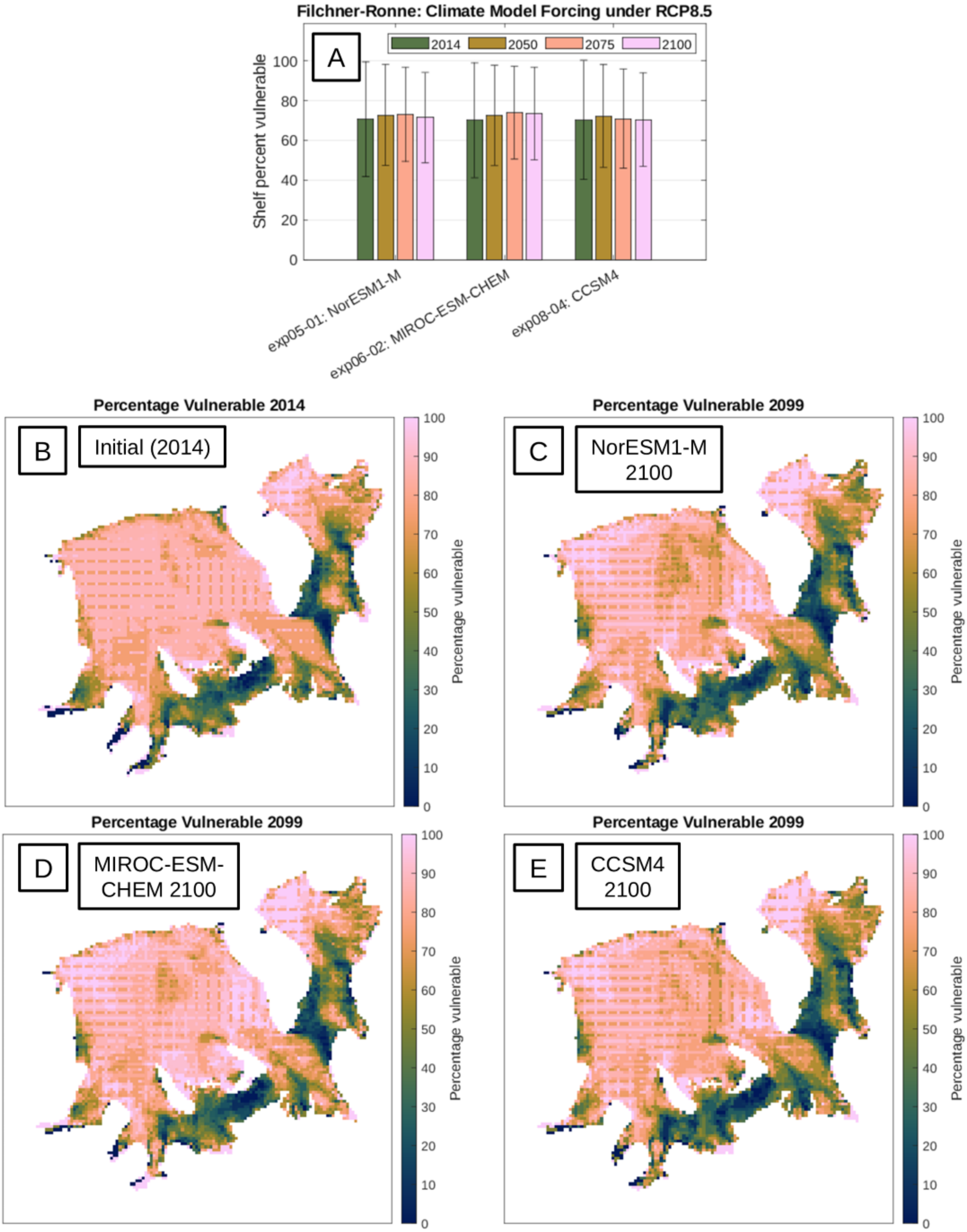

Figure S11: (A) Average shelf vulnerability fraction across ice sheet models in 2014, 2050, 2075, and 2100 using RCP8.5 with three climate models; (B) initial per-pixel vulnerability agreement across models; (C) 2100 vulnerability agreement driven by NorESM1-M; (D) 2100 vulnerability agreement driven by MIROC-ESM-CHEM; and (E) 2100 vulnerability agreement driven by CCSM4 for the Filchner-Ronne.

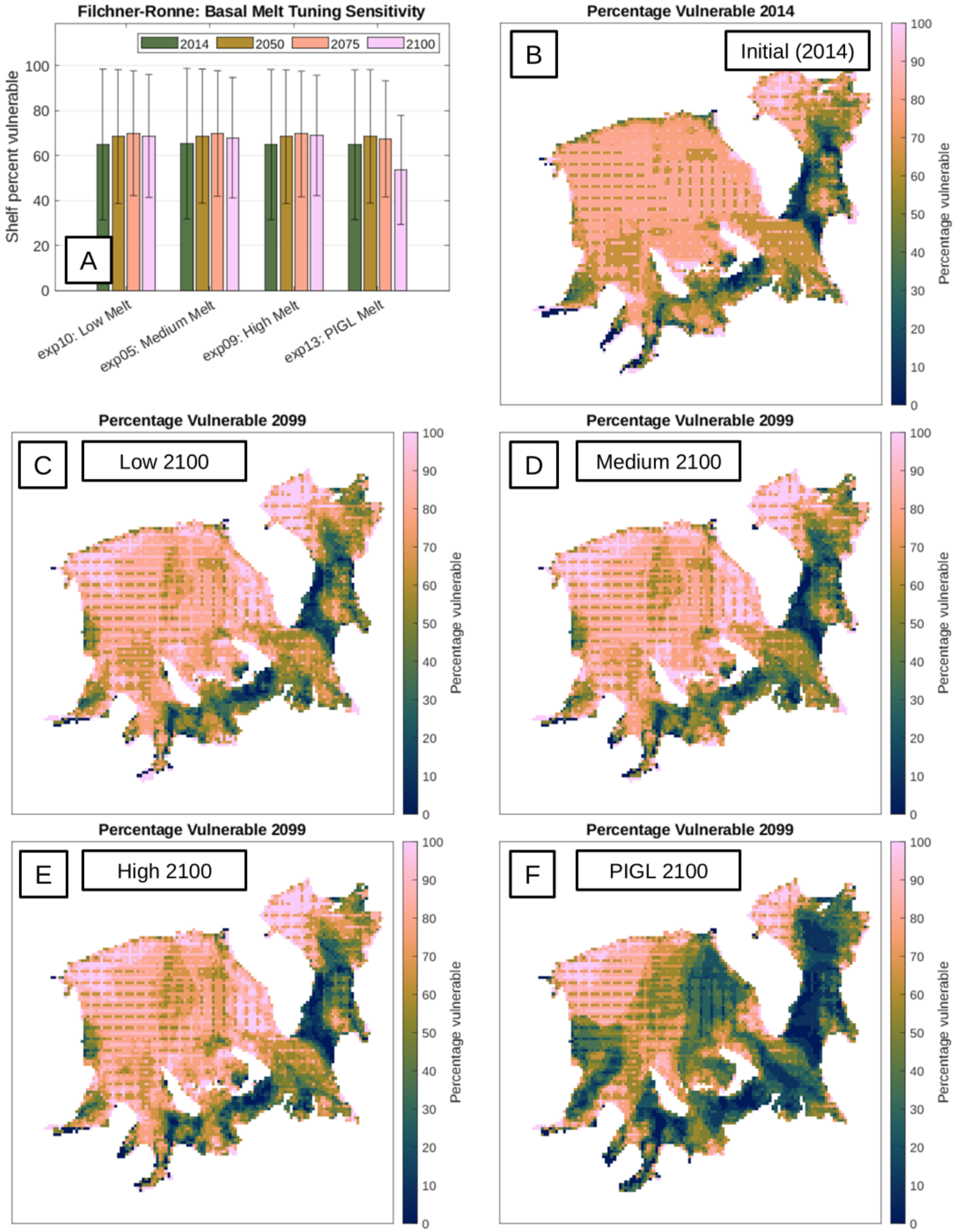

Figure S12: (A) Average shelf vulnerability fraction across ice sheet models in 2014, 2050, 2075, and 2100 using RCP8.5 with for basal melt parametrization tunings; (B) initial per-pixel vulnerability agreement across models; and 2100 vulnerability agreement with the (C) Low, (D) Medium, (E) High, and (F) PIGL basal melt parametrization tunings for the Filchner-Ronne.

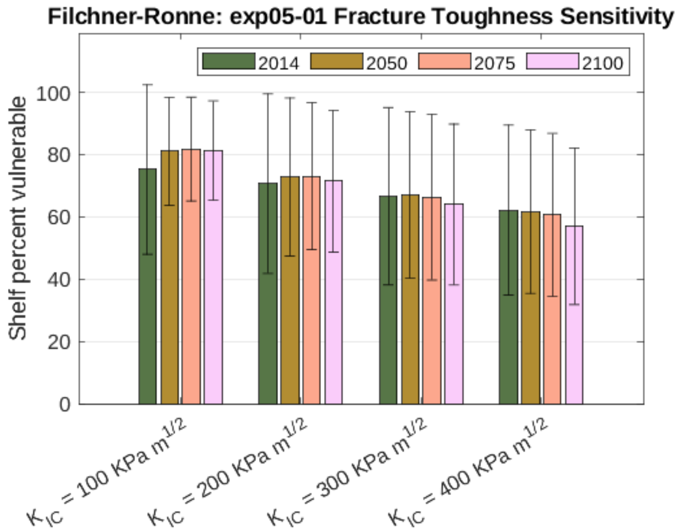

Figure S13: Average shelf vulnerability fraction across ice sheet models in 2014, 2050, 2075, and 2100 with fracture toughness values of 100, 200, 300, and 400 $KPa\ m^{1/2}$ under the RCP8.5 forcing with the NorESM1-M climate model for the Filchner-Ronne shelf.

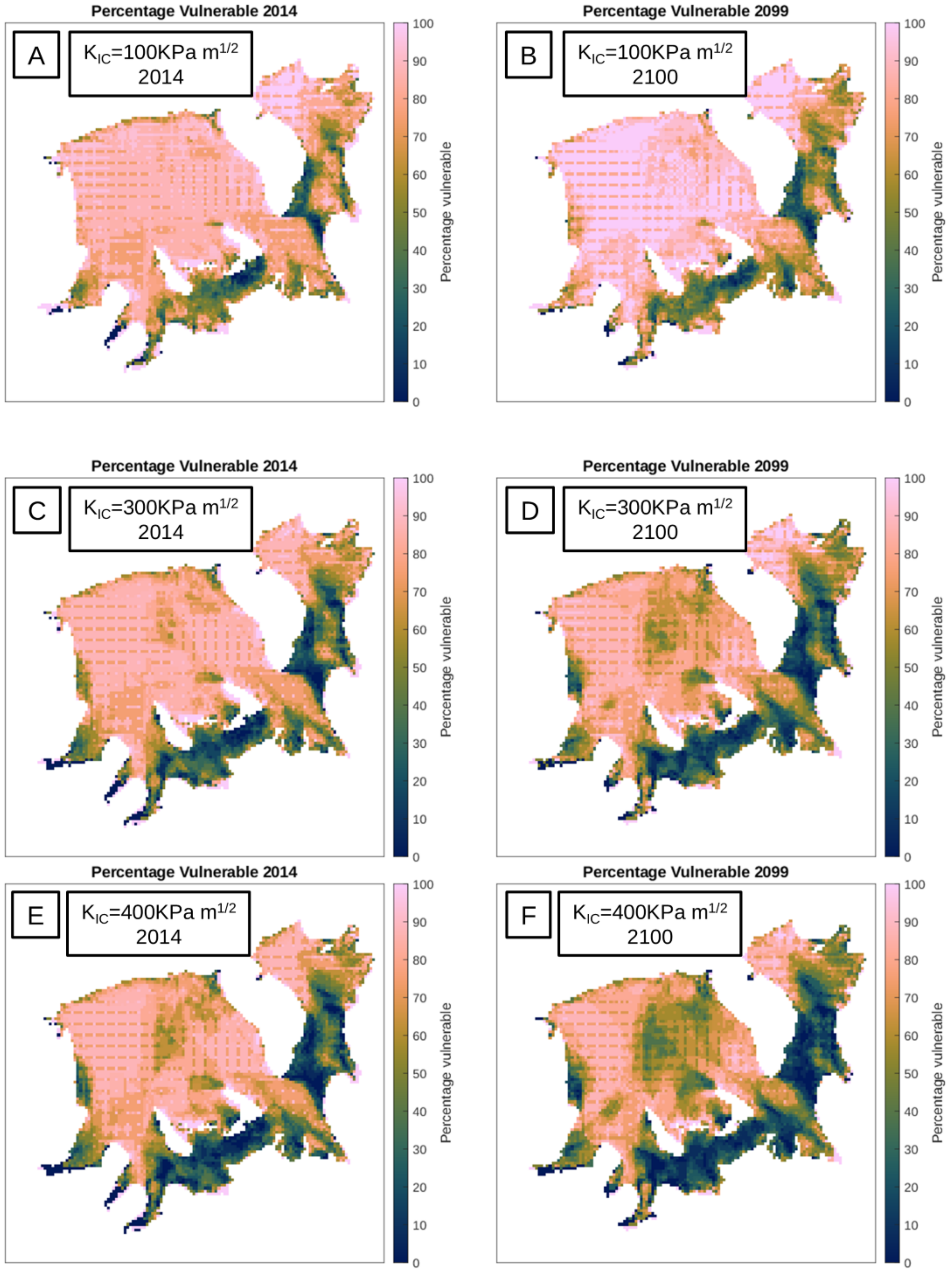

Figure S14: Initial and 2100 per-pixel vulnerability agreement across ice sheet models under RCP8.5 with NorESM1-M postprocessed with fracture toughness values of (A,B) 100, (C,D) 300, and (E,F) 400 $KPa\ m^{1/2}$ for the Filchner-Ronne. The equivalent plots with 200 $KPa\ m^{1/2}$ can be found as panels B and C of Fig. S3.

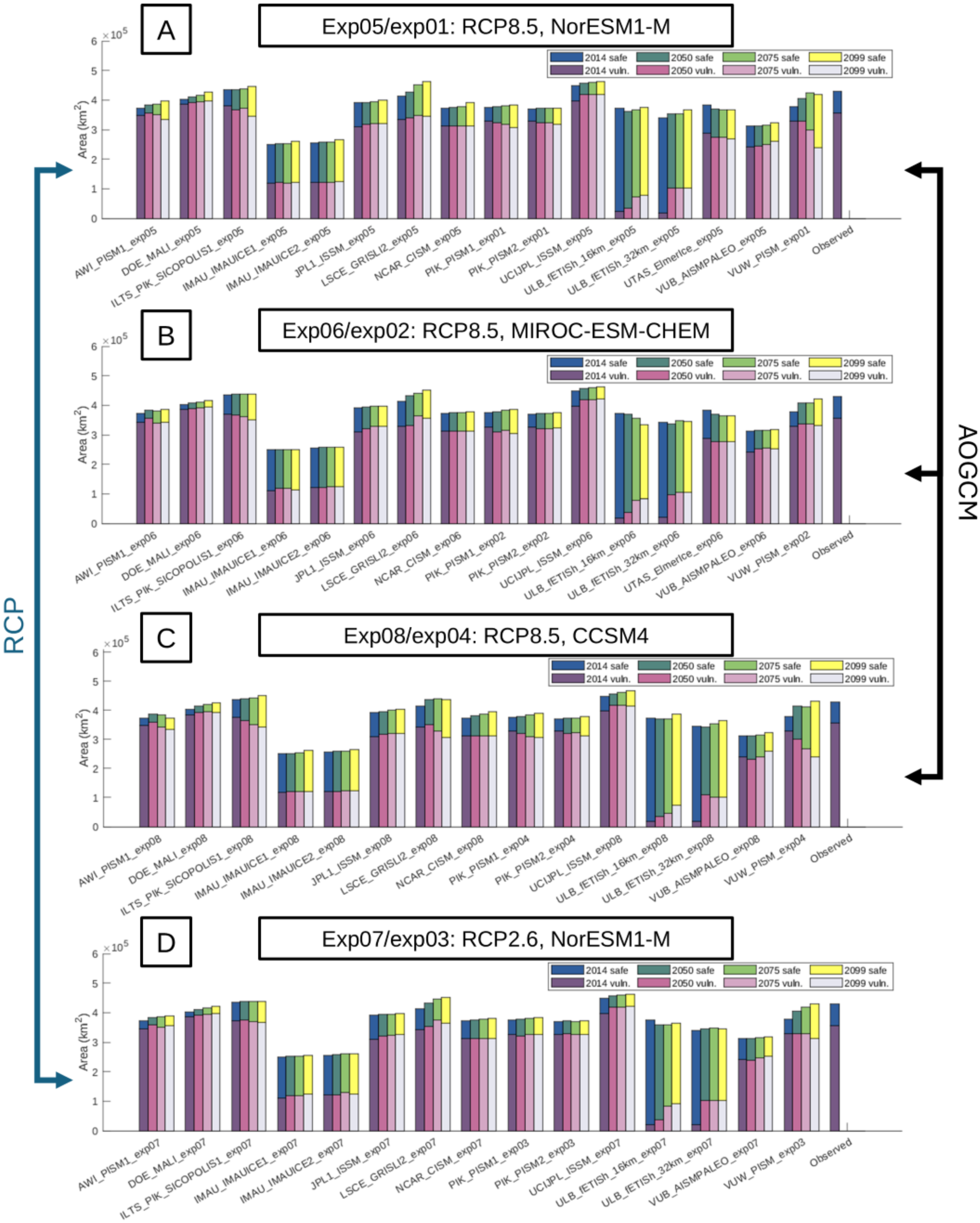

Figure S15: Vulnerable and safe ice shelf areas in each ice sheet model in 2014, 2050, 2075, and 2100 driven by (A) NorESM1-M with RCP8.5, (B) MIROC-ESM-CHEM with RCP8.5, (C) CCSM4 with RCP8.5, and (D) NorESM1-M with RCP2.6 for the Filchner-Ronne. Arrows indicate the analyses providing averages for the climate scenario (RCP) and climate model (AOGCM) analyses. The fracture toughness used is 200 $KPa\ m^{1/2}$.

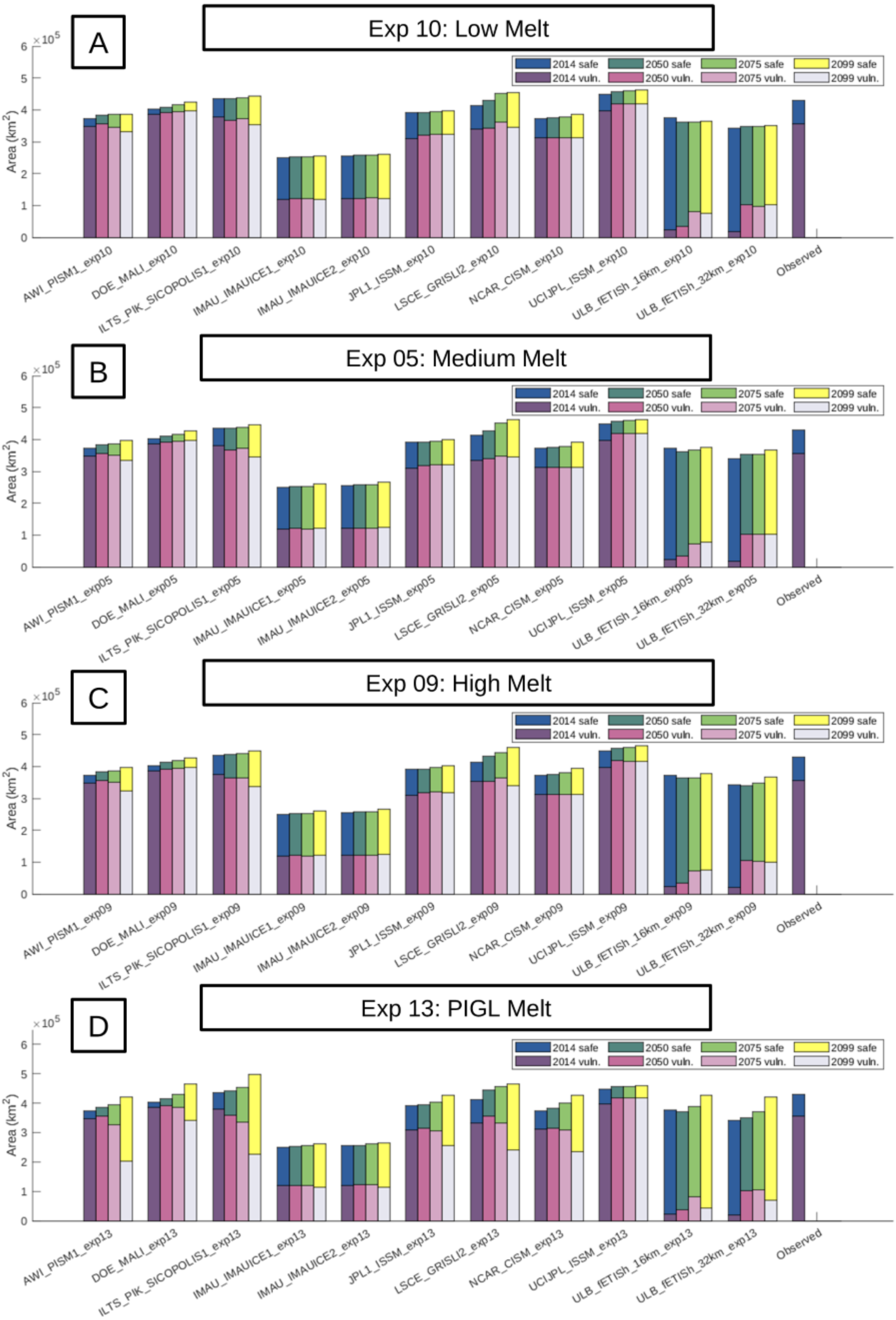

Figure S16: Vulnerable and safe ice shelf areas in each ice sheet model in 2014, 2050, 2075, and 2100 driven by the (A) low, (B) medium, (C) high, and (D) PIGL basal melt parametrizations for the Filchner-Ronne. The ice sheet models for all these experiments were driven by NorESM1-M under RCP8.5 and the fracture toughness used was $KPa\ m^{1/2}$.

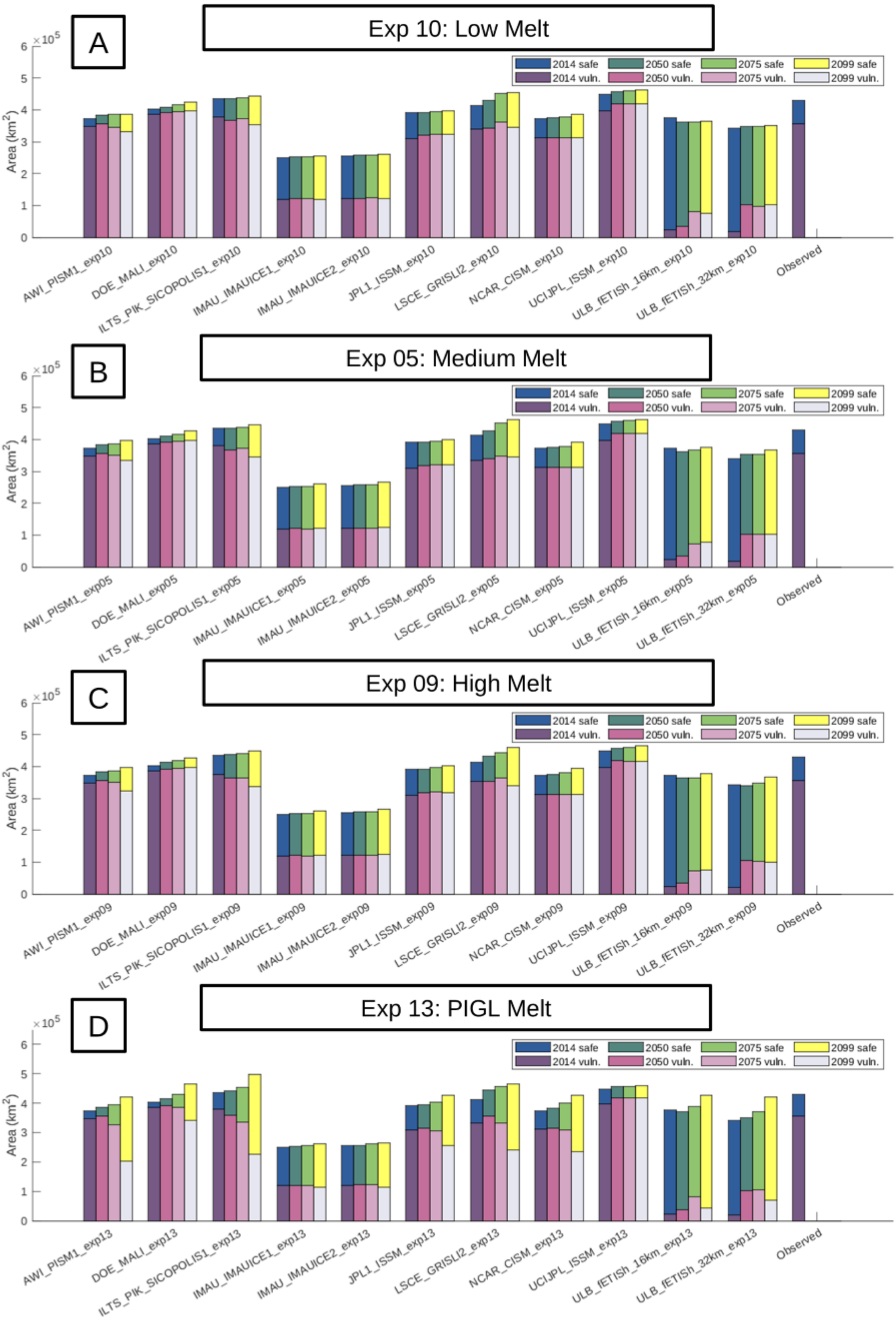

Figure S17: Vulnerable and safe ice shelf areas in each ice sheet model in 2014, 2050, 2075, and 2100 driven by NorESM1-M under RCP8.5 (exp05 and exp01) postprocessed with fracture toughenss values of (A) 100, (B) 200, (C) 300, and (D) 400 $KPa\ m^{1/2}$.

S2.3 Amery

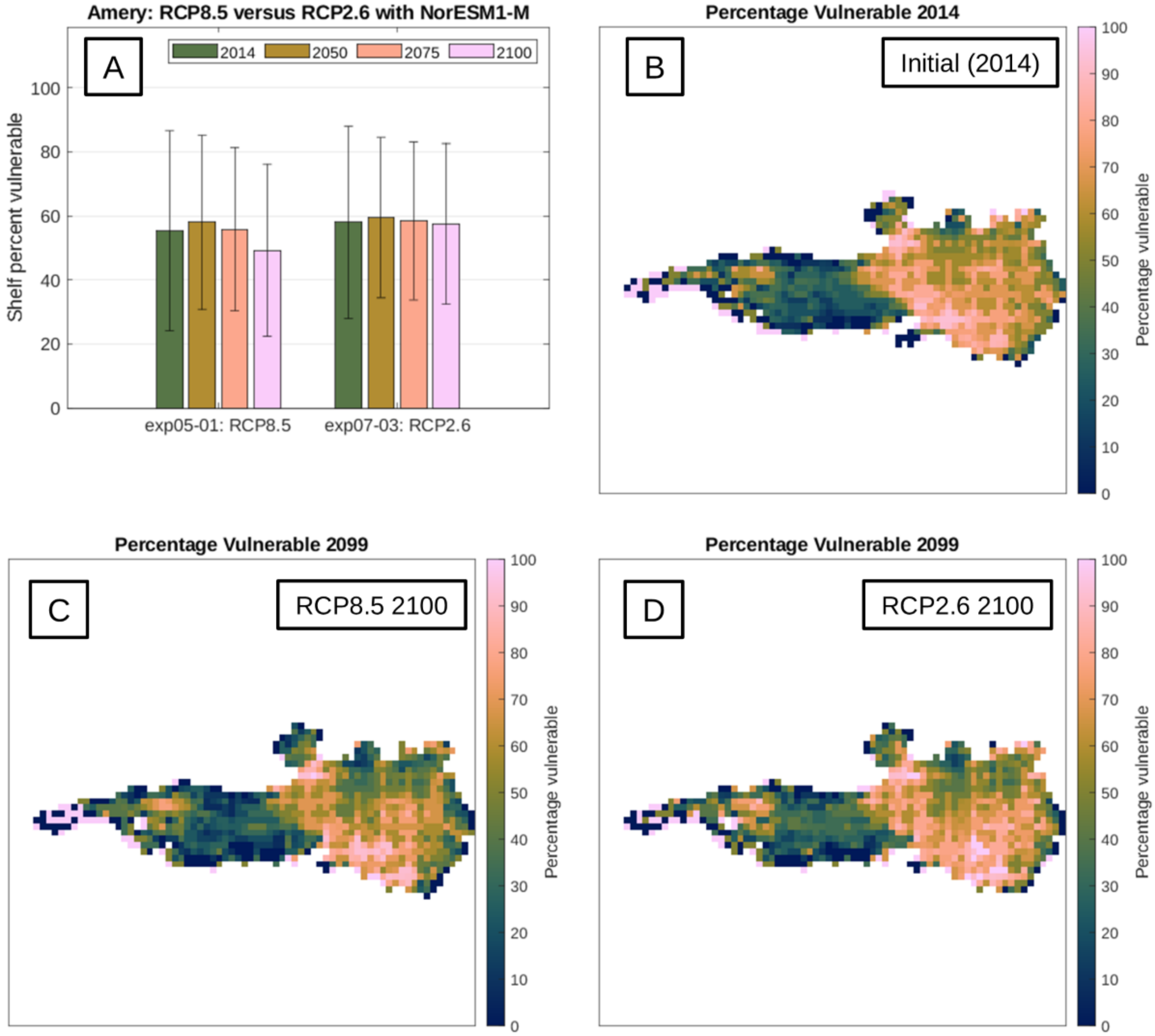

Figure S18: (A) Average shelf vulnerability fraction across ice sheet models in 2014, 2050, 2075, and 2100 under RCP8.5 and RCP2.6; (B) initial per-pixel vulnerability agreement across models; (C) 2100 vulnerability agreement under RCP8.5; and (D) 2100 vulnerability agreement under RCP2.6 driven by the NorESM1-M climate model for the Amery.

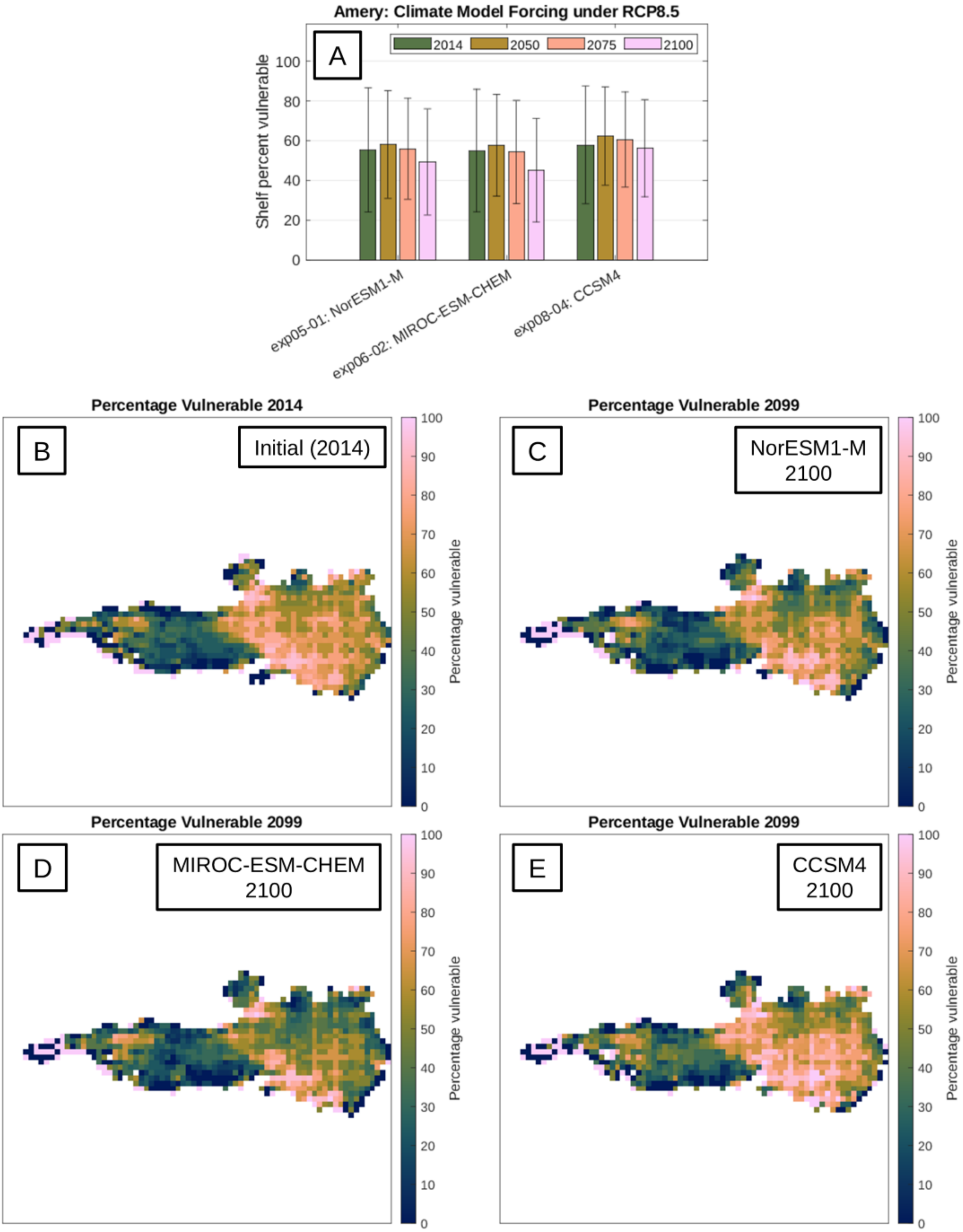

Figure S19: (A) Average shelf vulnerability fraction across ice sheet models in 2014, 2050, 2075, and 2100 using RCP8.5 with three climate models; (B) initial per-pixel vulnerability agreement across models; (C) 2100 vulnerability agreement driven by NorESM1-M; (D) 2100 vulnerability agreement driven by MIROC-ESM-CHEM; and (E) 2100 vulnerability agreement driven by CCSM4 for the Amery.

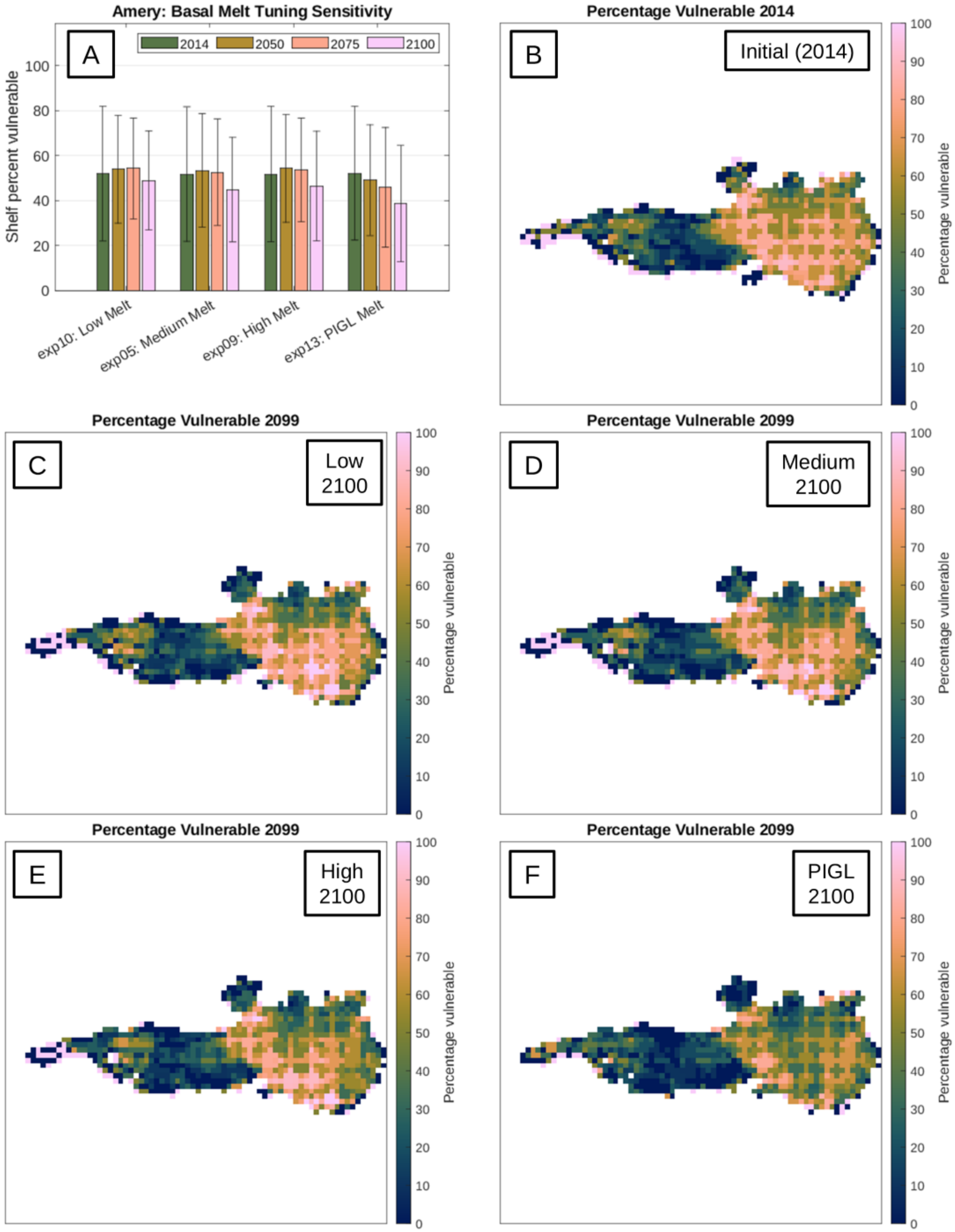

Figure S20: (A) Average shelf vulnerability fraction across ice sheet models in 2014, 2050, 2075, and 2100 using RCP8.5 with for basal melt parametrization tunings; (B) initial per-pixel vulnerability agreement across models; and 2100 vulnerability agreement with the (C) Low, (D) Medium, (E) High, and (F) PIGL basal melt parametrization tunings for the Amery.

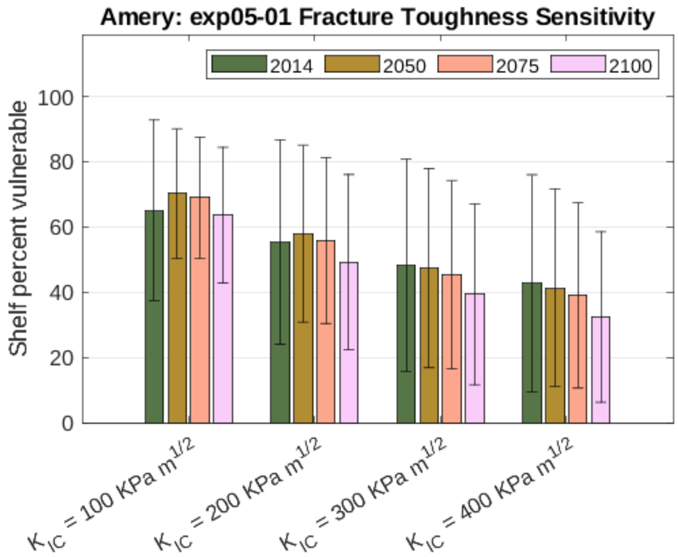

Figure S21: Average shelf vulnerability fraction across ice sheet models in 2014, 2050, 2075, and 2100 with fracture toughness values of 100, 200, 300, and 400 $KPa\ m^{1/2}$ under the RCP8.5 forcing with the NorESM1-M climate model for the Amery shelf.

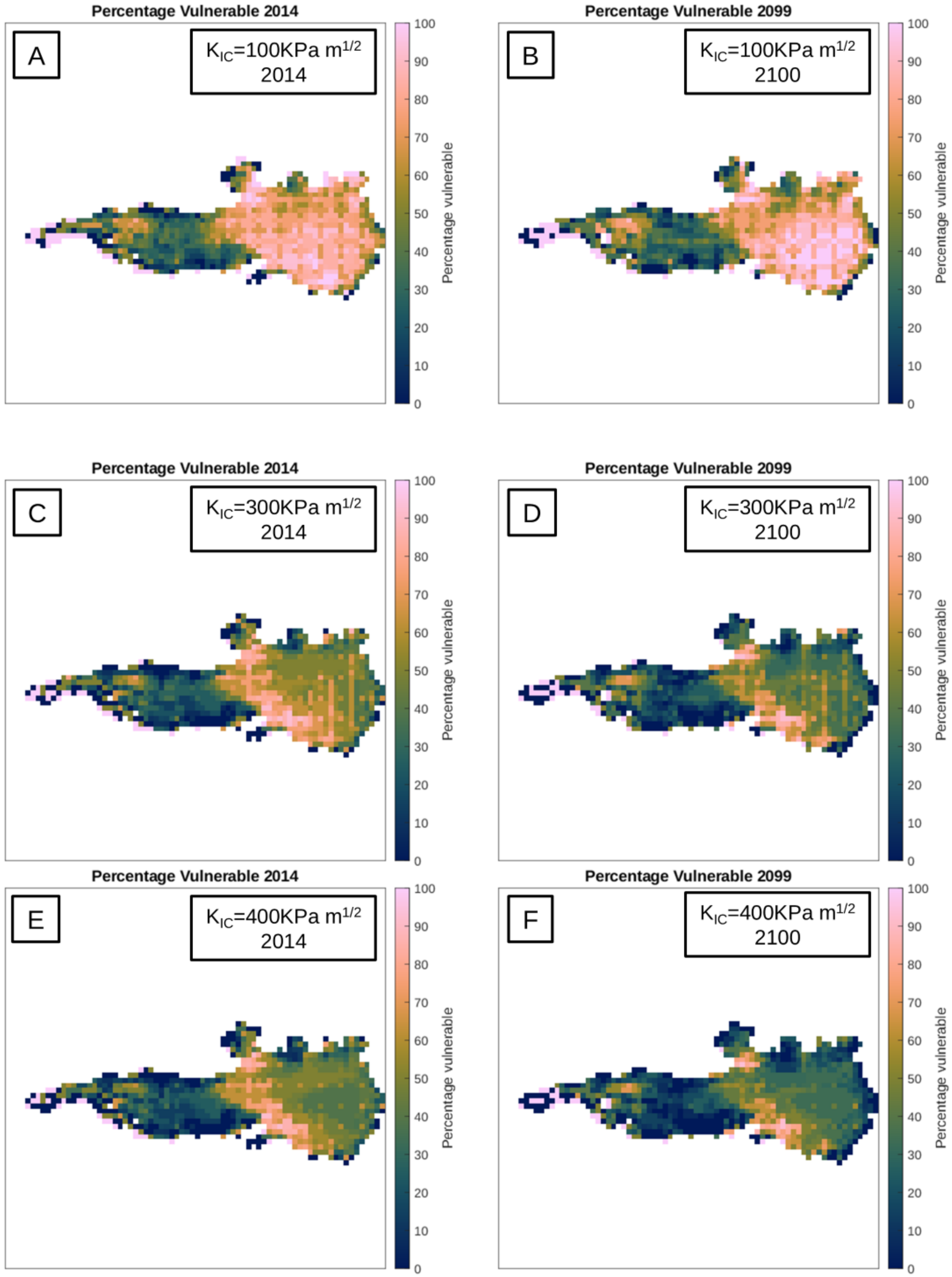

Figure S22: Initial and 2100 per-pixel vulnerability agreement across ice sheet models under RCP8.5 with NorESM1-M postprocessed with fracture toughness values of (A,B) 100, (C,D) 300, and (E,F) 400 $KPa\ m^{1/2}$ for the Amery. The equivalent plots with 200 $KPa\ m^{1/2}$ can be found as panels B and C of Fig. S3.

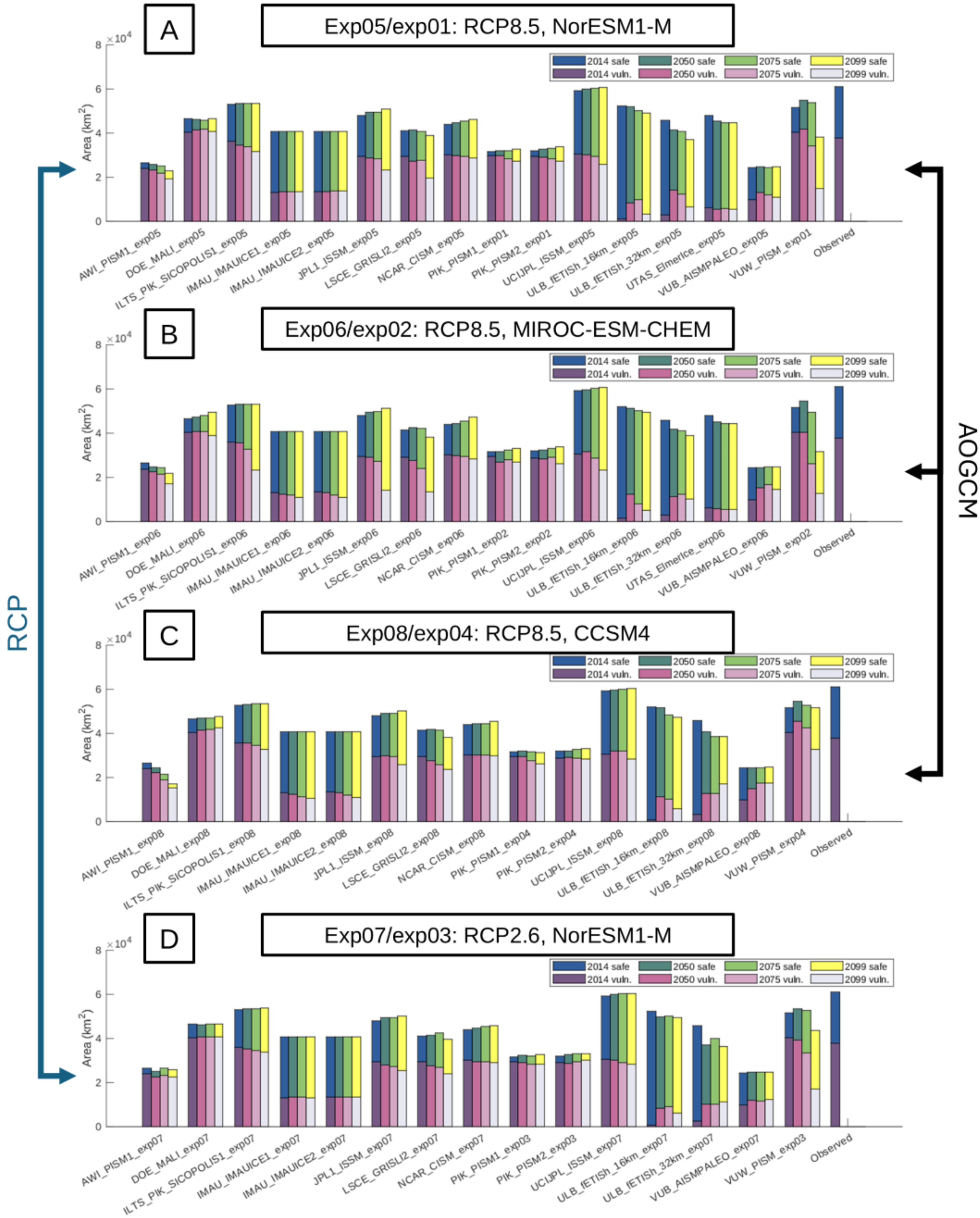

Figure S23: Vulnerable and safe ice shelf areas in each ice sheet model in 2014, 2050, 2075, and 2100 driven by (A) NorESM1-M with RCP8.5, (B) MIROC-ESM-CHEM with RCP8.5, (C) CCSM4 with RCP8.5, and (D) NorESM1-M with RCP2.6 for the Amery. Arrows indicate the analyses providing averages for the climate scenario (RCP) and climate model (AOGCM) analyses. The fracture toughness used is 200 $KPa\ m^{1/2}$.

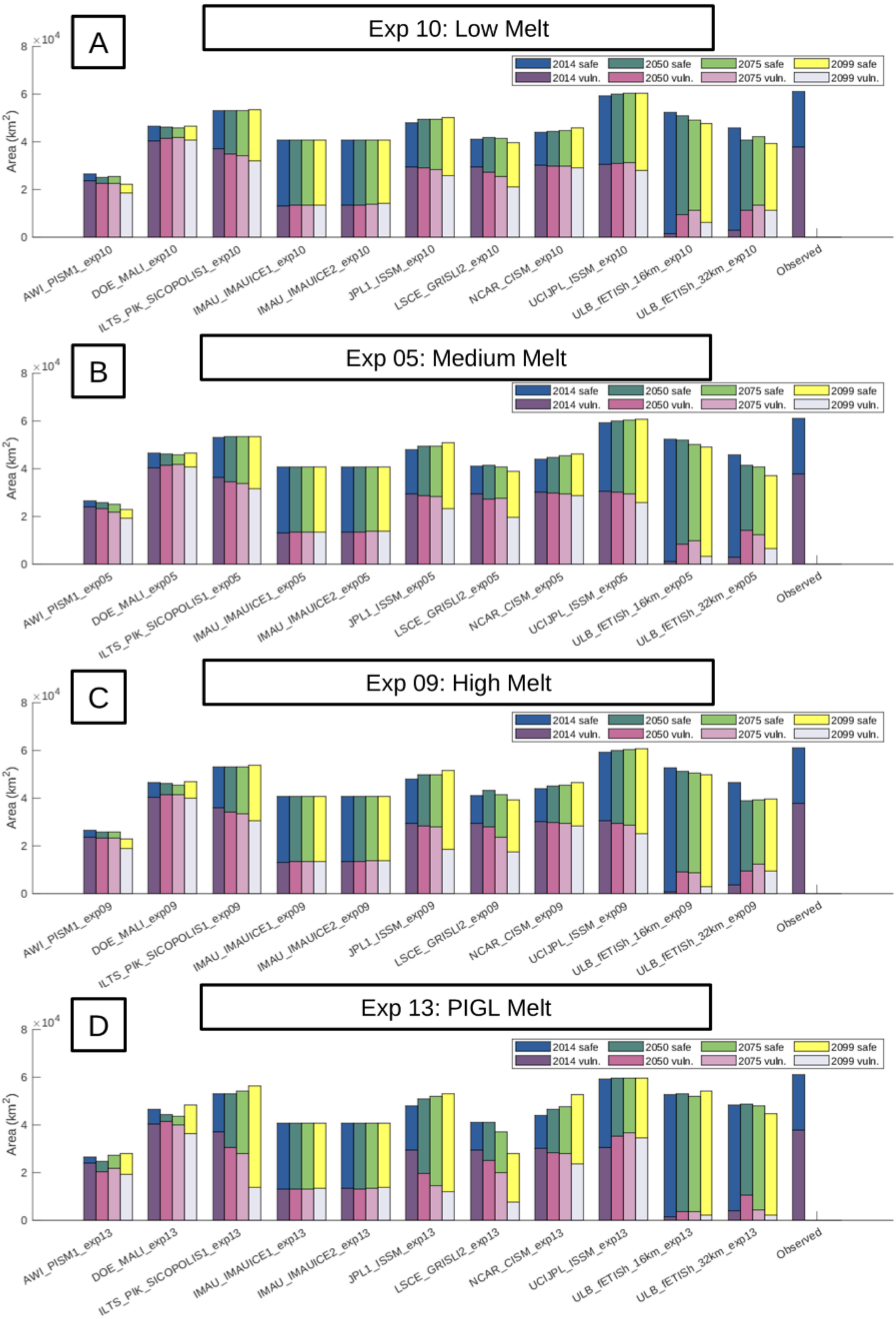

Figure S24: Vulnerable and safe ice shelf areas in each ice sheet model in 2014, 2050, 2075, and 2100 driven by the (A) low, (B) medium, (C) high, and (D) PIGL basal melt parametrizations for the Amery. The ice sheet models for all these experiments were driven by NorESM1-M under RCP8.5 and the fracture toughness used was $KPa\ m^{1/2}$.

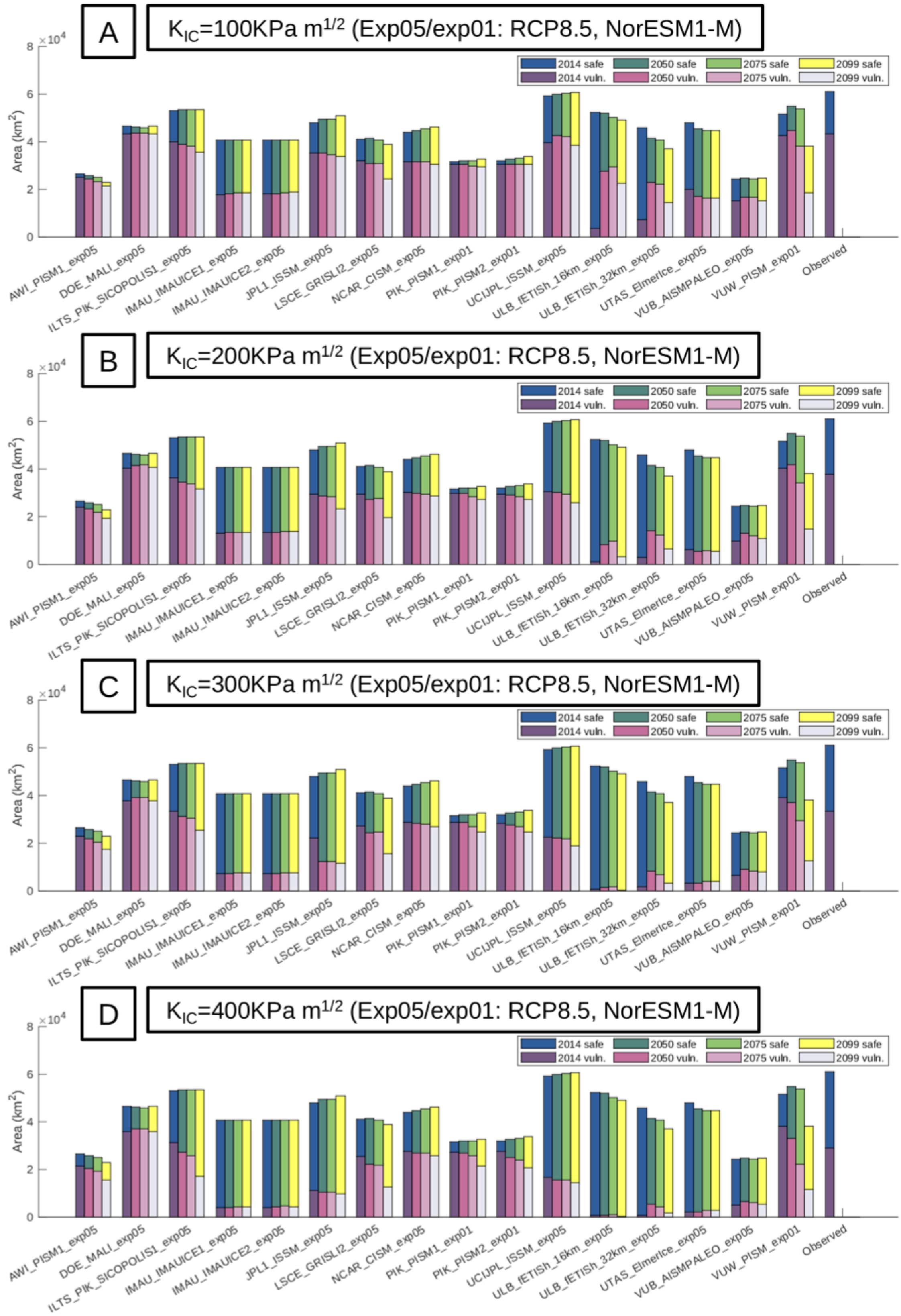

Figure S25: Vulnerable and safe ice shelf areas in each ice sheet model in 2014, 2050, 2075, and 2100 driven by NorESM1-M under RCP8.5 (exp05 and exp01) postprocessed with fracture toughenss values of (A) 100, (B) 200, (C) 300, and (D) 400 $KPa\ m^{1/2}$.

S2.4 Larsen C

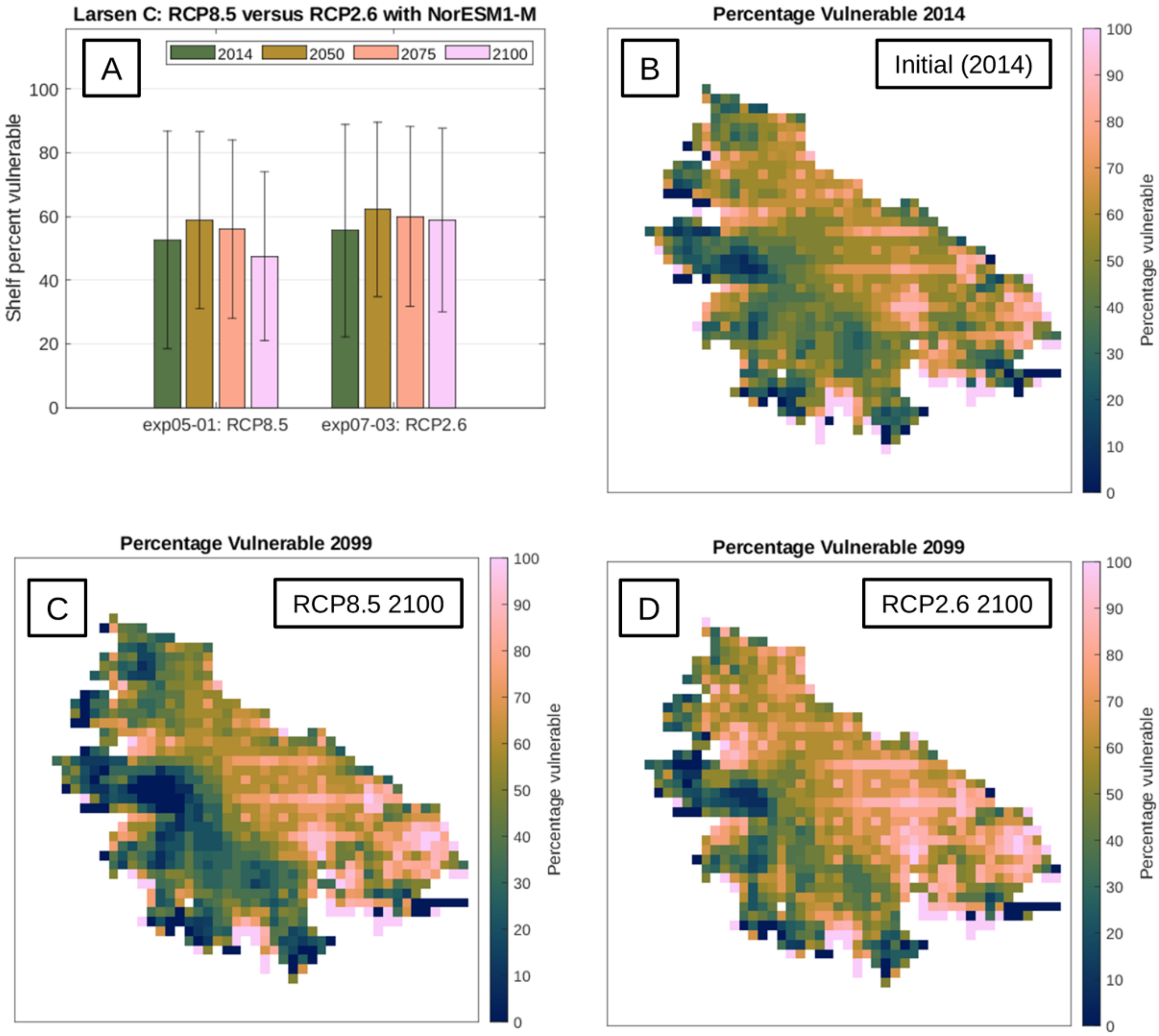

Figure S26: (A) Average shelf vulnerability fraction across ice sheet models in 2014, 2050, 2075, and 2100 under RCP8.5 and RCP2.6; (B) initial per-pixel vulnerability agreement across models; (C) 2100 vulnerability agreement under RCP8.5; and (D) 2100 vulnerability agreement under RCP2.6 driven by the NorESM1-M climate model for the Larsen C.

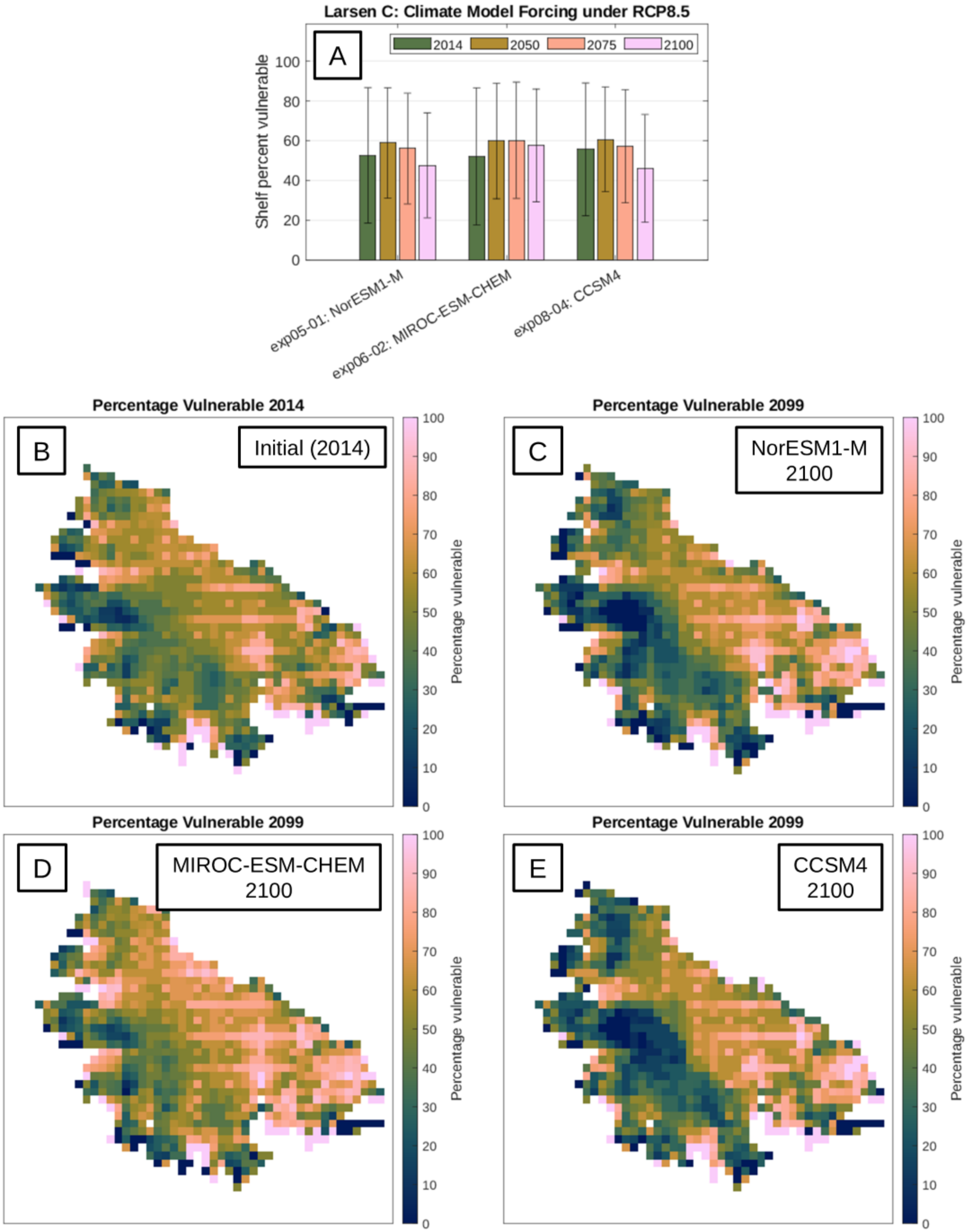

Figure S27: (A) Average shelf vulnerability fraction across ice sheet models in 2014, 2050, 2075, and 2100 using RCP8.5 with three climate models; (B) initial per-pixel vulnerability agreement across models; (C) 2100 vulnerability agreement driven by NorESM1-M; (D) 2100 vulnerability agreement driven by MIROC-ESM-CHEM; and (E) 2100 vulnerability agreement driven by CCSM4 for the Larsen C.

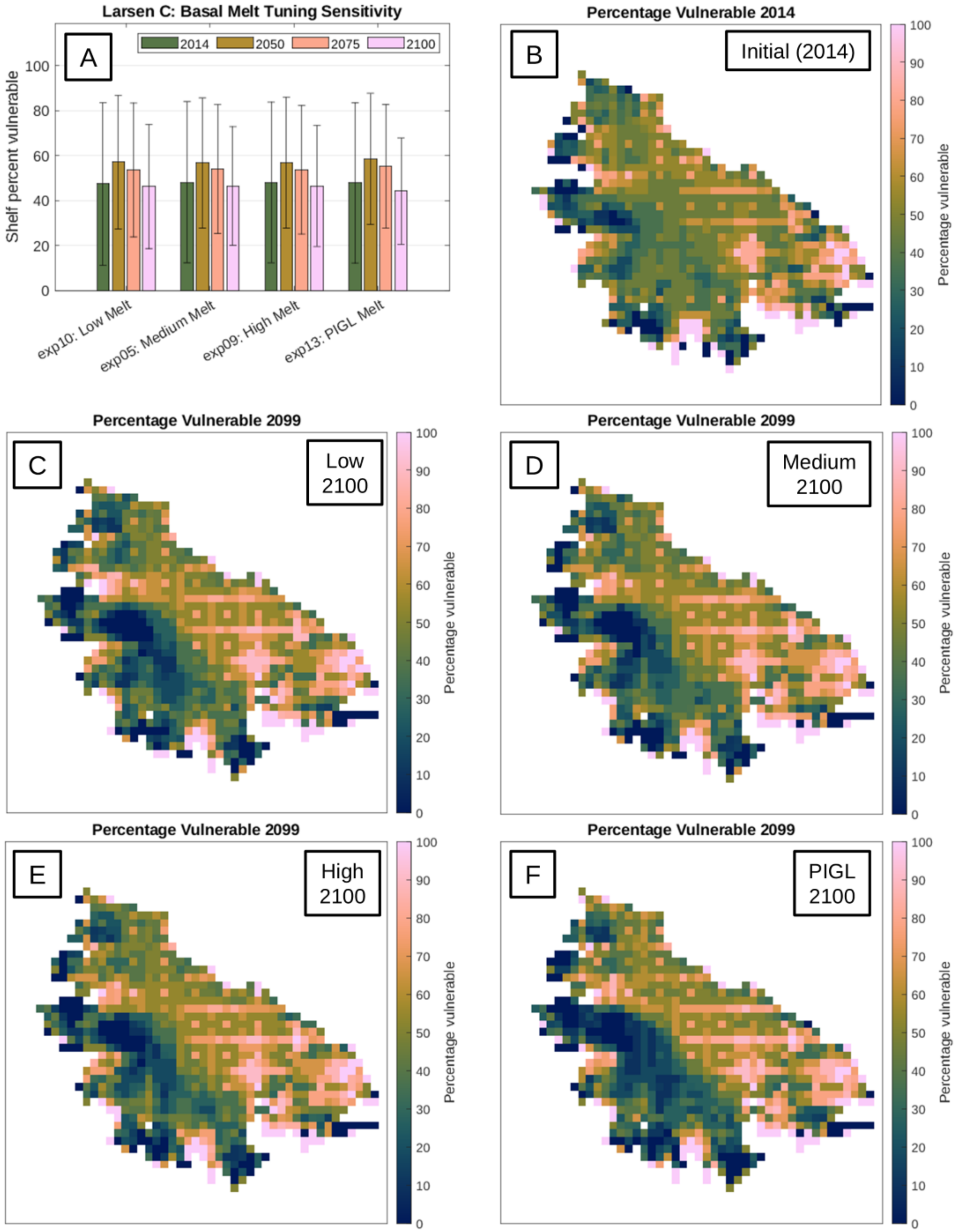

Figure S28: (A) Average shelf vulnerability fraction across ice sheet models in 2014, 2050, 2075, and 2100 using RCP8.5 with for basal melt parametrization tunings; (B) initial per-pixel vulnerability agreement across models; and 2100 vulnerability agreement with the (C) Low, (D) Medium, (E) High, and (F) PIGL basal melt parametrization tunings for the Larsen C.

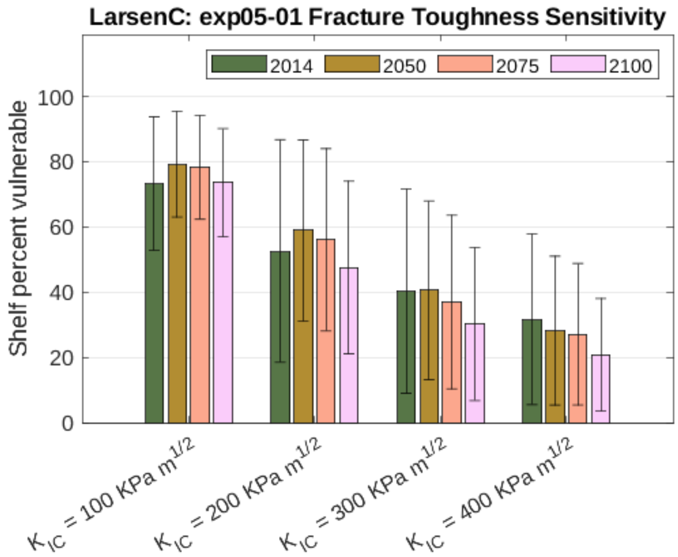

Figure S29: Average shelf vulnerability fraction across ice sheet models in 2014, 2050, 2075, and 2100 with fracture toughness values of 100, 200, 300, and 400 $KPa\ m^{1/2}$ under the RCP8.5 forcing with the NorESM1-M climate model for the Larsen C shelf.

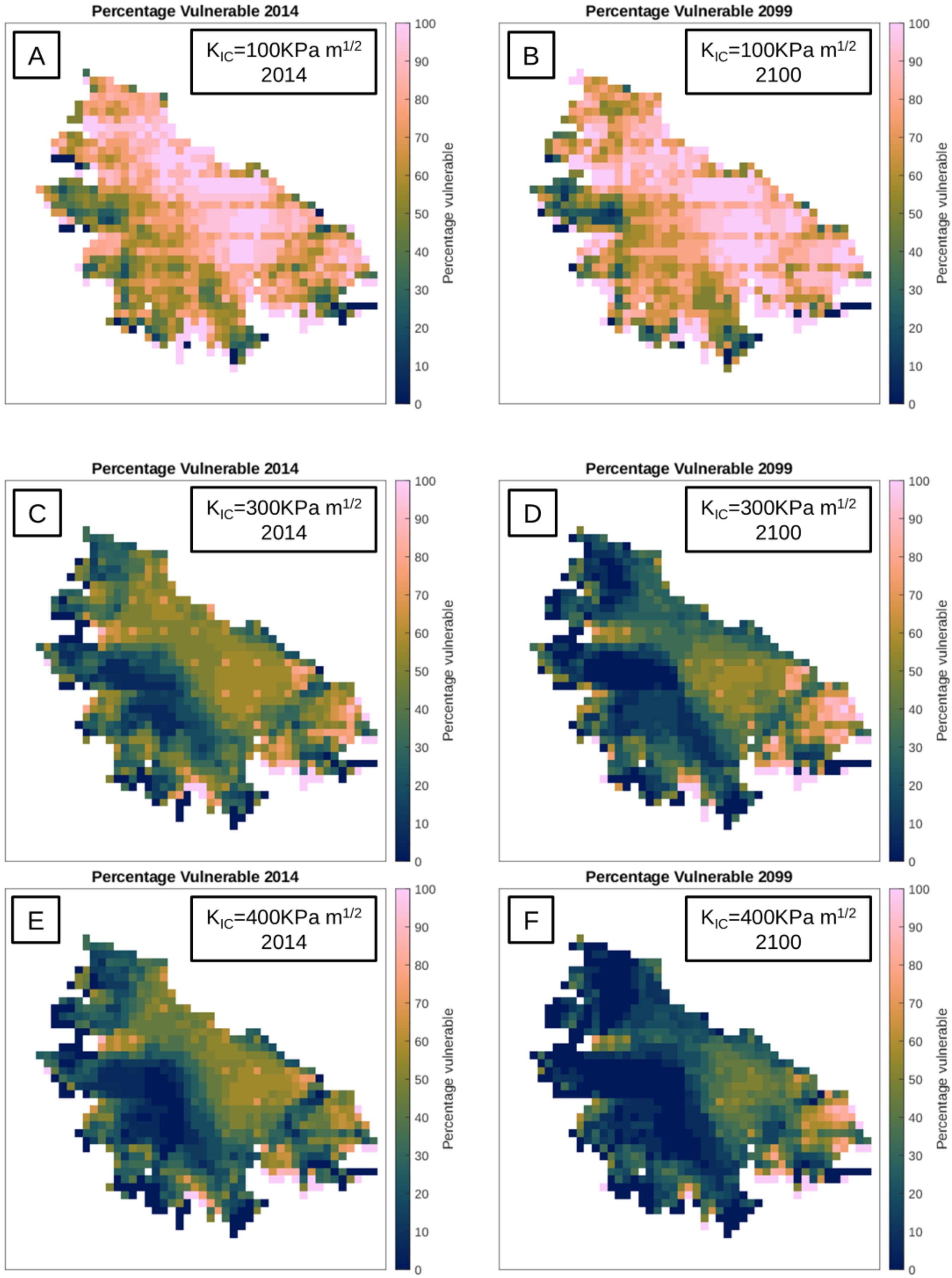

Figure S30: Initial and 2100 per-pixel vulnerability agreement across ice sheet models under RCP8.5 with NorESM1-M postprocessed with fracture toughness values of (A,B) 100, (C,D) 300, and (E,F) 400 $KPa\ m^{1/2}$ for the Larsen C. The equivalent plots with 200 $KPa\ m^{1/2}$ can be found as panels B and C of Fig. S3.

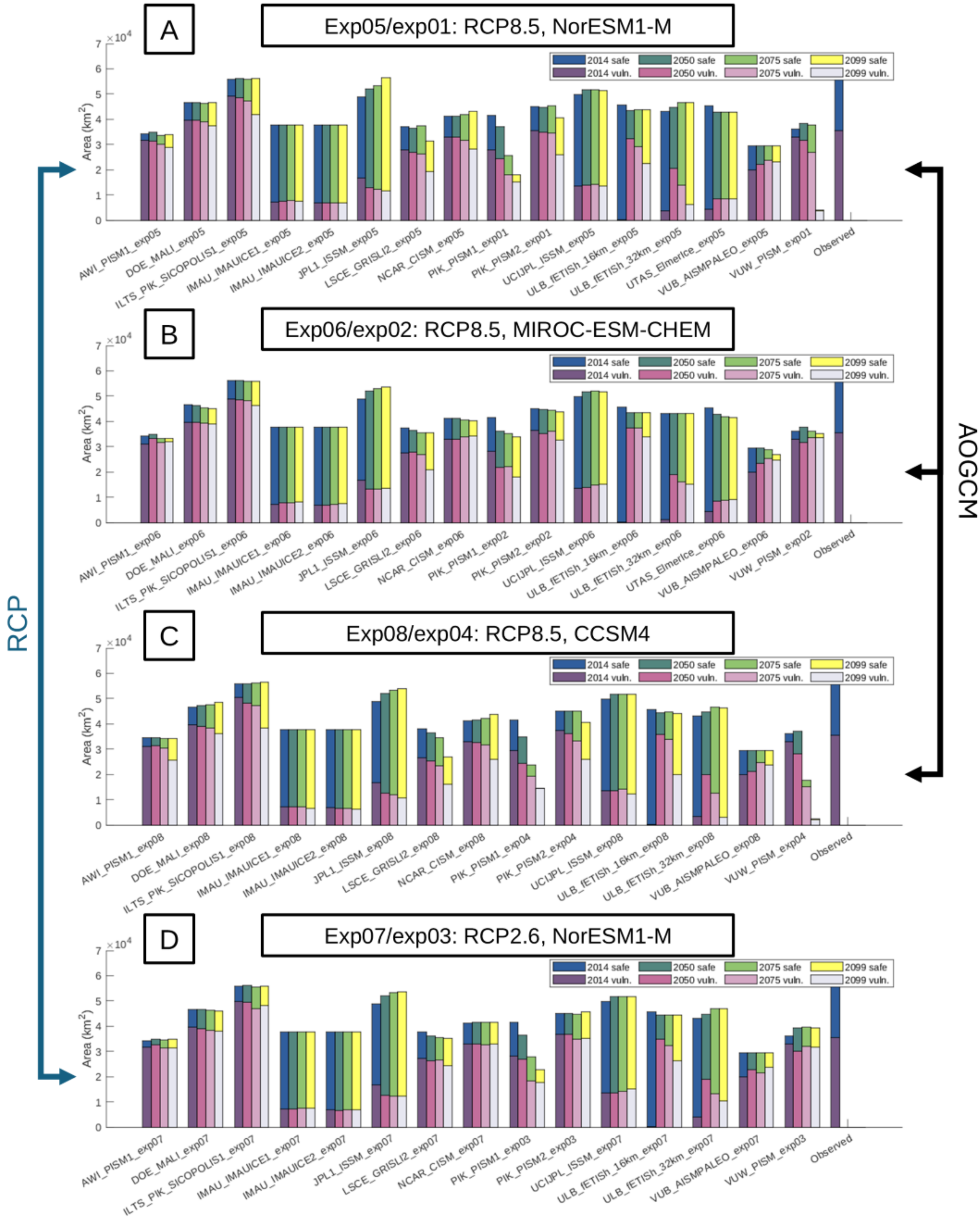

Figure S31: Vulnerable and safe ice shelf areas in each ice sheet model in 2014, 2050, 2075, and 2100 driven by (A) NorESM1-M with RCP8.5, (B) MIROC-ESM-CHEM with RCP8.5, (C) CCSM4 with RCP8.5, and (D) NorESM1-M with RCP2.6 for the Larsen C. Arrows indicate the analyses providing averages for the climate scenario (RCP) and climate model (AOGCM) analyses. The fracture toughness used is 200 $KPa\ m^{1/2}$.

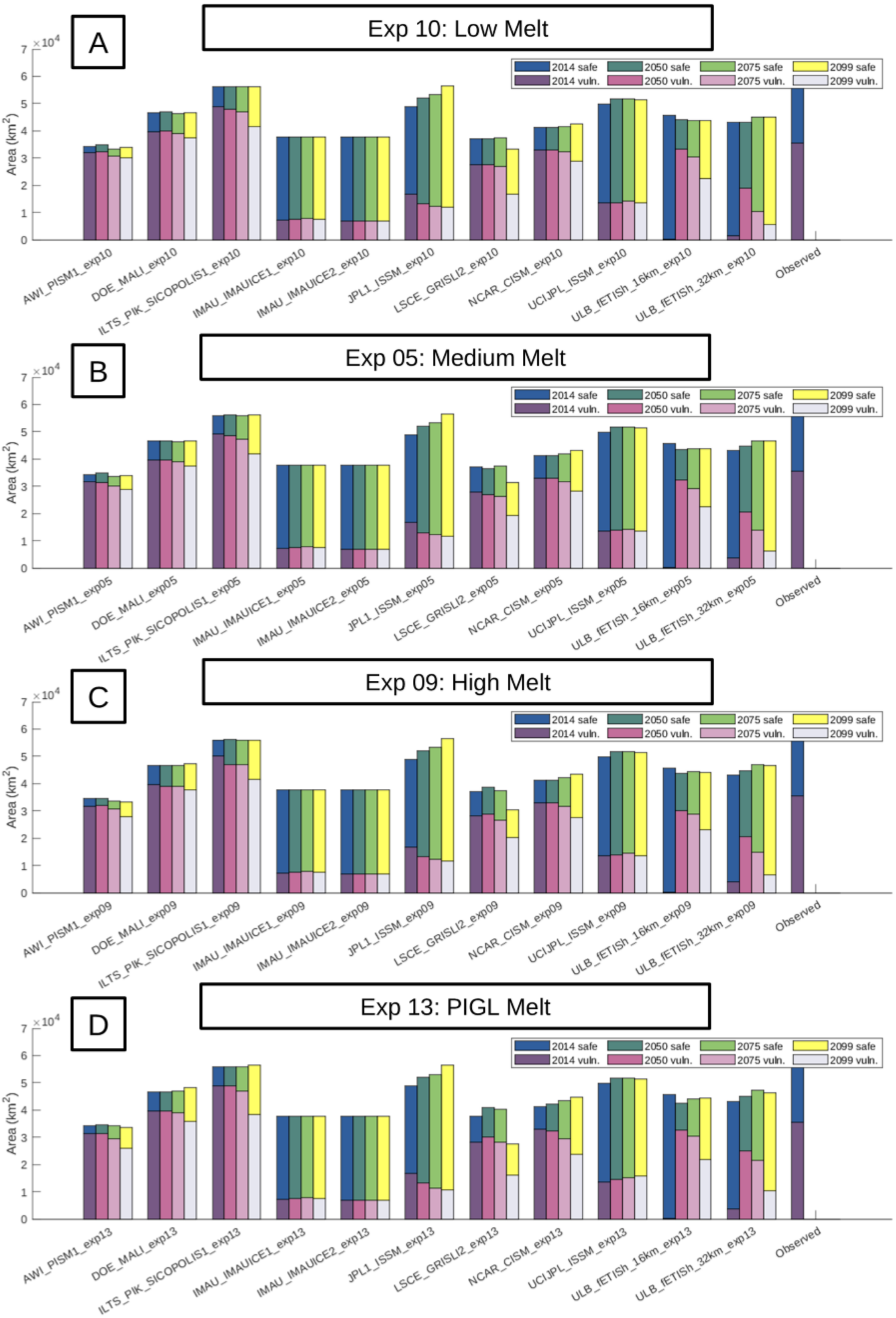

Figure S32: Vulnerable and safe ice shelf areas in each ice sheet model in 2014, 2050, 2075, and 2100 driven by the (A) low, (B) medium, (C) high, and (D) PIGL basal melt parametrizations for the Larsen C. The ice sheet models for all these experiments were driven by NorESM1-M under RCP8.5 and the fracture toughness used was $KPa\ m^{1/2}$.

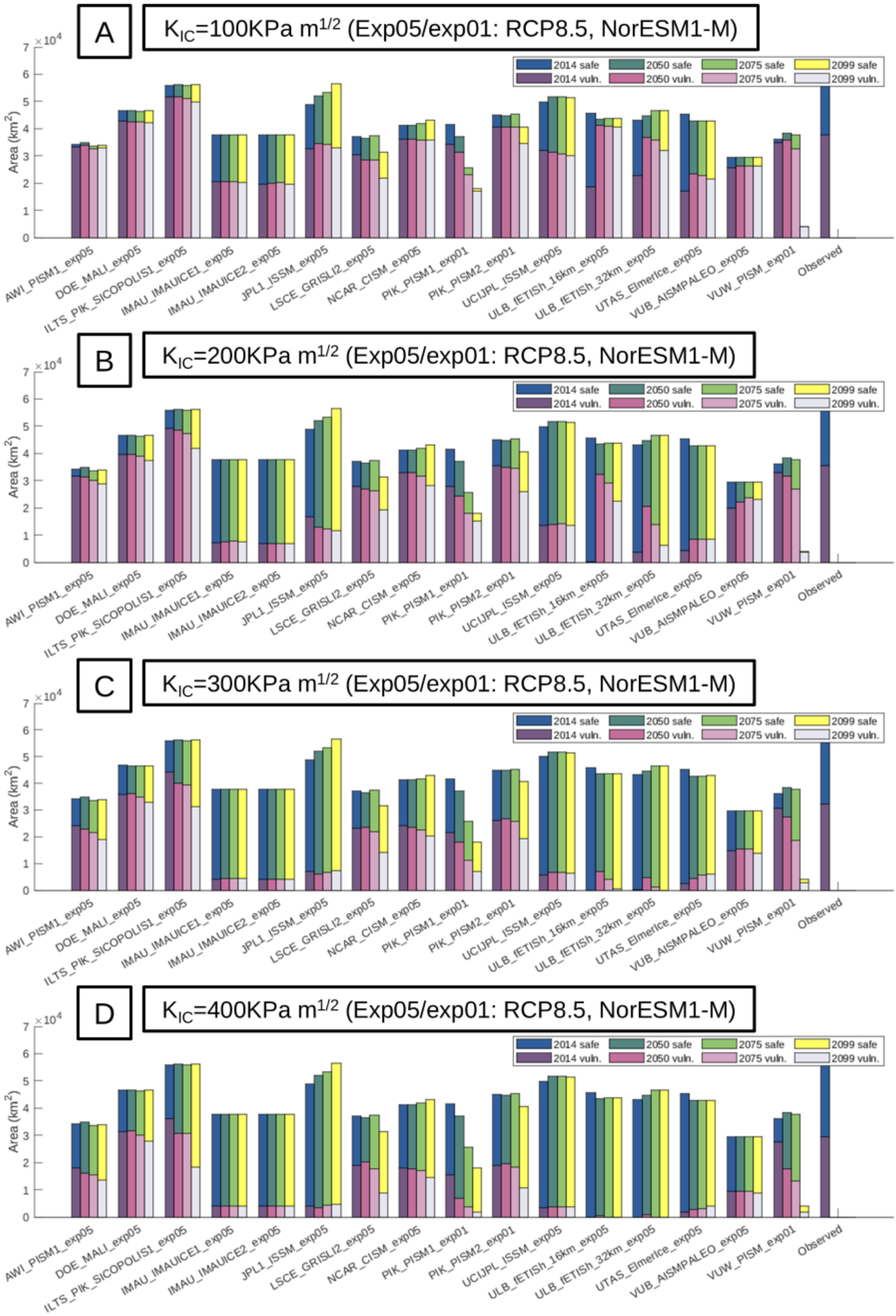

Figure S33: Vulnerable and safe ice shelf areas in each ice sheet model in 2014, 2050, 2075, and 2100 driven by NorESM1-M under RCP8.5 (exp05 and exp01) postprocessed with fracture toughenss values of (A) 100, (B) 200, (C) 300, and (D) 400 $KPa\ m^{1/2}$.